Characterisation and optimality of open quantum system dynamics

Eoin O'Connor

15413458

The thesis is submitted to University College Dublin in fulfillment of the requirements for the degree of Doctor of Philosophy in Physics

UCD School of Physics

Head of School: Prof. Emma Sokell
Principal Supervisor: Assistant Prof. Steve Campbell
Research Studies Panel: Prof. Emma Sokell
Prof. Peter Duffy

October 27, 2023

Contents

Abstract

We develop tools to characterise the dynamics of open quantum systems. We start by introducing the concept of action quantum speed limits (QSLs). Unlike conventional geometric methods, these QSLs intricately depend on the instantaneous speed, offering bounds on the minimal time needed to connect states. The instantaneous speed along fixed trajectories is shown to be an important and optimisable degree of freedom, as exemplified through the thermalising qubit case. Beyond discussing the feasibility of geometric QSLs, we also critically examine their interpretation in terms of different metric choices. It is revealed that these open-system QSL times provide indications of optimality concerning geodesic paths, rather than being strict minimal time indicators.

Distinguishability, based on distance metrics employed in deriving QSLs (in particular the Fisher information), is also the key concept in the field of metrology. We consider the use of open system dynamics as a model to explore parameter estimation. We investigate how the presence of correlation between measurement results affects the Fisher information. These correlations are introduced through a sequential measurement scheme, where the same probe is measured multiple times in succession without allowing for equilibration. We prove that, for there to be any advantage in precision as a result of these correlations, there must be information encoded into the system-environment interaction term related to the parameter that we are trying to estimate. To emphasise this, we consider the specific case of temperature estimation where the thermalisation rate of the probe contains additional information about the temperature. The sequential scheme can be viewed as a form of collisional quantum thermometry, which further allows additional freedoms in the protocol, e.g. by introducing stochasticity in the waiting time between collisions. We establish that incorporating randomness in this manner leads to a significant expansion of the parameter range for achieving advantages over typical equilibrium approaches to thermometry. Intriguingly, we demonstrate that in certain settings optimal measurements can be performed locally, highlighting the limited role of genuine quantum correlations in this advantage.

Finally, we delve into the statistics of the work done on a quantum system via a two-point measurement scheme. The Shannon entropy of the work distribution is shown to possess a general upper bound tied to initial diagonal entropy and a distinct quantum term associated with the relative entropy of coherence. This approach is shown to capture signatures of underlying physics across diverse scenarios. In particular, through an in-depth exploration of the Aubry-André-Harper model, we illustrate how the entropy of the work distribution provides a useful tool for characterising the localisation transition. We further explore the use of the entropy of the work distribution as a tool for identifying the mobility edge in a generalised Aubry-André-Harper model.

Collectively, these results provide a toolbox to assess the optimality, either in terms of the dynamical paths taken, utility for metrological tasks, or ability to spotlight relevant physical properties of the model, for the dynamics of complex quantum systems.

Statement of Original Authorship

I hereby certify that the submitted work is my own work, was completed while registered as a candidate for the degree stated on the Title Page, and I have not obtained a degree elsewhere on the basis of the research presented in this submitted work

Publications and Collaborations

This thesis is based on the following publications:

- E. O'Connor, G. Guarnieri, and S. Campbell., "Action quantum speed limits", *Phys. Rev. A* **103**(2), 022210 (2021) [1]
- E. O'Connor, B. Vacchini, and S. Campbell., "Stochastic Collisional Quantum Thermometry", *Entropy* **23**(12), 1634 (2021) [2]
- A. Kiely, E. O'Connor, T. Fogarty, G.T. Landi and S. Campbell., "Entropy of the quantum work distribution", *Phys. Rev. Research* **5**(2), L022010 (2023) [3]
- E. O'Connor, G.T. Landi and S. Campbell., "Information rates in sequential Metrology", (In Progress)

Acknowledgements

I am incredibly grateful to my supervisor, Steve Campbell, for trusting in me to be his first PhD student. I would like to thank him for his ever-present guidance and selfless support. You are building a great group and community at UCD, long may it last. On that note, I thank all of the CATS group members, Anthony for his endless insight and accurate calculation, Eoin for keeping me fit and motivated, and George for some necessary distractions. Additionally, I am grateful for all of those who I have shared the office with over the last 4 years, along with all of the administrative staff in the School of Physics for their constant support.

I would like to thank Barış Çakmak for welcoming me to Istanbul and taking the time to show me around the city and the university. I would also like to thank Gabriel Landi for hosting me at the University of São Paulo, thank you for keeping me alive and for inspiring many creative research ideas. Thanks to Giacomo Guarnieri and Bassano Vacchini for sharing their incredible expertise during our projects together.

I am incredibly lucky to have such a strong core group of family and friends that have been there for me before, during and hopefully long after my PhD. Their presence has been both a source of inspiration for my work and a necessary escape from it. Particular thanks to my parents, Ken and Nicola, who have always given me the freedom and encouraged me to pursue my dreams, and have provided a rock-solid support for me to do just that. I couldn't have done it without you.

List of Figures

Chapter 1

Introduction

Quantum mechanics, at its most fundamental level, deals with the evolution of vectors in a Hilbert space. These vectors evolve in time via unitary evolution. This evolution is completely time reversible and can be achieved by applying the conjugate transpose of the unitary. At the quantum level there is no arrow of time, no straightforward way to distinguish between the past and the future. Yet, for humans, we remember the past but can only predict the future, there is a clear asymmetry there. Human beings are finite creatures, we interact with the world via our senses. When our senses are not sufficient or not accurate enough, we build measurement devices. For example, we have thermal imaging devices that can detect wavelengths of light outside the visible range and allow us to see at night. We have precise thermometers that allow us to distinguish between temperatures that are far too fine for our own senses to differentiate. We have also built measurement devices that can measure quantities our own senses are incapable of detecting such as a magnetometer for measuring magnetic field strength or a Geiger counter for detecting the products of radioactive decay. Devices like these give us access to tiny length scales where quantum effects dominate. One crucial component of all measuring devices, humans included, is that information is lost in the measurement process. We are not Laplace's demon, and neither is the measurement device, when we interact with a system we, in turn, change the system and become part of a larger, interconnected system. It is interactions and correlations between tiny systems that eventually lead to all the phenomena of everyday life [5].

The concept of open quantum systems is where we can first start to see these properties appear and the first hints of time asymmetry start to emerge. Open quantum systems lean into the fact that our measurements only give us partial information about our system and there are multiple configurations of the system that could have resulted in that outcome. The theory of open quantum systems allows us to assign a probability to each of these configurations. This formalism combines the concept of superposition of quantum states with classical probabilities that arise from incomplete information. Understanding the transition between quantum and classical physics has been a topic of interest for a long time but only in recent years has significant progress been made with quantum thermodynamics [6] investigating the appearance of an arrow of time from time reversible unitary dynamics. Additionally, Quantum Darwinism [7] aims to explain how quantum

states, which are impossible to duplicate [8], can become classical states that all observers agree about.

All these results rely on the concept of open quantum systems. A common theme throughout this thesis will be understanding this connection between superposition and probability, and quantifying their effects on state manipulation, parameter estimation and thermodynamic quantities. In Chapter 2 we look at the concept of the distance between pure quantum states and show that it is related to the distance between classical probability distributions. This observation allows us to generalise the notion of distance to open quantum systems. We use these distance measures to put fundamental limits on the time that it takes to evolve from one quantum state to another. These distance measures also play a crucial role in quantum metrological settings, where the distinguishability between quantum states allows us to rigorously determine the ability for a quantum system to act as a precise quantum sensor. We explore this in the context of an open system acting as a probe in Chapter 3. At the end of the day, measurement results will always be classical bits of information because humans need to understand them. Still, quantum systems provide us with new tools to gain additional precision in our measurements over classical systems. Finally, Chapter 4 considers alternative tools to characterise a quantum evolution. We look at the thermodynamic quantity of work and see that the entropy of the work distribution can be split into a classical and a quantum component. The quantum component proves to be a useful tool for capturing key features of quantum systems including phase transitions and avoided crossings.

One other common theme seen throughout the thesis is the interplay between theory, simulation, and experiment. It is often easy, as a theorist to get caught up in proving the latest theorem and lemma or deriving a new, marginally tighter lower bound without stopping to think of the implications in practice. This is a place where simulations can be effective, simulations allow us to test our theories and quantify the size of effects. Simulations also have some pitfalls, in real world experiments there can often be limitations in experimental equipment or the addition of noise that is not always present in simulations. These are common concerns that we try to navigate throughout the thesis.

While throughout the thesis we will introduce important concepts and techniques within the particular contexts that they are needed, nevertheless there are a few overarching tools that will be recurring related to the simulations of quantum dynamics and which we introduce in the remainder of this Chapter.

1.1 Closed quantum systems

A quantum system is completely described by its state vector, which we will denote using Dirac notion as $|\psi\rangle$. State vectors are unit vectors in a complex Hilbert space, $\mathscr{H}$, i.e. $\langle\psi|\psi\rangle = 1$, where $\langle\phi|\psi\rangle$ is the inner product on $\mathscr{H}$ that maps the ordered pair of vectors $\{|\phi\rangle, |\psi\rangle\}$ to $\mathbb{C}$ [9].

The time evolution of quantum states in Hilbert space is described by the Schrödinger equation,

$$i\hbar\frac{d}{dt}\left|\psi(t)\right\rangle = H\left|\psi(t)\right\rangle, \tag{1.1}$$

where H is the time-independent Hamiltonian of the system and $\hbar$ is the reduced Planck constant. To calculate the state vector at any time we can simply integrate Eq. (1.1) to give

$$\left|\psi(t)\right\rangle = \exp\left[-\frac{i(t-t_0)H}{\hbar}\right]\left|\psi(t_0)\right\rangle. \tag{1.2}$$

This means that we can express the time evolution of the state using the operator,

$$U(t,t_0) \equiv \exp\left[-\frac{i(t-t_0)H}{\hbar}\right]. \tag{1.3}$$

We can immediately see that U is unitary since H is Hermitian. It is possible to change the Hamiltonian by applying, for example, an external magnetic field. In this case the Hamiltonian can be time dependent and the solution to the Schrödinger equation is a time-ordered exponential [10]

$$U(t,t_0) = T_{\leftarrow}\exp\left[-\frac{i}{\hbar}\int_{t_0}^{t} dsH(s)\right]. \tag{1.4}$$

Properties of a quantum system that can be measured are known as observables. Observables are Hermitian operators that perform a linear map on $\mathscr{H}$. An observable, A, can be decomposed as

$$A = \sum_j a_j P_j \tag{1.5}$$

where P_j is an orthogonal projection onto the span of the eigenvectors with eigenvalue a_j. When the observable, A, is measured, the outcome a_j is obtained with a probability given by

$$p(a_j) = \left\langle\psi|P_j|\psi\right\rangle. \tag{1.6}$$

During this measurement, the system is projected onto the eigenspace of A and the system state after obtaining measurement result a_j is

$$\left|\psi\right\rangle \to \frac{P_j\left|\psi\right\rangle}{\sqrt{p(a_j)}}. \tag{1.7}$$

The average value of the measurement result can be written as

$$\begin{aligned}\mathbf{E}(A) &= \sum_j a_j p(a_j) \\ &= \sum_j a_j \langle\psi|P_j|\psi\rangle \\ &= \langle\psi|A|\psi\rangle \equiv \langle A\rangle.\end{aligned} \tag{1.8}$$

Sometimes it is useful to describe a quantum system as an ensemble of orthogonal states, $|\psi_i\rangle$, with respective probabilities p_i, such as the state of the system after a measurement has been performed but before the measurement is read. It is most convenient to represent this ensemble as a density matrix,

$$\rho = \sum_j p_j \left|\psi_j\right\rangle\!\left\langle\psi_j\right| . \tag{1.9}$$

By definition, the density matrix is Hermitian and has a trace of 1. Using Eq. (1.1) it is simple to derive an equivalent equation for the density matrix

$$\begin{aligned}i\hbar\frac{d}{dt}\rho &= \sum_j i\hbar p_j \left(\frac{d}{dt}\left|\psi_j\right\rangle\right)\left\langle\psi_j\right| + \left|\psi_j\right\rangle\left(\frac{d}{dt}\left\langle\psi_j\right|\right) \\ &= \sum_j p_j H \left|\psi_j\right\rangle\!\left\langle\psi_j\right| + \left|\psi_j\right\rangle\!\left\langle\psi_j\right| H \\ &= \left[H, \rho\right].\end{aligned} \tag{1.10}$$

This is known as the Von-Neumann equation. When the ensemble contains more than one state vector, the corresponding density matrix is referred to as being *mixed*. States that are not mixed are referred to as pure. The average value or expectation value of a measurement on the observable, A, can be written in density matrix formulation as

$$\langle A\rangle = \mathrm{Tr}\left[A\rho\right]. \tag{1.11}$$

1.1.1 Kraus Operators

Another scenario where the density matrix formulation is necessary is when we have two quantum systems coupled together. We will call one of them S, with Hilbert space $\mathscr{H}_S$, and the other, the environment, E, with Hilbert space $\mathscr{H}_E$. Let us assume that the system and environment start in a pure product state,

$$\left|\psi\right\rangle\!\left\langle\psi\right|_S \otimes \left|0\right\rangle\!\left\langle 0\right|_E . \tag{1.12}$$

where $|0\rangle$ can be any pure state on $\mathscr{H}_E$ and we can construct an orthonormal basis of $\mathscr{H}_E$, $\{|j\rangle_E\}$, such that $|0\rangle$ is an eigenvector. The evolution of the system and environment is described by a

unitary evolution U_{SE}

$$|\psi_{SE}\rangle\langle\psi_{SE}| = U_{SE}\left(|\psi\rangle\langle\psi|_S \otimes |0\rangle\langle 0|_E\right) U_{SE}^\dagger. \tag{1.13}$$

We can rewrite this in terms of the environment basis $\{|j\rangle_E\}$

$$\begin{aligned}
|\psi_{SE}\rangle\langle\psi_{SE}| &= \left(\sum_k \mathbf{I}_S \otimes |k\rangle\langle k|_E\right) U_{SE}\left(|\psi\rangle\langle\psi|_S \otimes |0\rangle\langle 0|_E\right) U_{SE}^\dagger \left(\sum_j \mathbf{I}_S \otimes |j\rangle\langle j|_E\right) \\
&= \sum_k \sum_j \left(\mathbf{I}_S \otimes \langle k|_E\right) U_{SE} \left(\mathbf{I}_S \otimes |0\rangle_E\right) \left(\mathbf{I}_S \otimes \langle 0|_E\right) U_{SE}^\dagger \left(\mathbf{I}_S \otimes |j\rangle\langle j|_E\right) |\psi\rangle\langle\psi|_S \otimes |k\rangle\langle j|_E \\
&= \sum_k \sum_j \left(K_k |\psi\rangle\langle\psi|_S K_j^\dagger\right) \otimes |k\rangle\langle j|_E ,
\end{aligned} \tag{1.14}$$

where $\mathbf{I}_S$ and $\mathbf{I}_E$ are the identity operators acting on $\mathscr{H}_S$ and $\mathscr{H}_E$ respectively. We have defined the so-called Kraus operator on $\mathscr{H}_S$ [11],

$$K_k = \left(\mathbf{I}_S \otimes \langle k|_E\right) U_{SE} \left(\mathbf{I}_S \otimes |0\rangle_E\right). \tag{1.15}$$

Kraus operators are not unique as they can be defined for any orthogonal basis on $\mathcal{H}_E$. The Kraus operators satisfy the following property,

$$\begin{aligned}
\sum_k K_k^\dagger K_k &= \sum_j \left(\mathbf{I}_S \otimes \langle 0|_E\right) U_{SE}^\dagger \left(\mathbf{I}_S \otimes |k\rangle_E\right) \left(\mathbf{I}_S \otimes \langle k|_E\right) U_{SE} \left(\mathbf{I}_S \otimes |0\rangle_E\right) \\
&= \left(\mathbf{I}_S \otimes \langle 0|_E\right) U_{SE}^\dagger \left(\mathbf{I}_S \otimes \left(\sum_k |k\rangle\langle k|_E\right)\right) U_{SE} \left(\mathbf{I}_S \otimes |0\rangle_E\right) \\
&= \left(\mathbf{I}_S \otimes \langle 0|_E\right) U_{SE}^\dagger U_{SE} \left(\mathbf{I}_S \otimes |0\rangle_E\right) \\
&= \mathbf{I}_S
\end{aligned} \tag{1.16}$$

If we want to measure an observable, A, that acts only on $\mathscr{H}_S$ we can do that by measuring the observable $A \otimes \mathbf{I}_E$ on $\mathscr{H}_{SE}$

$$\begin{aligned}
\langle A\rangle &= \langle\psi_{SE}| \left(A \otimes \mathbf{I}_E\right) |\psi_{SE}\rangle \\
&= \mathrm{Tr}\left[\left(A \otimes \mathbf{I}_E\right) |\psi_{SE}\rangle\langle\psi_{SE}|\right] \\
&= \sum_k \sum_j \mathrm{Tr}\left[\left(A K_k |\psi\rangle\langle\psi|_S K_j^\dagger\right) \otimes |k\rangle\langle j|_E\right] \\
&= \sum_k \sum_j \mathrm{Tr}\left[A K_k |\psi\rangle\langle\psi|_S K_j^\dagger\right] \mathrm{Tr}\, |k\rangle\langle j|_E \\
&= \mathrm{Tr}\left[A \left(\sum_j K_j |\psi\rangle\langle\psi|_S K_j^\dagger\right)\right] \\
&= \mathrm{Tr}\left[A \rho_S\right]
\end{aligned} \tag{1.17}$$

where we have defined

$$\rho_S = \sum_j K_j \left|\psi\right\rangle\!\left\langle\psi\right|_S K_j^\dagger, \tag{1.18}$$

which is often called the reduced state of S. The reduced state can also be found by taking the partial trace over the degrees of freedom of the environment,

$$\begin{aligned}\rho_S &= \mathrm{Tr}_E \left[\left|\psi_{SE}\right\rangle\!\left\langle\psi_{SE}\right|\right] \\ &= \sum_j \left(\mathbf{I}_S \otimes \left\langle j\right|_E\right) U_{SE} \left(\left|\psi\right\rangle\!\left\langle\psi\right|_S \otimes \left|0\right\rangle\!\left\langle 0\right|_E\right) U_{SE}^\dagger \left(\mathbf{I}_S \otimes \left|j\right\rangle_E\right) \\ &\equiv \mathcal{E}(\left|\psi\right\rangle\!\left\langle\psi\right|_S).\end{aligned} \tag{1.19}$$

The map $\mathcal{E}(\cdot)$ is known as a completely positive trace preserving (CPTP) map. This tells us that even when the system-environment state is initially in a pure product state, the state of the system after interaction can only be expressed using a density matrix.

We can see, by analysing Eq. (1.14) that performing a projective measurement on E in the basis $\{\left|j\right\rangle\}$ will leave S in the reduced state

$$\rho_S^j = \frac{M_j \left|\psi\right\rangle\!\left\langle\psi\right|_S M_j^\dagger}{p(j)}, \tag{1.20}$$

where

$$\begin{aligned}p(j) &= \mathrm{Tr}\left[M_j \left|\psi\right\rangle\!\left\langle\psi\right|_S M_j^\dagger\right] \\ &= \left\langle\psi\right|_S M_j M_j^\dagger \left|\psi\right\rangle_S \\ &= \left\langle\psi\right|_S E_j \left|\psi\right\rangle_S\end{aligned} \tag{1.21}$$

We can think of this as a more general kind of measurement on $\mathscr{H}_S$, known as a positive operator-valued measure (POVM). A POVM, most generally, can be defined as a set of positive, Hermitian operators that sum to unity. We can define the probability of measuring E_j on any state ρ

$$p(j) = \mathrm{Tr}\left[E_j \rho_S\right]. \tag{1.22}$$

Neumark's theorem [12] shows that any POVM on $\mathscr{H}_S$ can be realised as a projective measurement on separate Hilbert space $\mathscr{H}_B$ in exact analogy with Eq. (1.14).

1.1.2 Quantum master equations

The Hamiltonian that generates U_{SE} can be broken up into three parts,

$$H(t) = H_S \otimes \mathbf{I}_E + \mathbf{I}_S \otimes H_E + H_I(t), \tag{1.23}$$

H_S is the system Hamiltonian, H_E is the environment Hamiltonian and H_I describes the system-environment interaction. It can be incredibly difficult to model the evolution of the reduced system state, ρ_S, because, in principle, it requires keeping track of the entire system-environment state at all times. However, we can apply a number of approximations in order to significantly simplify this problem. The first assumption we make is that there is weak coupling between the system and the environment. This implies that the effect of the system on the environment is small. Therefore, the combined system environment state can be approximated as a product state

$$\rho_{SE} \approx \rho_S(t) \otimes \rho_E. \tag{1.24}$$

This is often referred to as the Born approximation. The next approximation we apply is the Markov approximation. The Markov approximation is valid when the environmental correlations decay before the reduced state of the system has changed significantly in the interaction picture. The final approximation required is the rotating wave approximation. The rotating wave approximation holds when the timescale of the system Hamiltonian, H_S, is much shorter than that of the interaction Hamiltonian, H_I. The exact mathematical details of these approximations can be found in Ref. [10]. The result of these approximations allow us to write the map describing the system evolution in the form

$$\mathcal{E}_{t_1} \circ \mathcal{E}_{t_2}(\cdot) = \mathcal{E}_{t_1+t_2}(\cdot). \tag{1.25}$$

This is known as the Markov semi-group property [10]. The semi-group property allows us to express the map $\mathcal{E}_t(\cdot)$ in exponential form

$$\mathcal{E}_t(\cdot) = \exp\left(\mathcal{L}t\right)(\cdot) \tag{1.26}$$

giving a differential equation for the evolution of the reduced state of S

$$\frac{d}{dt}\rho_S(t) = \mathcal{L}(\rho_S(t)). \tag{1.27}$$

This allows us to expand $\mathcal{L}$ in terms of $\mathcal{E}$ in the limit [10]

$$\mathcal{L}(\rho_S) = \lim_{\epsilon \to 0} \frac{1}{\epsilon} \left(\mathcal{E}_\epsilon(\rho_S) - \rho_S\right)) \tag{1.28}$$

Any operator on $\mathscr{H}_S$ can be expressed in a basis of orthonormal operators C_i on $\mathscr{H}_S$ that satisfy the relations,

$$\mathrm{Tr}\left[C_i^\dagger C_j\right] = \delta_{ij} \tag{1.29}$$

$$A = \sum_{i=1}^{N^2} C_i \,\mathrm{Tr}\left[C_i^\dagger A\right]. \tag{1.30}$$

We can expand the Kraus operators, and subsequently $\mathcal{E}$ in this basis, leading to the representation,

$$\mathcal{E}_t(\rho_S) = \sum_{i,j=1}^{N^2} c_{ij}(t) C_i \rho_S C_j^\dagger \tag{1.31}$$

with

$$c_{ij}(t) = \sum_k \mathrm{Tr}\left[C_i K_k^\dagger\right] \mathrm{Tr}\left[K_k C_j^\dagger\right]. \tag{1.32}$$

By choosing $C_{N^2} = \frac{1}{\sqrt{N}}\mathbf{I}_S$ we can sub Eq. (1.31) into Eq. (1.28) to get a closed form for $\mathcal{L}$ [10]

$$\mathcal{L}(\rho_S) = -i\left[H_S, \rho_S\right] + \sum_{i,j=1}^{N^2-1} a_{ij}\left(C_i \rho_S C_j^\dagger - \frac{1}{2}\left\{C_j^\dagger C_i, \rho_S\right\}\right) \tag{1.33}$$

where

$$a_{ij} = \lim_{\epsilon \to 0} \frac{c_{ij}(\epsilon)}{\epsilon}. \tag{1.34}$$

Then since the matrix (c_{ij}) is positive, (a_{ij}) is too, and can therefore be diagonalised to give the standard form of the Lindblad master equation,

$$\mathcal{L}(\rho_S) = -i\left[H_S, \rho_S\right] + \sum_{j=1}^{N^2-1} \gamma_j\left(L_j \rho_S L_j^\dagger - \frac{1}{2}\left\{L_j^\dagger L_j, \rho_S\right\}\right), \tag{1.35}$$

which will be a recurring tool, particularly in Chapters 2 and 3.

Chapter 2

Action Quantum Speed Limits

Time has always proved to be a tricky concept in physics. Its intrinsic directionality, commonly quantified through the notion of entropy production, allows us to uniquely define a "before" and an "after", and therefore time dictates the evolution of a system, i.e. its transformation between different configurations (or states). Despite its contentious nature, time still appears as a coordinate in all of our most fundamental theories, including quantum mechanics. The theory of quantum computation, for one, considers time a key resource to optimize, since it relates to the number of elementary computational operations that can be performed [13]. A basic question naturally arises: Is there a lower bound on the time it can take to transform between a given initial and final target states? This is the questions that we will explore in this Chapter. Sections 2.1 to 2.3.1 represent a summary and expansion on known results in the field, while the remainder of the Chapter contains original results adapted from Ref. [1], mainly derived by me with the guidance of collaborators.

2.1 Introduction

In thermodynamics a slow, continuous expansion of a gas will result in a different final state to a series of fast expansions with a waiting time in between, even if the total process time and total expansion are the same [14]. When dealing with continuous phase transitions, the Kibble-Zurek mechanism tells us that the density of topological defect formation depends on the instantaneous speed at which the control parameter is varied across the phase transition [15, 16]. In quantum control it is common for the size of the control pulse to tend to 0 at both end points, this is useful for practical reasons, but also helps to minimise the effects of noise and timing errors [17]. The common theme among all these processes is, they depend on the instantaneous speed of the process. Quantum speed limits (QSLs) place a fundamental limit on the minimal time that a system can evolve from one quantum state to another. They have been applied to all the above problems [18–20] but as we will see, most quantum speed limits depend only on the path taken between the initial and final states and are insensitive to the instantaneous speed along that path. We derive a new family of QSLs that are sensitive to this degree of freedom which we

call *action* QSLs [1]. This is explicitly shown in a paradigmatic example of a qubit thermalizing with an environment modelled using a generalized amplitude-damping channel (GADC). Due to their construction, finding the best way to traverse a path is naturally suited to be tackled with quantum optimal control theory [21].

The chapter is organized as follows. First, we will give a brief background and history of the inspiration for QSLs and detail their original derivations. Secondly, we will introduce the framework of quantum information geometry and show how it can be applied to the space of density matrices. We will then use this framework to explore the concept of QSLs in open quantum systems. Then, we will present the results of the publication [1] in which we introduce action QSLs as an alternative to the geometric approach and establish that they provide consistent bounds when the path is optimally traversed. We will show how it is possible to use optimal control techniques to find the optimal solution to these action QSLs. Finally, we will detail how these results relate to the broader field of QSLs and to other fields such as quantum thermodynamics.

2.1.1 Uncertainty Relations

Putting bounds or limitations on complex physical processes is a common thread of investigation in all areas of science. In quantum mechanics, these bounds appear not just at a practical level, but at a fundamental level. In his seminal paper [22] Heisenberg used the theory of the Compton effect to argue that there is an uncertainty principle for position and momentum observables

$$\Delta x \Delta p \gtrsim \hbar. \tag{2.1}$$

Heisenberg also proposed a heuristic argument based on classical canonical variables that there should be a similar principle for energy and time operators

$$\Delta E \Delta t \gtrsim \hbar. \tag{2.2}$$

Soon after, Robertson derived a more solid bound related to non-commuting observables [23]. Robertson used that fact that the variance of any Hermitian operator O can be written as a symmetric inner product, $\Delta O^2 = \langle O^2 \rangle - \langle O \rangle^2 = \langle \psi | \left(O - \langle O \rangle \right)\left(O - \langle O \rangle \right) | \psi \rangle$. Then by applying the Cauchy-Schwarz inequality,

$$\langle u, u \rangle \langle v, v \rangle \geq |\langle u, v \rangle|^2, \tag{2.3}$$

to two Hermitian operators A and B we get

$$\Delta A^2 \Delta B^2 \geq |\langle AB + A\langle B \rangle + B\langle A \rangle + \langle A \rangle \langle B \rangle \rangle|^2. \tag{2.4}$$

Then we do the same with $A \to -B$ and $B \to A$, take the square root and add each together to get

$$\begin{aligned} 2\Delta A \Delta B &\geq |\langle AB + A\langle B\rangle + B\langle A\rangle + \langle A\rangle\langle B\rangle\rangle| + |\langle -BA - B\langle A\rangle - A\langle B\rangle - \langle B\rangle\langle A\rangle\rangle| \\ &\geq |\langle AB - BA\rangle| = |\langle [A,B]\rangle|, \end{aligned} \tag{2.5}$$

where the second step is a consequence of the triangle inequality. This inequality is much more powerful than the original uncertainty principles as it allows us to obtain uncertainty relations between any two observables. The variances in Eq. (2.5) are best thought of as statistical properties of measurements performed on an ensemble of identically prepared states rather than a simultaneous measurement of both observables [24]. We can now derive an exact version of the position-momentum uncertainty principle from the fact that their canonical commutation relation is given by $[x, p] = i\hbar$,

$$\Delta x \Delta p \geq \frac{\hbar}{2}. \tag{2.6}$$

As powerful as Eq (2.5) is, not every quantity of interest can be associated with a specific operator. In particular, time has always been a controversial issue in quantum mechanics [25]. Many modern quantum mechanics textbooks tell us that time and space are treated differently in quantum mechanics, space is an operator and time is a parameter [26]. But this misunderstanding stems from the failure to distinguish between the position variable of a particle, and the space coordinate as it appears in relativity or classical mechanics [27–29]. Indeed, this caused some problems with defining the position operator in relativistic quantum mechanics [30]. So, we might want to define in analogy to the position operator, a time operator. We want an operator $\boldsymbol{t}$ and a corresponding canonical momentum $\boldsymbol{\eta}$ that satisfy,

$$[\boldsymbol{\eta}, H] = 0, \quad [\boldsymbol{t}, H] = i\hbar, \tag{2.7}$$

because this would give us the relation

$$\frac{\partial \langle \boldsymbol{t}\rangle}{\partial t} = \frac{i}{\hbar}\langle [H, \boldsymbol{t}]\rangle = 1. \tag{2.8}$$

If we want the spectrum of the time operator to be continuous and span the entire real axis, then the spectrum of the Hamiltonian must also span the entire real axis, but this is not the case for many physically relevant systems [29]. This just means that in such systems there is no time operator or there is only a cyclic or discrete approximation of the time operator. This fact has sparked a recent resurgence in the field of quantum clocks [31]. In fact, it is likely impossible to create a perfect clock at finite power [32].

2.1.2 Mandelstam-Tamm Bound

The first major progress in understanding how to correctly interpret the energy time uncertainty principle came from the work of Mandelstam and Tamm [33] (MT). They note that one common interpretation of the energy time uncertainty relation derives from the relationship between energy and frequency for monochromatic light. This energy cannot be identified with the observable associated with energy in non-relativistic quantum mechanics [33], the Hamiltonian. In order to derive an uncertainty relation based on the Hamiltonian they simply considered the Robertson uncertainty bound (2.5) with $A = H$, the Hamiltonian, and $B = |\psi_0\rangle\langle\psi_0|$, the projector onto the initial state. The expectation values are calculated as $\langle O\rangle = \langle\psi_t| O |\psi_t\rangle$. By applying the von-Neumann equation,

$$[H, O] = -i\hbar\frac{dO}{dt} \tag{2.9}$$

on the right-hand side, we get,

$$\Delta H\sqrt{\langle B\rangle - \langle B\rangle^2} = \frac{\hbar}{2}\left|\frac{d\langle B\rangle}{dt}\right|, \tag{2.10}$$

using the fact that $B^2 = B$. We can then rearrange and integrate both sides to obtain,

$$\int_0^\tau dt\Delta H \geq \hbar\arccos|\langle\psi_\tau|\psi_0\rangle| \tag{2.11}$$

Then by assuming a time-independent Hamiltonian we find that the minimum evolution time required for a quantum system to unitarily evolve from an initial pure state $|\psi_i\rangle$ to an orthogonal final state $|\psi_f\rangle$ is given by,

$$\tau \geq \tau_{QSL}^{MT} = \frac{\pi}{2}\frac{\hbar}{\Delta H} \tag{2.12}$$

This formulation is essentially a reordering of the energy-time uncertainty relation where Δt is replaced by the time interval τ. Mandelstam and Tamm relate this bound to the broadening of spectral lines by defining a minimum "half-life" time of a given state [33]. This re-interpretation of the energy-time uncertainty relation has been termed the quantum speed limit (QSL) time. This equation puts a fundamental limit on a number of quantum processes such as the rate of information transfer [34], the rate of entropy production [35], the rate of information processing [36] and the fastest optimal control protocols [37].

It is easy to see from equation (2.11) that the results can be generalised to non-orthogonal states [38, 39] and time-dependent Hamiltonians [40]. In this scenario the minimum evolution time is bounded by

$$\tau \geq \tau_{\mathsf{QSL}} = \frac{\hbar L_A(|\psi_0\rangle, |\psi_\tau\rangle)}{\Delta E_\tau}. \tag{2.13}$$

where $L_A(|\psi_0\rangle, |\psi_\tau\rangle) = \arccos|\langle\psi_0|\psi_\tau\rangle|$ is the Bures angle for pure states and $\Delta E_\tau = \int_0^\tau dt\Delta H$ is the time averaged variance of the Hamiltonian. Anandan and Aharonov [40] showed, importantly, that Eq. (2.13) can be understood from a purely geometric perspective as a consequence of the

properties of the Fubini-Study metric on the Riemannian manifold of quantum states. In particular, they showed that in this metric, the geodesic length is given by the Bures angle and the path length of any unitary dynamics is given by $\Delta E_\tau/\hbar$. Therefore Eq. (2.13) simply follows from the fact that the geodesic length is always smaller than the actual path length.

2.1.3 Margolus-Levitin Bound

In quantum computation one measure of speed is the number of distinct, i.e. orthogonal, states that a system passes through in a given time. Margolus and Levitin [41] (ML) were able to put a bound on this speed which is remarkably similar to the MT bound. They started by expanding the initial state, $|\psi_0\rangle = \sum_n c_n |E_n\rangle$, in the energy basis of the Hamiltonian $H = \sum_n E_n |E_n\rangle\langle E_n|$, we also re-normalise so that $E_0 = 0$. Then, by applying the Schrödinger equation to this initial state we can write the time-evolved state as

$$|\psi_t\rangle = \sum_n c_n \exp\left(\frac{-iE_n t}{\hbar}\right)|E_n\rangle\,. \tag{2.14}$$

By considering the real part of the overlap between the initial state and the time-evolved state, $S_t \equiv \langle\psi_0|\psi_t\rangle = \sum_n |c_n|^2 \exp(-iE_n t/\hbar)$, and applying the inequality, $\cos(x) \geq 1 - 2/\pi(x + \sin(x))$, which holds for $x \geq 0$,

$$\begin{aligned} \mathrm{Re}(S_t) &= \sum_n |c_n|^2 \cos(E_n t/\hbar) \\ &\geq \sum_n |c_n|^2 \left[1 - \frac{2}{\pi}\left(\frac{E_n t}{\hbar} + \sin\left(\frac{E_n t}{\hbar}\right)\right)\right] \\ &= 1 - \frac{2}{\pi}\frac{\langle H\rangle}{\hbar}t + \frac{2}{\pi}\,\mathrm{Im}(S_t). \end{aligned} \tag{2.15}$$

When the initial and final state are orthogonal we have $S_\tau = 0$, which implies that both $\mathrm{Re}(S_\tau) = 0$ and $\mathrm{Im}(S_\tau) = 0$. From this we can rearrange to get the ML bound

$$\tau \geq \tau_{QSL}^{ML} = \frac{\pi}{2}\frac{\hbar}{\langle H - E_0\rangle}. \tag{2.16}$$

The crucial difference here is that the bound depends on the mean energy $\langle H\rangle$ of the initial state instead of the variance ΔH. Extending the ML bound, even to just non-orthogonal pure states, has proven to be a real challenge. Giovannetti *et al.* [42, 43] proposed an extension to the ML bound in the form

$$\tau \geq \alpha(\epsilon)\frac{\hbar}{\langle H - E_0\rangle}, \tag{2.17}$$

with $\epsilon = |S_\tau|^2$. They were able to derive implicit upper and lower bounds on $\alpha(\epsilon)$ and showed numerically that these bounds were approximately equal. Hörnedal, Niklas and Sönnerborn [44] showed analytically that the $\alpha(\epsilon)$ derived by this upper and lower bound is exact and is always

saturable. The function can be defined as

$$\alpha(\epsilon) = \min_{z^2 \leq \epsilon} \frac{1+z}{2} \arccos\left(\frac{2\epsilon - 1 - z^2}{1 - z^2}\right). \tag{2.18}$$

The minimum value of z can be defined implicitly by

$$\arccos\left(\frac{2\epsilon - 1 - z^2}{1 - z^2}\right) = \frac{2z}{1-z}\sqrt{\frac{1-\epsilon}{\epsilon - z^2}}. \tag{2.19}$$

Recently a dual version of the ML bound was also derived [45], it takes the form,

$$\tau \geq \alpha(\epsilon) \frac{\hbar}{\langle E_{\max} - H \rangle}. \tag{2.20}$$

Understanding and developing on the MT and ML bounds has been the focus of sustained work. A number of papers have focused on expanding the geometric interpretation of these results [46–50] and extending them to mixed states [51, 52]. The MT and ML bounds have also been used to investigate the speed of quantum control [53–55], the effect of correlations on evolution time [56–58], and many other quantum phenomena [59–63].

2.1.4 Saturating QSL Bounds

Having fundamental bounds on the evolution time of your system is important, but it is equally important to understand if and when those bounds can be achieved. For the MT bound let us start by writing the Hamiltonian in the energy basis $H = \sum_k E_k |E_k\rangle\langle E_k|$, we can write any pure state in this basis so we have, $|\psi_0\rangle = \sum_k c_k |E_m\rangle$ and $|\psi_t\rangle = \sum_k c_k e^{-iE_k t/\hbar} |E_k\rangle$, we can now calculate the overlap

$$\begin{aligned} |S_t|^2 &= |\langle \psi_0 | \psi_t \rangle|^2 \\ &= \sum_{k,l} |c_k|^2 |c_l|^2 e^{-i(E_k - E_l)t/\hbar} \\ &= \sum_{k,l} |c_k|^2 |c_l|^2 \cos(E_k - E_l)t/\hbar. \end{aligned} \tag{2.21}$$

The final line follows from the fact that $|S_t|^2$ is real. Levitin and Toffoli [64] showed that the MT bound can be derived in an analogous way to the ML bound by applying a trigonometric inequality,

$$\cos x \geq 1 - \frac{2}{\pi^2}(2x \sin x - x^2), \tag{2.22}$$

with equality for $x \in \{-\pi, 0, \pi\}$. So, applying this to Eq. (2.21) we get

$$|S_t|^2 \geq 1 - \frac{4}{\pi^2}\Bigg(\sum_{k,l} |c_k|^2 |c_l|^2 (E_k - E_l)(t/\hbar) \sin(E_k - E_l)t/\hbar \tag{2.23}$$
$$+ \frac{1}{2} \sum_{k,l} |c_k|^2 |c_l|^2 (E_k - E_l)^2 (t/\hbar)^2 \Bigg).$$

If we look at the first term in the brackets we see that it is simply $t\frac{d\left(|S_t|^2\right)}{dt}$ and since we know that $|S_t|^2$ is non-negative then its derivative must be zero whenever $|S_t|^2 = 0$. Next we calculate the variance of the Hamiltonian,

$$\Delta H^2 = \langle H^2 \rangle - \langle H \rangle^2 = \sum_k |c_k|^2 E_k^2 - \left(\sum_k |c_k|^2 E_k \right)^2 \tag{2.24}$$
$$= \frac{1}{2} \sum_k |c_k|^2 E_k^2 + \frac{1}{2} \sum_l |c_l|^2 E_l^2 - \sum_{k,l} |c_k|^2 |c_l|^2 E_k E_l \tag{2.25}$$
$$= \frac{1}{2} \sum_k |c_k|^2 E_k \left(E_k - \sum_l |c_l|^2 E_l \right) + \frac{1}{2} \sum_l |c_l|^2 E_l \left(E_l - \sum_k |c_k|^2 E_k \right) \tag{2.26}$$
$$= \frac{1}{2} \sum_{k,l} |c_k|^2 |c_l|^2 (E_k - E_l)^2. \tag{2.27}$$

So now we can sub this into Eq. (2.23) and by choosing a time τ such that $|S_\tau|^2 = 0$ we get

$$0 \geq 1 - \left(\frac{2\tau \Delta H}{\pi \hbar} \right)^2. \tag{2.28}$$

We can see that by rearranging this we can exactly recover the MT bound in Eq. (2.12). Now, in order to saturate this inequality, for every term in Eq. (2.21) we have to either saturate Eq. (2.22) or have one of $|c_k|^2$ or $|c_l|^2$ equal to zero. Therefore, if $|c_k|^2 \neq 0$ and $|c_l|^2 \neq 0$ we need $(E_k - E_l)t/\hbar \in \{-\pi, 0, \pi\}$. So, this means that our initial state must be a superposition of only two energy levels. In principle, we could have additional energy levels that are degenerate, but we know that any linear combination of degenerate eigenstates is also an eigenstate with the same eigenvalue. In order to saturate the MT bound we also need $|S(t)|^2 = 0$, so subbing this superposition into Eq. (2.21) we get

$$0 = |c_-|^4 - |c_-|^2 |c_+|^2 + |c_+|^4 \tag{2.29}$$
$$|c_-|^2 = |c_+|^2 \tag{2.30}$$
$$c_- = e^{-i\phi} c_+. \tag{2.31}$$

Then using the fact that $|c_-|^2 + |c_+|^2 = 1$ we can write the initial state as

$$|\psi(0)\rangle = \frac{1}{\sqrt{2}}\left(|E_-\rangle + e^{-i\phi}|E_+\rangle\right). \tag{2.32}$$

Therefore, in order to saturate the MT bound our initial state must be in an equal superposition of two energy eigenstates. Alternatively, we could think of some initial state $|\psi\rangle$ and an orthogonal final state $\left|\psi^\perp\right\rangle$, then the Hamiltonian that saturates the MT bound must have the eigenstates of the form,

$$|E_-\rangle = \frac{1}{\sqrt{2}}\left(|\psi\rangle + e^{-i\phi}\left|\psi^\perp\right\rangle\right); \quad |E_+\rangle = \frac{1}{\sqrt{2}}\left(|\psi\rangle - e^{-i\phi}\left|\psi^\perp\right\rangle\right). \tag{2.33}$$

As mentioned earlier, Anandan and Aharonov [40] proved that the evolution path that saturates the MT bound can be thought of as a geodesic path on a Riemannian manifold. This means that the path between two orthogonal states is also a geodesic path for all the intermediate states. This, combined with that fact that if we have two arbitrary pure quantum states, $|\psi\rangle$ and $|\varphi\rangle$, we can always decompose $|\varphi\rangle$ as,

$$|\varphi\rangle = \cos\theta|\psi\rangle + \sin\theta e^{i\phi}\left|\psi^\perp\right\rangle, \tag{2.34}$$

tells us that in order to saturate the MT bound (2.13) between any two pure states $|\psi\rangle$ and $|\varphi\rangle$ the Hamiltonian must have eigenvectors of the form in Eq. (2.33). This was also proved by Brody *et. al.* [48] using a slightly different method.

The inequality $\cos(x) \geq 1 - 2/\pi(x + \sin(x))$ used to define the ML bound also happens to obtain equality for $x = 0$ or $x = \pi$. Levitin and Toffoli [64] used this fact to show that, in exactly the same way as for the MT bound, the ML bound is also saturated when the initial state is of the form in Eq. (2.32). Therefore, although the MT and ML bounds are not always equal, they are both saturated using the Hamiltonian defined in Eq. (2.33). Interestingly, this only applies for orthogonal states since the generalised ML bound, Eq. (2.17), is not a geodesic bound, therefore, intermediate states do not necessarily share the same optimal path. Similarly, the dual ML bound in Eq. (2.20) is also not saturable at the same time as either the MT or ML bound for non-orthogonal states.

2.1.5 Open System QSLs

Extending the notion of QSLs to open quantum systems has not been straightforward. A number of different methods have been tried. Perhaps the most common approach has been to take inspiration from the derivation of the ML bound by taking a distance measure between quantum states and applying an inequality, such as the triangle or Cauchy-Schwarz, to its time derivative [65–76]. This approach generally provides simpler bounds but often at the cost of not being saturable for most initial and final states.

Another approach has been to take inspiration from the work of Anandan and Aharonov [40] on

the MT bound and derive a geometric speed limit on the space of open quantum systems [77–85]. One problem that this approach runs into is that there are infinitely many possible Riemannian metrics that can be defined on the space of open quantum systems [78, 86, 87]. Additionally, these speed limits are not simultaneously saturable in general. This has led to a lot of confusion in the field over how to choose what speed limit to use.

There has also been a lot of interest in deriving speed limit like bounds for specific kinds of systems such as ultracold gases [88], continuous variable systems [89], thermal states [90] and macroscopic systems [91]. Other papers have made use of these QSLs to shed light on concepts such as non-Markovianity [92,93], irreversibility [94], optimal transport [95], quantum batteries [96] and quantum control [55, 97, 98]. More detail on all this and more can be found in the following reviews on the subject [99, 100].

2.2 Quantum information geometry

We now outline some of the technical details that underpin the derivation of geometric approaches to defining QSLs. Information geometry provides us with the tools to establish metrics from which families of QSLs follow.

In classical information theory, a real-valued random variable $X : \Omega \to \mathbb{R}$ is a function that maps from a space of possible outcomes, $\omega \in \Omega$, to the real line. Each of these possible outcomes occurs with probability $p(\omega)$. We can calculate the correlation between two real-valued random variables X and Y as,

$$\mathsf{Cov}_p(X, Y) = \sum_{\omega \in \Omega} (X(\omega) - \mathsf{E}_p(X))(Y(\omega) - \mathsf{E}_p(Y))p(\omega), \tag{2.35}$$

where $\mathsf{E}_p(X) = \sum_{\omega \in \Omega} X(\omega)p(\omega)$ is the expectation value of the random variable X. This is usually referred to as the covariance of X and Y. We get the standard definition of covariance by setting $p(\omega) = 1/|\Omega|$, where $|\Omega|$ is the number of elements in Ω. The covariance of X with itself $\mathsf{Cov}_p(X, X) = \sigma_p^2(X)$ is equal to the variance of X.

We can also define the inner product in the space of real-valued random variables as ,

$$\langle A, B \rangle_p = \sum_{\omega \in \Omega} A(\omega)B(\omega)p(\omega). \tag{2.36}$$

It is easy to see then that,

$$\mathsf{Cov}_p(X, Y) = \langle (X(\omega) - \mathsf{E}_p(X)), (Y(\omega) - \mathsf{E}_p(Y)) \rangle_p. \tag{2.37}$$

So, when A and B have zero expectation value, (2.36) can be thought of as a measure of the correlation between the two variables [101]. If we consider the set of probability distributions p_θ

parametrized by a single real number θ then we can define the logarithmic derivative,

$$\frac{d\log p_\theta(\omega)}{d\theta}|_{\theta=\theta_0} = \frac{1}{p_{\theta_0}(\omega)}\frac{dp_\theta(\omega)}{d\theta}|_{\theta=\theta_0}. \tag{2.38}$$

The Fisher information is defined as the variance of the logarithmic derivative, but the expectation of the logarithmic derivative is zero so we can also write it as,

$$F_\theta = \left\langle \frac{d\log p_\theta(\omega)}{d\theta}, \frac{d\log p_\theta(\omega)}{d\theta} \right\rangle_{p_\theta}. \tag{2.39}$$

The Fisher information is an important quantity in classical information theory and perhaps most famously appears in the Cramér-Rao bound [102, 103].

If we allow A, B and p to be the diagonal elements of the commuting Hermitian matrices X, Y and ρ respectively. Then the inner product in Eq. (2.36) is equal to $\mathrm{Tr}[X\rho Y]$. In order to deal with the geometry of quantum states, we want to generalise $X, Y \in M_n(\mathbb{C})$ to the set of complex $n \times n$ matrices, and ρ to a positive, semi-definite Hermitian operator of trace 1. In this scenario the order of the matrices in the trace is important. We define the inner product,

$$\langle X, Y\rangle_\rho = Tr[(\mathbf{K}_\rho(X))^\dagger Y], \tag{2.40}$$

where $\mathbf{K}_\rho(Y)$ is a positive (super)operator. This is the most general form of inner product on this space [87] that satisfies

$$\langle aX, bY\rangle_\rho = \bar{a}b\langle X, Y\rangle_\rho \tag{2.41}$$

$$\langle X, X\rangle_\rho \geq 0. \tag{2.42}$$

Let $\mathbf{T}$ be a completely positive, trace preserving (CPTP) map. An inner product is monotone if

$$\langle X, Y\rangle_\rho \geq \langle \mathbf{T}(X), \mathbf{T}(Y)\rangle_{\mathbf{T}(\rho)} \tag{2.43}$$

for all $\mathbf{T}$. Petz [87] showed that this is equivalent to the condition,

$$\mathbf{K}_\rho^{-1} \geq \mathbf{T}^\dagger \mathbf{K}_{\mathbf{T}(\rho)}^{-1}\mathbf{T}. \tag{2.44}$$

Petz was also able to show that if we impose a symmetry condition, $\langle X, Y\rangle_\rho = \langle Y^\dagger, X^\dagger\rangle_\rho$, then there is a one to one correspondence between operator monotone functions f that satisfy $f(t) = tf(t^{-1})$ and monotone inner products [87] i.e. Eq. (2.43) given by,

$$\mathbf{K}_\rho = \mathbf{R}_\rho^{1/2} f(\mathbf{L}_\rho \mathbf{R}_\rho^{-1})\mathbf{R}_\rho^{1/2}, \tag{2.45}$$

where $\mathbf{R}_\rho(X) = X\rho$ and $\mathbf{L}_\rho(X) = \rho X$. For any two Hermitian matrices A and B for which $A - B \geq 0$, i.e. is positive semi-definite, an operator monotone function f satisfies $f(A) - f(B) \geq$

0.

Given the relationship in Eq. (2.44) it makes sense to analyse the dual inner product [101] given by

$$\langle A, B\rangle_\rho^{(D)} = Tr[A^\dagger(\mathbf{K}_\rho^{-1}(B))]. \tag{2.46}$$

If we associate $A = \mathbf{K}_\rho(X)$ and $B = \mathbf{K}_\rho(Y)$ we can see that

$$\langle A, B\rangle_\rho^{(D)} = \langle X, Y\rangle_\rho \tag{2.47}$$

The set of all Hermitian, positive-definite, $n\times n$ matrices of trace 1, $\mathscr{M}_n$, is a smooth manifold, so we can make it a Riemannian manifold by equipping its tangent space with a positive-definite inner product $\mathbf{g}$. For any set of smooth local coordinates on $\mathscr{M}_n$, given by m real-valued functions $(\theta^1, .., \theta^m)$, we can calculate the metric tensor components,

$$g_{i,j} := \mathbf{g}\left(\frac{\partial}{\partial\theta^i}, \frac{\partial}{\partial\theta^j}\right). \tag{2.48}$$

This defines a Riemannian metric on $\mathscr{M}_n$. If we define this inner product to be the dual inner product $\langle A, B\rangle_\rho^{(D)}$ defined in Eq. (2.46), this metric has a number of interesting properties. Consider the set of quantum states ρ_θ parameterized by a single real number θ. The distance between ρ_θ and $\rho_{\theta+\epsilon}$ is $\sqrt{\left\langle \frac{d\rho}{d\theta}, \frac{d\rho}{d\theta}\right\rangle_\rho^{(D)}}$. When $\frac{d\rho}{d\theta}$ and ρ_θ commute we get

$$\mathbf{K}_{\rho,c}^{-1}\left(\frac{d\rho}{d\theta}\right) = \frac{1}{\rho_\theta}\frac{d\rho}{d\theta}, \tag{2.49}$$

for any f, giving the classical Fisher information, $\left\langle \frac{d\rho}{d\theta}, \frac{d\rho}{d\theta}\right\rangle_{\rho,c}^{(D)} = F_\theta$. Let us look at some specific examples of operator monotone functions now. $f_s(t) = (1+t)/2$ gives us $\mathbf{K}_{\rho,s} = (\mathbf{R}_\rho + \mathbf{L}_\rho)/2$. In order to calculate the inner product we define $\mathbf{K}_{\rho,s}^{-1}(\frac{d\rho}{d\theta}) = L_\rho$ which gives $\frac{d\rho}{d\theta} = \frac{1}{2}(L_\rho\rho + \rho L_\rho)$. This operator, L_ρ, is known as the symmetric logarithmic derivative (SLD) and is an important quantity in quantum metrology as we will see in Chapter 3. When we sub this into the inner product we get

$$\left\langle \frac{d\rho}{d\theta}, \frac{d\rho}{d\theta}\right\rangle_{\rho,s}^{(D)} = \mathrm{Tr}\left[\frac{d\rho}{d\theta}\mathbf{K}_{\rho,s}^{-1}\left(\frac{d\rho}{d\theta}\right)\right] = \mathrm{Tr}\left[\frac{1}{2}(L_\rho\rho + \rho L_\rho)L\right] = \mathrm{Tr}\Big[\rho L_\rho^2\Big] \tag{2.50}$$

which is the quantum Fisher information $\mathcal{F}_\theta(\rho)$. So, for this reason the metric defined by $\mathbf{K}_{\rho,s} = 1/2(\mathbf{R}_\rho + \mathbf{L}_\rho)$ is usually called the SLD metric, the quantum Fisher information metric, or the Bures metric. We can define some other important metrics using the same method, for example $f_b(t) = \int_0^1 t^\lambda d\lambda$ giving $\mathbf{K}_{\rho,b} = \int_0^1 \mathbf{R}_\rho^{1-\lambda}\mathbf{L}_\rho^\lambda d\lambda$ which is usually referred to as the Bogoliubov metric or the Kubo-Mori metric.

Finally, if we consider the case of the Bures metric with pure states and unitary evolution we

have $i\hbar\frac{d|\psi\rangle}{d\theta} = H|\psi\rangle$ and $L_\rho = \frac{2}{i\hbar}H$ giving

$$\left\langle \frac{d\rho}{d\theta}, \frac{d\rho}{d\theta} \right\rangle_{\rho,p}^{(D)} = \frac{2}{i\hbar}\operatorname{Tr}\left[\frac{d(|\psi\rangle\langle\psi|)}{d\theta}H\right] = \frac{2}{i\hbar}\operatorname{Tr}\left[(|d\psi\rangle\langle\psi| + |\psi\rangle\langle d\psi|)H\right] = \\ = 2\langle d\psi|d\psi\rangle + 2\langle\psi|d\psi\rangle\langle d\psi|\psi\rangle, \quad (2.51)$$

where $|d\psi\rangle = \frac{d\psi}{d\theta}$. This metric is known as the Fubini-study metric and can also be derived as an extension of the classical Fisher information metric to complex projective Hilbert spaces [104]. As discussed above this is the metric that Anandan and Aharonov [40] used to derive the MT bound for time-dependent Hamiltonians and non-orthogonal pure states (2.13).

2.3 Open System Quantum Speed Limits

The first attempt at generalising QSLs to open systems can be traced back to the work of Braunstein and Caves [47]. They used the fact that the infinitesimal form of the Bures distance [105],

$$L_B(\rho_1,\rho_2)^2 = 2\left[1 - \sqrt{F_B(\rho_1,\rho_2)}\right], \quad (2.52)$$

with $F_B(\rho_1,\rho_2) = \left[\operatorname{Tr}\sqrt{\sqrt{\rho_1}\rho_2\sqrt{\rho_1}}\right]^2$, can be expressed [106] in terms of the SLD inner product in Eq. (2.50)

$$L_B(\rho,\rho+d\rho)^2 = \frac{1}{4}\langle d\rho, d\rho\rangle_{\rho,s}^{(D)} = \frac{1}{4}\operatorname{Tr}\left[d\rho\mathbf{K}_{\rho,s}^{-1}(d\rho)\right]. \quad (2.53)$$

While there is no explicit, basis-independent, way to express $\mathbf{K}_{\rho,s}^{-1}(A)$, we can express it in a specific basis. For example, when written in the diagonal basis of the density matrix $\rho = \sum_j p_j|j\rangle\langle j|$ we get [47]

$$\mathbf{K}_{\rho,s}^{-1}(A) = 2\sum_{j,k}\frac{\langle j|A|k\rangle}{p_j+p_k}|j\rangle\langle k|. \quad (2.54)$$

If we now assume unitary dynamics described by the von-Neumann equation [100]

$$i\hbar\frac{d\rho}{dt} = [H,\rho] = [H - \langle H\rangle,\rho] = [\delta H,\rho]. \quad (2.55)$$

We can combine the above equations to obtain,

$$\left(\frac{dL_B}{dt}\right)^2 = \frac{1}{2\hbar^2}\sum_{j,k}\frac{(p_j-p_k)^2}{p_j+p_k}|\langle j|\delta H|k\rangle|^2 \leq \frac{1}{2\hbar^2}\sum_{j,k}(p_j+p_k)|\langle j|\delta H|k\rangle|^2 = \frac{\Delta H^2}{\hbar^2}, \quad (2.56)$$

where the inequality $(p_j-p_k)^2 \leq (p_j+p_k)^2$ follows from the fact that p_i is positive for all i. Then by taking the square root of both sides and integrating we get the following inequality,

$$\int_0^{L_B(\rho_0,\rho_\tau)} dL_B \leq \frac{1}{\hbar}\int_0^\tau dt\Delta H. \quad (2.57)$$

It is easy to see that this bound can never be saturated by a mixed state since the inequality in Eq. (2.56) is only saturated when $p_i p_j = 0$ for all $i \neq j$ and this is only true for pure states [47]. We can see that the final time τ does not appear explicitly in the above inequality so in order to get a bound on the time we must use the trick of multiplying both sides by τ and rearranging we obtain a QSL like inequality,

$$\tau \geq \frac{\hbar}{\Delta E_\tau} L_B(\rho_0, \rho_\tau), \tag{2.58}$$

where ΔE_τ is the time averaged variance of the Hamiltonian $\Delta E_\tau = \frac{1}{\tau}\int_0^\tau dt \Delta H$. So now we have derived a QSL for mixed states and time-dependent Hamiltonians. This trick of forcing in time by multiplying both sides is a very common technique used when deriving QSLs. This has led to some confusion regarding how to meaningfully interpret these bounds. By introducing action QSLs, such that time enters the picture more naturally, we demonstrate that some of these interpretive issues can be alleviated. Furthermore, through the following analysis we argue that there is no reason to expect that these QSL bounds place any meaningful limit on the actual minimum time, except in the limit of constant instantaneous speed (such as in the MT bound), but rather they provide a useful tool to characterise the dynamics.

There were three main papers that provided breakthroughs in extending QSLs to arbitrary system evolutions, described by CPTP maps. Taddei *et al.* [77] directly extended the work of Braunstein and Caves [47]. They showed that for any distance measure $L[F_B(\rho_1, \rho_2)]$ that depends on ρ_1 and ρ_2 solely via the Bures fidelity F_B the following inequality holds,

$$\sqrt{\frac{d^2 L(F_B)/dF_B^2}{2[dL(F_B)/dF_B]^3}}\Bigg|_{F_B \to 1} L[F_B(\rho_0, \rho_\tau)] \leq \int_0^\tau dt \sqrt{\frac{1}{4}\operatorname{Tr}\left[\frac{d\rho}{dt}\mathbf{K}_{\rho,s}^{-1}\left(\frac{d\rho}{dt}\right)\right]} = \int_0^\tau dt \sqrt{\frac{\mathcal{F}_t(\rho_t)}{4}}, \tag{2.59}$$

where $\mathcal{F}_t(\rho_t)$ is the quantum Fisher information with respect to t. In contrast to the Braunstein and Caves [47] result this bound can be saturated for mixed quantum states.

Another approach was followed by del Campo *et al.* [65]. They used the relative purity as their distance measure,

$$\mathcal{P}(\rho_0, \rho_\tau) = \frac{\operatorname{Tr}[\rho_0 \rho_\tau]}{\operatorname{Tr}[\rho_0^2]}. \tag{2.60}$$

Applying the Cauchy-Schwarz inequality to the time derivative of this measure gives the following bound,

$$|\dot{\mathcal{P}}(\rho_0, \rho_t)| \leq \frac{\sqrt{\operatorname{Tr}[(\mathcal{L}^\dagger \rho_0)^2)]\operatorname{Tr}[\rho_t^2]}}{\operatorname{Tr}[\rho_0^2]} \leq \frac{\sqrt{\operatorname{Tr}[(\mathcal{L}^\dagger \rho_0)^2)]}}{\operatorname{Tr}[\rho_0^2]}, \tag{2.61}$$

where $\mathcal{L}^\dagger$ is the Hermitian adjoint of the Lindbladian [107, 108]. Then, if we parameterize $\mathcal{P}(\rho_0, \rho_\tau) = \cos\theta$, with $\theta \in [0, \pi/2]$, integrating from initial to final state gives us a QSL,

$$\tau \geq \frac{|\cos\theta - 1| \operatorname{Tr}[\rho_0^2]}{\sqrt{\operatorname{Tr}[(\mathcal{L}^\dagger \rho_0)^2)]}} \geq \frac{4\theta^2 \operatorname{Tr}[\rho_0^2]}{\pi^2 \sqrt{\operatorname{Tr}[(\mathcal{L}^\dagger \rho_0)^2)]}}. \tag{2.62}$$

the clear advantage of this bound is that it depends only on the Lindbladian and the initial state, although, this comes at the disadvantage of only being saturable for very specific combinations of initial states and Lindbladians. They also derive equivalent bounds for time-dependent Lindbladians, and generic, CPTP evolutions, but at the cost of losing the time-independence of the right-hand side of the equation.

Not long after the above two papers were published Deffner and Lutz [66] developed another form of open system QSL. They specifically looked at the Bures angle for a pure initial state $|\psi_0\rangle$

$$L_A = \arccos\left(\sqrt{\langle\psi_0|\,\rho_\tau\,|\psi_0\rangle}\right). \tag{2.63}$$

They were able to obtain a number of QSL bounds of the form

$$\tau \geq \frac{1}{\Lambda_\tau^x}\sin^2[L_A(\rho_0,\rho_\tau)], \tag{2.64}$$

where $\Lambda_\tau^x = \frac{1}{\tau}\int_0^\tau \|\dot{\rho}_t\|_x$ and $\|A\|_x$ corresponds to the trace, Hilbert-Schmidt and operator norms which are specific cases of the Schatten p-norm, $\|A\|_p = (\mathrm{Tr}\left[\sqrt{A^\dagger A}\right]^p)^{\frac{1}{p}}$, for $p = 1, 2$ and ∞ respectively. The structure of the Schatten p-norm means that the operator norm bound is always the tightest. These bounds are some of the simpler open system QSLs but once again come at the cost of not being saturable in general [92].

2.3.1 Generalized Geometric Quantum Speed Limits

All of the above speed limits have their strengths and weaknesses, and much like in the case of the MT and ML bounds there is no single tightest QSL for all evolutions. Pires *et al.* [78] shed some light on this problem by proving that there are, in fact, infinitely many saturable QSLs for open quantum system dynamics. In order to prove this, they made use of the Riemannian metrics described in Section 2.2,

$$\mathbf{g}_\rho^f\left(\frac{d\rho}{dt},\frac{d\rho}{dt}\right) = \frac{1}{4}\left\langle\frac{d\rho}{dt},\frac{d\rho}{dt}\right\rangle_{\rho,f}^{(D)} = \frac{1}{4}\,\mathrm{Tr}\left[\frac{d\rho}{dt}\mathbf{K}_{\rho,f}^{-1}\left(\frac{d\rho}{dt}\right)\right], \tag{2.65}$$

where f denotes the symmetric, operator monotone that defines the specific metric. The arbitrary factor of $1/4$ is chosen so that the geodesic distance corresponds to well-known distance measures in specific metrics. Our manifold is the set of all Hermitian, positive-definite, $n \times n$ matrices of trace 1, $\mathscr{M}_n$. For any set of smooth local coordinates on $\mathscr{M}_n$, given by m real-valued functions $(\theta^1, .., \theta^m)$ we can write the above inner product as

$$\mathbf{g}_\rho^f\left(\frac{d\rho}{dt},\frac{d\rho}{dt}\right) = \sum_{j,k}^{m} g_{j,k}^f \frac{d\theta^j}{dt}\frac{d\theta^k}{dt}, \tag{2.66}$$

with $g^f_{j,k} = \mathbf{g}^f_\rho\left(\frac{\partial\rho}{\partial\theta^j}, \frac{d\rho}{d\theta^k}\right)$. Morozova and Chentzov [86]were also able to derive an explicit form of the inner product in terms of the spectral decomposition of $\rho = \sum_j p_j \left|j\right\rangle\!\left\langle j\right|$

$$\mathbf{g}^f_\rho\left(\frac{d\rho}{dt}, \frac{d\rho}{dt}\right) = \frac{1}{4}\left[\sum_j \frac{(d\rho_{jj})^2}{p_j} + 2\sum_{j<k} c_f(p_j, p_k)|d\rho_{jl}|^2\right], \tag{2.67}$$

where $d\rho_{jl} = \langle j|\, \frac{d\rho}{dt}\, |l\rangle$ and $c_f(x,y) = \frac{1}{yf(x/y)}$ depends on Morozova-Chentzov function, f, for the metric $\mathbf{g}^f_\rho$. It is easy to see from this formulation that there is a classical component, given by the Fisher information that is metric independent and a coherent quantum component that depends on f. We can think of the first of these two contributions as classical because, if we consider a classical process where the eigenvectors of our state stay fixed, and only p_j change with t, we have $\frac{d\rho}{dt} = \sum_j \frac{dp_j}{dt}\left|j\right\rangle\!\left\langle j\right|$. This tells us that $d\rho_{jl} = 0$ for $j \neq l$, and therefore, the second term in Eq. (2.67) is zero for such a process.

The derivation of these geometric QSL, in essence, relies on the simple and elegant consideration that the geodesic distance between any two points of a Riemannian metric is the shortest possible length connecting them. The path length is calculated by integrating the inner product along the curve γ, giving the inequality,

$$L_f(\rho_0, \rho_\tau) \geq \int_\gamma \sqrt{\mathbf{g}^f(d\rho, d\rho)} = \int_0^\tau dt \sqrt{\sum_{j,k}^m g^f_{j,k}\frac{d\theta^j}{dt}\frac{d\theta^k}{dt}} \equiv \ell^\gamma_f(\rho_0, \rho_\tau), \tag{2.68}$$

where $L_f(\rho_0, \rho_\tau)$ is the geodesic distance between ρ_0 and ρ_τ in the Riemannian metric $\mathbf{g}^f_\rho$. It is important to stress that Eq. (2.68) expresses a hierarchy among all possible paths connecting the two states ρ_0 and ρ_τ for a *fixed* metric $\mathbf{g}^f_\rho$, with equality obtained if and only if γ corresponds to a geodesic in that metric. In order to translate this inequality into a QSL for the evolution time as in Eq. (2.13), one usually introduces the path-average speed,

$$v^\gamma_f = \frac{1}{\tau}\ell^\gamma_f(\rho_0, \rho_\tau), \tag{2.69}$$

from which it straightforwardly follows that

$$\tau \geq \tau^\gamma_f = \frac{L_f(\rho_0, \rho_\tau)}{v^\gamma_f}. \tag{2.70}$$

This, essentially, equates to multiplying both sides by the evolution time, τ, so this inequality is still really only telling us about the ratio between the path length and the geodesic length. The fact that there are infinitely many symmetric, operator monotone functions, f, implies that there are infinitely many QSLs for open quantum systems. Additionally, each of these QSLs can be saturated by following the geodesic in the corresponding metric. Unfortunately, a closed form of the geodesic distance, $L_f(\rho_0, \rho_\tau)$, is only known for two of these metrics, for all other metrics we must rely on loose bounds or numerical calculations. Although, it is possible to derive QSLs with known

geodesic distances for other kinds of metrics that are not Riemannian and completely positive, as we will see below. As already mentioned, for pure states and unitary evolution, the Fubini-Study metric is the unique contractive Riemannian metric and leads to the MT bound. Furthermore, in this case the speed is related to a physical resource of the system, namely the (square root of the) energy variance of the initial state. Whenever open quantum systems and mixed states are considered, however, the non-uniqueness of $\mathbf{g}_\rho^f$ naturally brings forward an important question: is there a particular metric which gives rise to a QSL which is the tightest possible, therefore representing the ultimate lower bound on the evolution time?

The answer to the above question is actually very subtle. In Ref. [78] it was argued that, for any given path γ^* between two fixed initial and final states ρ_0, ρ_τ, the hierarchy of the MCP metrics reflects into the possibility to find, at least in principle, the geodesic which gives rise to the tightest geometric QSL bound to the evolution. The latter is given by,

$$\tau_{\mathrm{QSL}} = \tau_{f^*}^{\gamma^*} \leq \tau, \tag{2.71}$$

where the metric $\mathbf{g}_{f^*}$ is the metric such that its geodesic $L_{f^*}(\rho_0, \rho_\tau)$ is the closest to the actual given path γ^*, i.e.

$$f^* \text{ such that } \inf_f \delta_f^{\gamma^*} = \delta_{f^*}^{\gamma^*}, \tag{2.72}$$

with $\delta_f^{\gamma^*} \equiv \tau/\tau_f^{\gamma^*} - 1$.

Although it is possible to define and calculate the quantity, $\delta_{f^*}^{\gamma^*}$, it is essentially meaningless. An implicit idea in the definition of a hierarchy of QSL bounds is that only the tightest bound is valid since, it would seem on the surface, that saturating any of the other bounds would violate the tightest bound, but this is simply not true. Changing the path γ^* results in the path lengths changing differently in all metrics and the hierarchy rearranging itself. Once all the quantities entering the bound Eq. (2.71) are uniquely determined, i.e. once a path γ^* and start and end points are fixed, nothing more can be done to approach the QSL bound. Equivalently said, if a given path connecting two quantum states is not already optimal, in the sense that does not already coincide with a geodesic path according to some contractive Riemannian metric, then the geometric QSL bound is never saturable and will only provide an estimate of "how far from optimal" the evolution time is with respect to τ_{QSL}.

Thus, if we are free to choose the path connecting a given initial and target state, then the QSL bound for every metric $\mathbf{g}_\rho^f$ can be saturated simply by moving along a path which coincides to the geodesic for that metric. *A priori*, the choice of one metric over another may be dictated by the physics of the problem at hand, e.g. the average initial energy as in the ML bound or the initial energy variance as for the MT bound. Regardless though, the corresponding QSL bound can, in principle, be achieved. One possible middle ground would be to fix the dynamics, e.g. a specified master equation, but allow the initial and final states to change. In this scenario there is no single metric $\mathbf{g}_\rho^f$ which represents the tightest QSL for every possible choice of the path's boundary conditions.

2.3.2 Generalized amplitude damping channel

Let us provide an explicit demonstration of this for a simple paradigmatic example consisting of a qubit undergoing a generalized amplitude damping channel (GADC) modelled using the techniques outlined in Chapter 1. This ubiquitous situation describes a two-level quantum system undergoing equilibration with a large thermal bath, such that its evolution is described in terms of the following master equation (in interaction picture)

$$\dot{\rho}_t = \mathcal{L}(\rho_t) = \gamma\left(\sigma_-\rho_t\sigma_+ - \frac{1}{2}\Big\{\rho_t, \sigma_+\sigma_-\Big\}\right) + \Gamma\left(\sigma_+\rho_t\sigma_- - \frac{1}{2}\Big\{\rho_t, \sigma_-\sigma_+\Big\}\right) \tag{2.73}$$

where $\beta = \frac{1}{2}\ln\frac{\gamma}{\Gamma}$ denotes the inverse temperature of the bath in units of the qubit's energy.

While we will consider the dynamics (GADC) and the final state (i.e. the thermal state) fixed, we will vary the initial state ρ_0, thus resulting in a different path on the Bloch sphere for each starting configuration. We will focus on three important metrics for which their geodesics can be calculated and compute the respective QSL bound, Eq. (2.70). The first is the quantum Fisher information (QFI) metric (2.50) [46, 47, 109]. The geodesic distance in this metric is given by the Bures angle,

$$L_s(\rho,\sigma) = \arccos\left(\mathrm{Tr}\sqrt{\sqrt{\rho}\sigma\sqrt{\rho}}\right). \tag{2.74}$$

The resulting QSL reads [77]

$$\tau_s = \frac{L_s(\rho_0,\rho_\tau)}{\frac{1}{\tau}\int_0^\tau dt\sqrt{\mathcal{F}_t(\rho_t)}}. \tag{2.75}$$

The second metric we will consider is the one related to the Wigner-Yanase (WY) skew information metric [78]. The corresponding operator monotone function is $f_w(t) = (1/4)(\sqrt{t}+1)^2$. The geodesic distance in this metric is given by,

$$L_w(\rho,\sigma) = \arccos(\mathrm{Tr}[\sqrt{\rho}\sqrt{\sigma}]). \tag{2.76}$$

This geodesic distance was derived by Gibilisco and Isola [110,111] and is a quantum generalisation of the Bhattacharya angle. This metric is known as the WY metric because for unitary dynamics with time dependent Hamiltonian H_t we have [78, 111],

$$\ell_w^\gamma(\rho_0,\rho_\tau) = \sqrt{2}\frac{1}{\tau}\int_0^\tau dt\sqrt{I(\rho_t,H_t)}, \tag{2.77}$$

where $I(\rho,A) = -(1/2)\,\mathrm{Tr}\{[\sqrt{\rho},A]^2\}$ is the WY skew information of the self-adjoint matrix A. Finally, we will consider the metric based on the trace distance (TD) [72] which stems from a direct application of the triangle inequality [73] rather than being one of the Riemannian metrics defined in section 2.2. The distance is given by the trace norm,

$$L_t(\rho,\sigma) = \|\rho_0-\rho_\tau\|_1 = \mathrm{Tr}\sqrt{(\rho_0-\rho_\tau)^2}. \tag{2.78}$$

The geodesic paths are also known for all three of these metrics. In the following $p(t)$ is any function satisfying $p(0)=0$ and $p(\tau)=1$ that is monotonically increasing on that interval. The geodesic path for the QFI metric was derived by Uhlmann [112] and is given by,

$$\rho_t = \frac{[(p(t)\omega_\tau + (1-p(t))\omega_0)((p(t)\omega_\tau^\dagger + (1-p(t))\omega_0^\dagger))]}{\|p(t)\omega_\tau + (1-p(t))\omega_0\|^2} \tag{2.79}$$

where ω_0 is a purification of $\rho_0 = \omega_0\omega_0^\dagger$. Therefore if ρ_0 has a spectral decomposition $\rho_0 = \sum_i p_i \left|p_i\right\rangle\!\left\langle p_i\right|$ then we define, $\omega_0 = \sum_i \sqrt{p_i}\left|p_i\right\rangle\!\left\langle \phi_i\right|$, where $\left|\phi_i\right\rangle$ is another orthonormal basis of the Hilbert space, with ω_τ defined in terms of ω_0 as

$$\omega_\tau = \rho_0^{-1/2}(\rho_0^{1/2}\rho_\tau\rho_0^{1/2})^{1/2}\rho_0^{-1/2}\omega_0. \tag{2.80}$$

Similarly for the WY metric the geodesic path was derived by Gibilisco [111] and is given by,

$$\rho_t = \frac{\left((1-p(t))\sqrt{\rho_0} + p(t)\sqrt{\rho_\tau}\right)^2}{\mathrm{Tr}\left\{\left((1-p(t))\sqrt{\rho_0} + p(t)\sqrt{\rho_\tau}\right)^2\right\}}. \tag{2.81}$$

Finally, the TD geodesic path is simply a "straight line" between the initial and final states,

$$\rho_t = (1-p(t))\rho_0 + p(t)\rho_\tau. \tag{2.82}$$

Fig. 2.1(a) shows the result of the evaluation of the three QSL bounds as a function of the parameter, θ, which determines the initial state that, without any loss of generality, is taken to be pure $\rho_0(\theta) = \left|\Psi_0(\theta)\right\rangle\!\left\langle\Psi_0(\theta)\right|$, with $\left|\Psi_0(\theta)\right\rangle = \cos(\theta)\left|0\right\rangle + \sin(\theta)\left|1\right\rangle$. While for any given fixed path (i.e. in this case, fixed θ), one QSL is clearly tighter than the other, thus confirming Eq. (2.71), it is evident that none of them provides the tightest QSL for every parameter $\theta \in [0,\pi]$. The tightest bound for any given initial state is the one corresponding to the metric whose geodesic happens to be closest to the GADC dynamics for that particular choice of θ. We finally notice that for $\theta = 0, \pi/2$ all the bounds saturate because the GADC traces a geodesic path for all the considered metrics.

When we have a two-dimensional system, $\rho = \sum_{i,j=0}^{1}\rho_{ij}\left|j\right\rangle\!\left\langle i\right|$ where $\{\left|i\right\rangle\}$ is an arbitrary orthogonal basis, it can be parameterised by the Bloch sphere coordinates

$$\begin{aligned} u &= \rho_{01} + \rho_{10} \\ v &= i(\rho_{01} - \rho_{10}) \\ w &= \rho_{00} - \rho_{11}. \end{aligned} \tag{2.83}$$

The geodesic paths corresponding to each of the three metrics described above are shown in the Bloch sphere in Figs. 2.1(b), (c), (d) for different values of θ. The basis is chosen to be the energy basis. Figure 2.1(b) corresponds to the case of $\theta = 0$ where we initially start in the excited

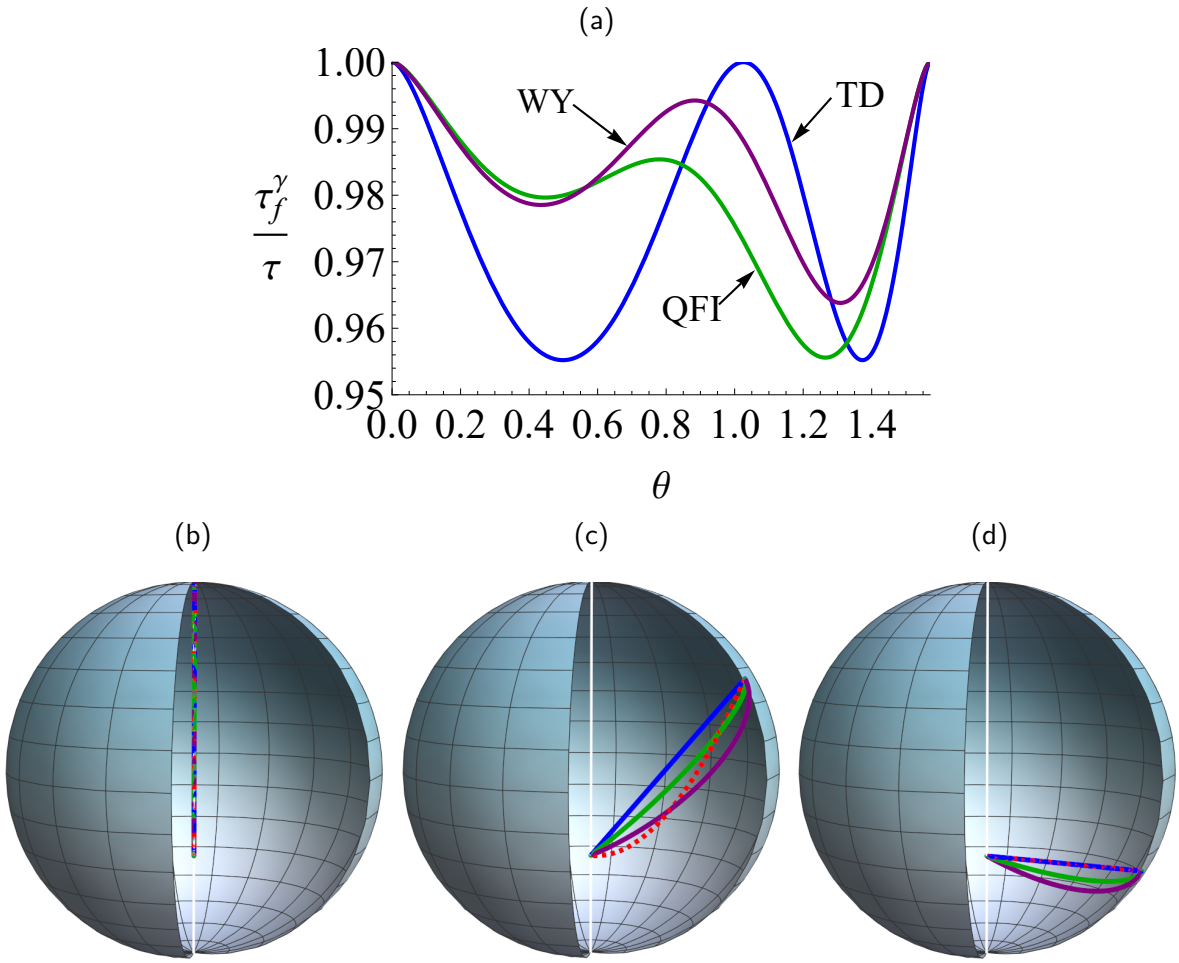

Figure 2.1: **(a)** Plot of the ratio, τ_f^γ/τ, between the quantum speed limit time and the evolution time for three different choices of metric $f = w, s, t$ (Wigner-Yanase, quantum Fisher information and trace distance, respectively), as a function of the initial state parameter θ with $\beta = 0.5$. The path γ corresponds to the GADC. **(b),(c),(d)** Bloch sphere representation of the three geodesic paths of a two-level system undergoing the GADC, Eq. (2.73), with $\beta = 0.5$. The straight, blue line corresponds to the TD geodesic path. The QFI geodesic corresponds to the solid, green curve. The remaining solid, purple line is the WY geodesic. Finally, the path followed by the GADC is shown in dashed, red. Initial states in **(b),(c),(d)** correspond to $\theta = 0, \pi/6, 1.0256$ respectively

state. Here all the geodesics coincide with the actual path that the GADC takes, and this makes sense since we see the QSL saturate at $\theta = 0$ in Fig. 2.1(a). As we discussed below Eq. (2.67) the metric can be split up into a classical and quantum component, both of which are strictly positive. Therefore, if the initial state and final states commute with each other, such as is the case for $\theta = 0, \pi/2$, then the geodesic path between those states will also commute at all times. This means that the quantum contribution to the metric is zero along the geodesic and all the Morozova and Chentzov [86] metrics share the same geodesic path. The geodesic path of the TD metric has the property that it is just a linear combination of the initial and final state, therefore if the initial and final state commute then the geodesic also commutes. For $\theta = \pi/6$ in Fig 2.1(c) none of the QSLs are saturated and it is not easy to tell which of the three will be the tightest. Finally, in Fig 2.1(d) we choose $\theta \approx 1$ so that our initial state has the same u Bloch sphere component as the thermal state. When this is the case, the GADC dynamics corresponds with the straight-line geodesic of the TD metric.

2.3.3 Qubit metrics

To understand why the metrics have the geodesics they do, we can take a closer look at the form of their metrics. We make the transformation to spherical coordinates in the Bloch sphere which are defined implicitly as

$$\begin{aligned} u &= r\sin\theta\cos\phi \\ v &= r\sin\theta\sin\phi \\ w &= r\cos\theta. \end{aligned} \tag{2.84}$$

In this basis we can calculate the eigenvalues,

$$E_0 = \frac{1}{2}(1-r); \quad E_1 = \frac{1}{2}(1+r), \tag{2.85}$$

and the corresponding eigenvectors,

$$|E_0\rangle = \begin{pmatrix} \sin\frac{\theta}{2} \\ -e^{i\phi}\cos\frac{\theta}{2} \end{pmatrix}; \quad |E_1\rangle = \begin{pmatrix} \cos\frac{\theta}{2} \\ e^{i\phi}\sin\frac{\theta}{2} \end{pmatrix}. \tag{2.86}$$

With this basis we can now calculate the metric tensor for the Morozova and Chentzov [86] metrics as defined in Eq. (2.67). In this coordinate frame, the first term, common to all of these metrics is,

$$\sum_j \frac{(d\rho_{jj})^2}{p_j} = \frac{dr^2}{1-r^2}. \tag{2.87}$$

Then the second term is going to depend on the specific metric that we are using, in particular, it depends on the Morozova-Chentzov function f that goes into $c_f(x,y) = \frac{1}{yf(x/y)}$. We can

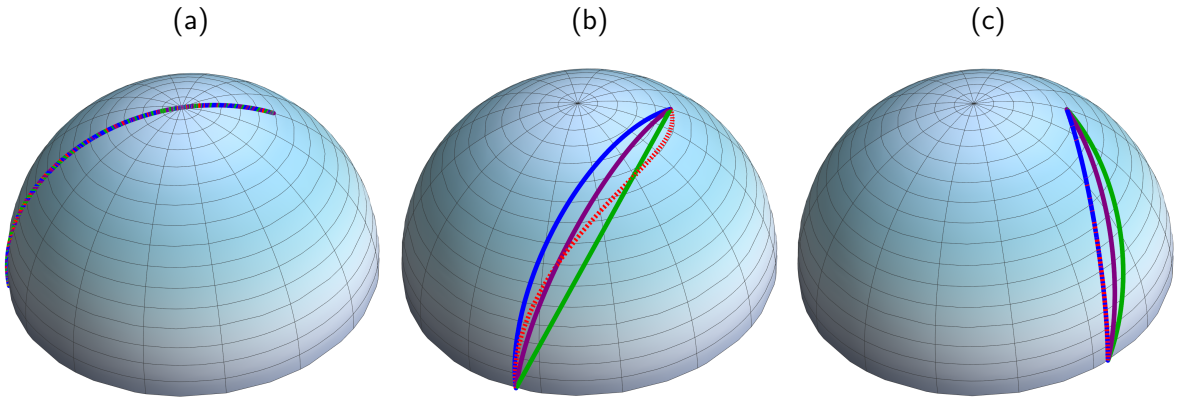

Figure 2.2: Representation of the three geodesic paths of a two-level system undergoing the GADC, Eq. (2.73), with $\beta = 0.5$ on the surface of a 2-sphere representing the QFI metric. The blue line corresponds to the TD geodesic path. The QFI geodesic corresponds to the solid, green curve. The remaining solid, purple line is the WY geodesic. Finally, the path followed by the GADC is shown in dashed, red. Initial states in **(a),(b),(c)** correspond to $\theta = 0, \pi/6, 1.0256$ respectively.

calculate the second term exactly and it gives us,

$$\sum_{j<k} c_f(p_j, p_k)|d\rho_{jl}|^2 = \frac{r^2(d\theta^2 + \sin^2\theta d\phi^2)}{2f\left[\frac{1-r}{1+r}\right](1+r)}, \tag{2.88}$$

so then combining these two terms together we get the line element,

$$ds^2 = \frac{1}{4}\left(\frac{dr^2}{1-r^2} + \frac{r^2(d\theta^2 + \sin^2\theta d\phi^2)}{f\left[\frac{1-r}{1+r}\right](1+r)}\right). \tag{2.89}$$

The first interesting thing we can do with this metric is restrict ourselves to pure states, for this we have $r = 1$ and $dr = 0$ leaving us with,

$$ds^2 = \frac{1}{8f\,[0]}\left(d\theta^2 + \sin^2\theta d\phi^2\right). \tag{2.90}$$

This is just the metric of a 2-sphere. Additionally, the coordinates are exactly the spherical coordinates in the Bloch sphere, this tells us that for pure states that the geodesics are the great circles of the Bloch sphere and since any two pure states can be represented in a two-dimensional subspace we now know the geodesic path between any two pure states. This is another way to prove the result for saturating the ML bound from Sec. 2.1.4. So, all the Morozova and Chentzov metrics agree about the geodesic path for pure states confirming the fact that there is only one unique, contractive, Riemannian metric over the pure states (up to a constant factor).

Now we can look at this in more detail for specific metrics. The QFI metric is defined by the

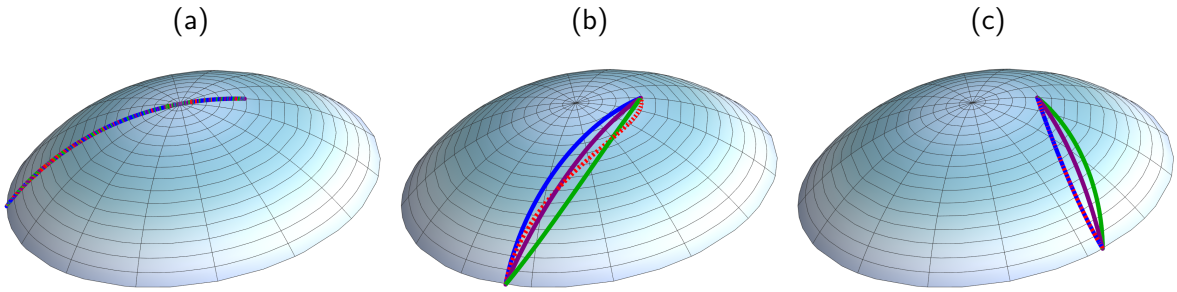

Figure 2.3: Representation of the three geodesic paths of a two-level system undergoing the GADC, Eq. (2.73), with $\beta = 0.5$ on the surface of a 2-sphere representing the WY metric. The blue line corresponds to the TD geodesic path. The QFI geodesic corresponds to the solid, green curve. The remaining solid, purple line is the WY geodesic. Finally, the path followed by the GADC is shown in dashed, red. Initial states in **(a),(b),(c)** correspond to $\theta = 0, \pi/6, 1.0256$ respectively.

Morozova-Chentzov function $f(t) = (1+t)/2$, subbing this into Eq. (2.89) we get

$$ds^2 = \frac{1}{4}\left(\frac{dr^2}{1-r^2} + r^2(d\theta^2 + \sin^2\theta d\phi^2)\right) \tag{2.91}$$

then by making the substitution $r = \sin\xi$ we end up with

$$ds^2 = \frac{1}{4}\left(d\xi^2 + \sin^2\xi\left(d\theta^2 + \sin^2\theta d\phi^2\right)\right), \tag{2.92}$$

which is the metric of a 3-sphere of radius $1/2$ embedded in 4-dimensional Euclidean space using the hyper-spherical coordinates,

$$\begin{aligned} x_0 &= r\sin\xi\sin\theta\sin\phi \\ x_1 &= r\sin\xi\sin\theta\cos\phi \\ x_2 &= r\sin\xi\cos\theta \\ x_3 &= r\cos\xi. \end{aligned} \tag{2.93}$$

Then we know that the geodesics in the QFI metric are just the great circles of this sphere. More specifically if we look at the parameters we see that $\arcsin r = \xi \in \{0, \pi/2\}$, whereas for a full 3-sphere this would run all the way to π. This means that the space of two-dimensional quantum states equipped with the QFI metric is isomorphic to a 3-dimensional hemisphere in 4-dimensional Euclidean space. The maximally mixed state is at the north pole and pure states are on the rim of the hemisphere, i.e. $\xi = 0, \pi/2$ respectively.

For the example of the GADC in Sec. 2.3, we chose initial and final states with $\phi = 0$ and all the intermediate states also have $\phi = 0$ so this simplifies our metric to the metric of a 2-sphere embedded in the 3-dimensional Euclidean space. This means that it is now possible to visualise the paths as we do in Fig 2.2. We can see that all of our pure initial states lie on the boundary of

the hemisphere. The QFI geodesic takes the geodesic path of the sphere which is just the great circle.

We can also perform a similar analysis on the WY metric which has the Morozova-Chentzov function, $f(t) = (1/4)(\sqrt{t}+1)^2$, this leaves us with the metric

$$ds^2 = \frac{1}{4}\left(\frac{dr^2}{1-r^2} + \frac{r^2(d\theta^2 + \sin^2\theta d\phi^2}{\left(\sqrt{1-r}+\sqrt{1+r}\right)^2}\right) \tag{2.94}$$

then by making the substitution $r = 1/2\sin\xi$ we end up with

$$ds^2 = d\xi^2 + \sin^2\xi\left(d\theta^2 + \sin^2\theta d\phi^2\right). \tag{2.95}$$

So once again we end up with a 3-sphere, this time of radius 1 and $\xi \in \{0, \pi/4\}$, we can think of this as the top $1/4$ of the 3-sphere. By once again restricting to $\phi = 0$ and looking at the GADC map, we plot different geodesics paths in this metric in Fig 2.2. This time the WY geodesic corresponds to the great circle of the sphere. Although there is no general equation for the geodesic in every Morozova-Chentzov metric it may be possible to solve this geodesic equation and find a general solution for two-dimensional sub-spaces. This would be particularly useful because it would give us the geodesic path and distance between any two pure states in each metric.

For the trace distance QSL the equivalent of this line element is given by

$$\begin{aligned} ds^2 &= \left\|\frac{d\rho}{dt}\right\|_1^2 \\ &= \frac{1}{2}\left(du^2 + dv^2 + dw^2\right), \end{aligned} \tag{2.96}$$

which is exactly the metric of the Bloch sphere. This explains why the trace distance geodesics are straight lines in Bloch sphere plots.

2.4 Action Quantum Speed Limits

The previous section highlights that when open quantum systems are considered, there is no single contractive, Riemannian metric for which the corresponding geometric QSL bound is the tightest unless the path and endpoints are fixed. Fixing a path is therefore a necessary requirement in order to have a well-defined unique and tightest QSL bound Eq. (2.71) such that Eq. (2.72) holds. If every parameter of the problem is fixed, however, unless a given dynamics already coincides with a geodesic path according to some metric (e.g. in the case of a GADC channel with $\theta = 0, \pi$ in the above example), then the geometric QSL time provides a quantitative indication of how far the traversed path is from the optimal path, according to the specific metric in question. Nevertheless, despite what the name might suggest, the geometric quantum speed limit time is completely insensitive to the actual instantaneous speed.

This simple observation represents the starting point for introducing our new family of QSLs.

The instantaneous speed at which a given path is travelled is an important degree of freedom. Indeed, the varying speed of evolution provides a vital tool in many physical settings, for example every thermodynamic cycle of any driven engine is crucially dependent on the speed at which the protocol is performed [14] and high-fidelity control can be achieved by varying the speed with which some time-dependent ramp is applied such that the dynamics slows down when energy gaps close, which applies to understanding the dynamics across quantum phase transitions in light of the Kibble-Zurek mechanism [19, 113]. The generation of defects during such a ramp will depend on how the system traverses the impulse regime, this information is not properly captured by considering only the average speed of the system over the entire ramp. The instantaneous speed around the start and end points is also vital for quantum control because no physical clock can perfectly characterize time [114].

We incorporate the instantaneous speed into the formulation of quantum speed limits by borrowing inspiration from recent developments in thermodynamic geometry [14, 115–121]. This can be achieved by applying the Cauchy-Schwarz inequality $\int_0^\tau h^2 dt \int_0^\tau f^2 dt \geq [\int_0^\tau fh\, dt]^2$ to the path length $\ell_f^\gamma(\rho_0, \rho_\tau)$. Specifically, by setting $h=1$, one has

$$\tau \int_0^\tau dt \sum_{jk=1}^{M} g_{jk} \frac{d\theta_j}{dt} \frac{d\theta_k}{dt} \geq \left(\int_0^\tau dt \sqrt{\sum_{jk=1}^{M} g_{jk} \frac{d\theta_j}{dt} \frac{d\theta_k}{dt}} \right)^2 \tag{2.97}$$

which leads to the following result,

$$\tau \geq \tau_a^\gamma = \frac{L_f(\rho_0, \rho_\tau)^2}{a_f^\gamma}, \tag{2.98}$$

where $a_f^\gamma = \int_0^\tau dt \sum_{jk=1}^{M} g_{jk} \frac{d\theta_j}{dt} \frac{d\theta_k}{dt}$ is known as the action or energy functional. Eq. (2.98) is the anticipated new family of QSLs which, in light of the above quantity and its interpretation, we name *action quantum speed limits*.

Most geometric QSLs display some peculiar behaviour when the target state is only approached asymptotically in the long-time limit such as in the case of the GADC or the damped Jaynes-Cummings model [92]. This is because the geometric QSLs depend on the average speed over the entire trajectory. Since the time to reach this final steady state is arbitrarily long, but the distance between the initial and the steady state is bounded, this leads to the QSL time scaling linearly with the evolution time in the long-time limit. This is not very physical since the system state is asymptotically close to the steady state and its instantaneous speed is essentially zero, yet the QSL bound is still getting larger. In order to fix this problem Mirkin *et. al.* [92] highlight that there is another way to define the QSL time that does not seem to have this problem. For any geometric bound the path length must be longer than the geodesic length. Therefore, there must exist some point along the actual evolution path where the distance travelled is equal to the

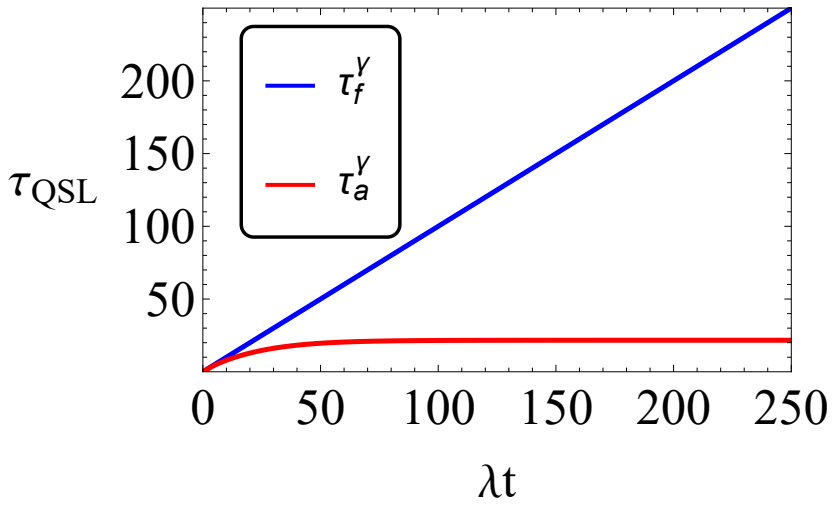

Figure 2.4: A comparison between the geometric and action QSL times for the GADC with master equation given by Eq. (2.73), with $T = 0$ and the initial state of $\theta = 0$. Results are qualitatively identical for all values of T and θ.

geodesic distance between the initial and final state, i.e.

$$L_f(\rho_0, \rho_\tau) = \int_0^{\tau_{\text{min}}} dt \sqrt{\sum_{j,k}^{m} g^f_{j,k} \frac{d\theta^j}{dt} \frac{d\theta^k}{dt}}. \tag{2.99}$$

While this does solve the issue of linear scaling in the QSL time with the driving time for most processes, we will still see this linear scaling when the actual evolution path is geodesic path since τ_{min} is just equal to the geometric QSL in this scenario. There are also a number of other conceptual problems with defining the QSL time like this, such as it not necessarily being symmetric if the process is played backwards. Action QSLs can address all of these problems without any of the extra conceptual baggage. In Fig. 2.4 we can see a comparison between the geometric QSLs and the action QSLs, we have chosen an initial state of $\theta = 0$ so that all of the metrics agree on the geodesic path. Clearly, the geometric QSL (and τ_{min}) displays this linear scaling in the long time limit but the action QSL flattens out instead. This can be understood from the fact that the action is the integral of the square of the instantaneous speed, which gets asymptotically smaller as the system approaches the steady state.

It is crucial to point out that, for any given path γ, Eq. (2.98) is saturated when γ is a geodesic and the speed along it, $\sqrt{\sum_{jk=1}^{M} g_{jk} \frac{d\theta_j}{dt} \frac{d\theta_k}{dt}}$ is constant. This means that, if a given path is already optimal in the sense that it coincides with a geodesic and thus saturates the geometric QSL, then the action QSL will also be saturated provided this path is traversed at a constant speed in the corresponding metric. Conversely, when a given path is not optimal, then Eq. (2.98) becomes more delicately dependent on this instantaneous speed, as we show explicitly below. This also explains why the action QSL can be so far from saturated in Fig 2.4 even though the path is a geodesic; the instantaneous speed is far from constant.

Another important consideration stems from the following inequality:

$$\frac{\tau_a^\gamma}{\tau} = \frac{L_f(\rho_0,\rho_\tau)^2}{\tau\, a_f^\gamma} \leq \frac{L_f(\rho_0,\rho_\tau)^2}{\tau^2 (v_f^\gamma)^2} = \left(\frac{\tau_f^\gamma}{\tau}\right)^2 \tag{2.100}$$

This result highlights the fact that the geometric QSL is a special instance, corresponding to the upper bound, of the action QSL. This physically indicates that, for every non-optimal path, any time-dependent profile for the speed will lead to a QSL bound which is going to be less than or equal to the geometric ideal QSL value. This is however an especially important property, as it implies that different strategies aimed at optimizing the speed for any given non-optimal path will reflect in the value of the action-QSL time which progressively approaches the bound given in Eq. (2.100). Due to the very structure of it involving the action a_f^γ, finding the optimal way to traverse a path is naturally suited to be solved by techniques borrowed from optimal control theory [21, 122–129].

Since there is no square root inside the integral in the action this means that we can split the integral up into its constituent components. The most obvious partition we can make would be the one in Eq. (2.67). Using this we can identify the classical and quantum contributions to the speed limit time. This could be used to compare different paths and gain a greater understanding of what is contributing to the QSL. The concept of splitting the denominator in the speed limit up has been employed before [81] but it can be expanded to many more scenarios with action QSLs.

2.5 Optimizing the Instantaneous Speed

As we have mentioned above a number of times, the standard geometric QSLs are insensitive to the instantaneous speed along the path. This means that there are a number of solutions that minimise the path length between any two points on our Riemannian metric. In Riemannian geometry, in order to get around this problem it is standard to use the Euler-Lagrange equation to derive a geodesic equation. The solutions to the Euler-Lagrange equation are the stationary points of the action, therefore the solution to this equation will be the geodesic that minimises the action and that is the geodesic that satisfies the standard geodesic equations,

$$\frac{d^2\theta^k}{dt^2} + \Gamma^k_{i,j}\frac{d\theta^i}{dt}\frac{d\theta^j}{dt} = 0, \tag{2.101}$$

where

$$\Gamma^k_{i,j} = \frac{1}{2} g^{lk}\left(\partial_i g_{lj} + \partial_j g_{li} - \partial_l g_{ij}\right), \tag{2.102}$$

are the Christoffel symbols. For action QSLs, minimising the action is equivalent to saturating the QSL.

This is all well and good for when we have full control over the system evolution but often there are constraints on the evolutions that are possible. We could try to incorporate these into the geodesic equations, such as when we restricted to pure states in Eq. (2.90) and derived the

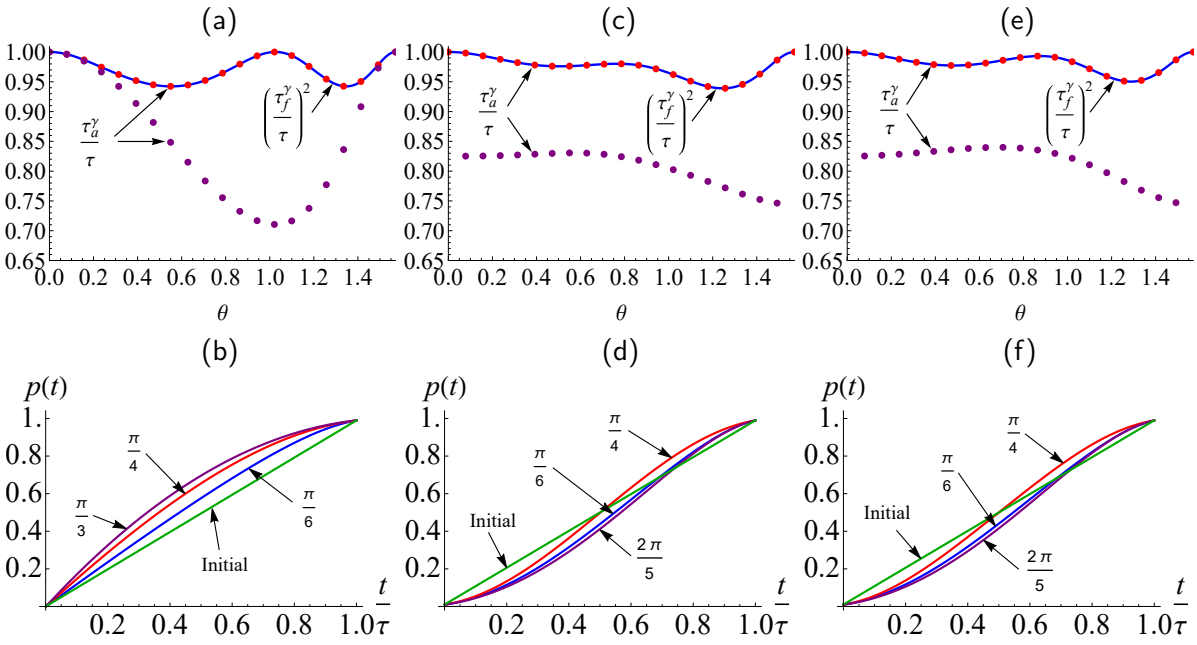

Figure 2.5: **(a)** The solid blue line shows the (square of the) geometric TD speed limit for the generalised amplitude damping channel with $\beta = 0.5$ (arbitrarily chosen). This QSL time is independent of $p(t)$ as long as $\dot{p}(t) > 0$. The purple points represent the value of the TD action QSL for our initial guess of constant $\dot{p}(t)$. The red points are the value of the TD action speed limit after optimising over all admissible $\dot{p}(t)$ with the desired start and end points. These points lie on the blue line demonstrating that we can use optimal control to saturate equation (2.100). **(b)** Shows the optimal function $p(t)$ for various values of θ as compared to our initial guess. **(c)** and **(d)** Are as for panels (a) and (b) except applied to the QFI speed limit. **(e)** and **(f)** Are as for panels (a) and (b) except applied to the WY speed limit.

MT bound, but this is not so simple in general. An alternative approach is to make use of optimal control techniques. We will constrain our evolution to a fixed path and a fixed driving time with freedom to change the instantaneous speed along the path. An example of this would be the path followed by the GADC used in Section 2.3. To explicitly account for the time-dependence along the path, we express this channel using the Kraus operators,

$$K_0(t) = \sqrt{c}\begin{pmatrix} \sqrt{1-p(t)} & 0 \\ 0 & 1 \end{pmatrix}, K_1(t) = \sqrt{c}\begin{pmatrix} 0 & 0 \\ \sqrt{p(t)} & 0 \end{pmatrix}, \tag{2.103}$$

$$K_2(t) = \sqrt{1-c}\begin{pmatrix} 1 & 0 \\ 0 & \sqrt{1-p(t)} \end{pmatrix}, K_3(t) = \sqrt{1-c}\begin{pmatrix} 0 & \sqrt{p(t)} \\ 0 & 0 \end{pmatrix}, \tag{2.104}$$

where $c = \frac{1}{2}(1 + \tanh\beta)$ and with β being the inverse temperature of the bath. The path is fixed by the value of β, while $p(t)$ describes how that path is traversed and must satisfy $p(0) = 0$ and $p(\tau) = 1$.

To identify the optimal time-dependent profile $p(t)$ for the dynamics we can make use of

Pontryagin's optimum principle [21, 122, 130]. The cost functional that we want to minimise is the action along our path,

$$a_f^\gamma = \int_0^\tau dt \sum_{jk=1}^{M} g_{jk} \frac{d\theta_j}{dt} \frac{d\theta_k}{dt} \equiv \int_0^\tau dt\, \mathscr{L}(\rho(t), \dot{\rho}(t), \dot{p}(t)). \tag{2.105}$$

In analogy with classical Lagrangian mechanics we can define the control Lagrangian, $\mathscr{L}(\rho(t), \dot{\rho}(t), \dot{p}(t))$ of the dynamics. $\dot{p}(t)$ is simply the time derivative of the ramp profile and can be thought of as the external control parameter. The difference between this method and just solving the Euler Lagrange equations is that we are not simply minimising the action but finding the protocol $p(t)$ that minimises the action subject to fixed initial and final states and fixed total evolution time. We then take the Legendre transform of the control Lagrangian to get the control Hamiltonian, which is analogous to the Hamiltonian in classical Hamiltonian mechanics. It is metric dependent and has no relation to the Hamiltonian that appears in the Schrödinger equation. We can now apply Pontryagin's optimum principle which states that the control protocol $\dot{p}^*(t)$ that minimises our action is given by,

$$\mathcal{H}(\dot{p}^*(t)) = \sup_{\dot{p}(t)\in\mathcal{A}} \mathcal{H}(\dot{p}(t)). \tag{2.106}$$

Here $\mathcal{A}$ represents the set of all admissible profiles. The advantage of transforming to the Hamiltonian is that it allows us to find the optimal profile by a point-wise optimisation rather than an optimisation of the action over the full function space of $p(t)$.

It is important to stress that to optimise the dynamics we must saturate the Cauchy-Schwarz inequality, which corresponds to finding the ramp profile that results in a constant speed in the metric. As we demonstrate by explicit example for non-geodesic paths, achieving a constant speed in the metric generally requires a non-trivial temporal ramp profile. In this case, the set of all admissible profiles $\mathcal{A}$ corresponds to all profiles that map our pure initial state to the thermal state, i.e.

$$\int_0^\tau dt\, \dot{p}(t) = p(\tau) - p(0) = 1. \tag{2.107}$$

In order to perform the optimisation, we use a modified gradient descent algorithm,

$$\dot{p}^{n+1} = \dot{p}^n + \epsilon \left(\frac{\partial \mathcal{H}^n}{\partial \dot{p}} - \frac{1}{\tau} \int_0^\tau dt\, \frac{\partial \mathcal{H}^n}{\partial \dot{p}} \right). \tag{2.108}$$

We add the final term in order to guarantee that Eq. (2.107) is always satisfied.

In Fig. 2.5 we display the result of the numerical implementation of optimal control strategies on $\dot{p}(t)$ and their impact on the associated QSL. First, it is immediately evident from Fig. 2.5(a) that different profiles of $p(t)$ (shown as dotted curves) lead to vastly different values of the action-QSL bound. We initially start by guessing that the optimal profile is a linear ramp $p(t) = t/\tau$, then we apply our modified gradient descent algorithm until we maximise the control Hamiltonian. We can see that, except for some specific initial states in the TD metric, the linear ramp (lower, purple dots) is clearly a non-optimal solution, as it results in a value markedly below the tightest

theoretical bound given by the geometric QSL (blue solid curve), Eq. (2.100). A fully optimized $\dot{p}(t)$ (red dots) demonstrates that we can saturate Eq. (2.100). In contrast, however, evaluating Eq. (2.70) using these two ramp profiles gives the same result (the solid blue curve in Fig. 2.5) thus confirming that geometric QSLs are insensitive to the instantaneous speed. In Fig. 2.5(b) we show the optimal profiles $p(t)$ which result in a constant metric speed, for different values of θ, i.e. for different fixed paths. A completely analogous treatment can be implemented for any other metric, e.g. for the QFI and WY action introduced above. The optimal protocols for $p(t)$ will of course be different given choice and path as determined by θ. This is shown in Fig. (2.5)(c)-(f) for the QFI and for the WY metrics, thus demonstrating the general validity of our approach.

2.6 Impact on the Interpretation of QSLs

The results of this chapter significantly clarify the interpretation of QSLs. Traditionally, they have been interpreted as putting a fundamental lower limit on the evolution of a system between an initial and a final state, but this is only one way to interpret them and often obscures precisely what the determination of a QSL is actually revealing. Almost all QSLs take the form

$$\tau \geq \tau_{\mathsf{QSL}} = \frac{f(\rho_0, \rho_\tau)}{g(\gamma)} \tag{2.109}$$

where τ is the total system evolution time, f is a distance-like function that depends exclusively on the initial and final state of the system and g is a function that depends on the path, γ, taken between the initial and final states, i.e. depends on ρ_t for $0 \leq t \leq \tau$. In order to understand what it would mean to achieve or saturate any QSL bound it is important to fix any two of the three quantities in this inequality. Allowing more than one quantity to vary would lead to significant ambiguity in the interpretation, for example if we keep only the distance fixed in the MT bound, Eq. (2.13), then the minimum time is not meaningful because we can always increase the variance of our Hamiltonian and reduce the minimum time. The most common way to interpret the quantum speed limit is to fix both $f(\rho_0, \rho_\tau)$ and $g(\gamma)$. It is important to note that we are not fixing the path, γ, itself only the real number output of $g(\gamma)$. It is usually assumed that the initial and final states are fixed, although this is not necessary for this interpretation to hold, only that $f(\rho_0, \rho_\tau)$ is fixed. In this interpretation, the QSL is a statement that τ is the minimum possible time for a system to evolve between two states a "distance", $f(\rho_0, \rho_\tau)$, apart subject to the constraint that $g(\gamma)$ is fixed for the evolution path. If a QSL is always saturable this means that there always exists such a path γ that saturates Eq. (2.109). This interpretation is most insightful when the quantity $g(\gamma)$ corresponds to an important property of our system that we need to keep fixed. Another approach would be to fix the evolution time and $g(\gamma)$ and allow only the "distance" between states to vary. The QSL bound can then be interpreted as the maximum possible "distance" a system could have evolved from an initial state for a specific value of $g(\gamma)$. This interpretation might be used when we want to maximise distinguishability between two states such as for measurement purposes [131] or when we want to minimise the effect of noise on

our system evolution [132]. The final interpretation involves fixing the evolution time and the "distance" between the initial and final states. In this case the QSL bound tells us the minimum possible value of $g(\gamma)$ for any evolution path between states a "distance" $f(\rho_0, \rho_\tau)$ away from each other with an evolution time τ. This interpretation is most relevant when we want to keep a fixed evolution time and minimising the value of $g(\gamma)$ is important to us.

All of these interpretations highlight the fact that it is important that the quantity $g(\gamma)$ is physically meaningful, but it is the final interpretation that emphasises this the most. We can understand the path that saturates the QSL as the path that minimises $g(\gamma)$ so it is vital that we choose a QSL bound that corresponds to a quantity $g(\gamma)$ that we want to minimise. This provided a significant portion of the motivation for introducing action QSLs.

Experiments and theoretical work relating to QSLs have often focused on reducing the QSL time such as by adding non-Markovianity [66, 133] but, as the above analysis highlights, it is more important that we look for processes that saturate the QSL bound because it will always be possible to lower the QSL time by increasing $g(\lambda)$. There has been a number of papers comparing optimal control times to quantum speed limit times [37, 134, 135] but not a lot of experimental realisations of such scenarios. One recent paper investigated the experimental performance of the ML and MT bounds for the motion of an atom in an optimal trap [45]. They found regimes where either bound could be tighter, suggesting that neither bound fully captures the physics of the problem. The MT bound has been shown to be practically relevant, at least in theory, in calculating the charging time for a quantum battery with a constant interaction strength [136, 137]. As far as we know, there has yet to be any demonstration of an open system QSL linked to an experimentally relevant optimisation.

A family of bounds that is similar in idea to QSLs is Lieb-Robinson bounds [138]. Lieb-Robinson bounds put a fundamental limit on the maximum velocity that correlations can spread through many-body quantum systems. Despite this similarity, no clear relation has been shown between the two bounds [100]. This highlights the fact that QSLs often neglect some practical considerations in systems such as the need for local interactions. While it is possible to apply the restriction of local interactions to QSLs [139] it is often more fruitful to apply techniques such as optimal control or Lieb-Robinson bounds in these scenarios.

Although we have only considered qubit systems in this analysis, the QSLs considered apply to systems of any dimension. One interesting property of geometric QSLs is that the optimal path between any two states is always contained within the span of the initial and final states [78]. In particular, this means that the Hilbert space needed to describe the optimal evolution between any two pure states is always two dimensional. We proved this for the MT bound in Eq. (2.34) but this applies more generally for all bounds considered in this Chapter so the Bloch sphere picture is not as restrictive as it may initially seem.

For action QSLs, the relationship between the action and classical Lagrangian mechanics means that it is natural to incorporate certain kinds of constraints, specifically those that can be formulated as a Lagrange multiplier problem where we restrict to a submanifold of states that

connect our initial and final states. It is an open question as to whether it is possible to incorporate constraints that restrict the kinds of system Hamiltonians or interactions that our system is subject to such as the local interactions considered in Lieb-Robinson bounds.

2.7 Conclusions and Outlook

In this chapter we introduced the notion of a quantum speed limit and showed how Riemannian geometry can be used to extend the concept to open quantum systems. If one has the freedom to choose any path connecting two states, then any and all of the infinite families of geometric QSL are saturable. While the existence of a unique and tightest lower bound for the evolution time is guaranteed once a path and dynamics are completely specified, these constraints necessarily leave no room for optimization if the dynamics does not already coincide with a geodesic path. Therefore, care must be taken in interpreting open system geometric QSL times: they provide a quantitative indication of how far a given path is from the geodesic rather than necessarily indicating an achievable minimal time. We also highlighted that these geometric QSL times are insensitive to how this path is traversed and are therefore agnostic to the instantaneous speed.

Nevertheless, this speed is an important and tunable degree of freedom. We have introduced a novel family of QSLs, termed action quantum speed limits, that explicitly depend on both the path and the instantaneous speed for a given metric. Our derivation relied on the same geometrical representation of quantum states and followed from the application of the Cauchy-Schwartz inequality to the path length. We established that the bound provided by the geometric QSL coincides with a special instance of the action QSL, specifically when the instantaneous speed of the latter is fully optimized along the path. We explicitly demonstrated this using optimal control techniques applied to a qubit undergoing a dynamics described in terms of a generalized amplitude damping channel for three choices of metric, the trace-distance, quantum Fisher information, and Wigner-Yanase skew information. While our formulation applies to arbitrary finite-dimensional systems, we expect that solving the optimal control problem becomes computationally more demanding for increasing system size. Our results provide a means to quantitatively assess the optimality of a given dynamical process from a purely geometric perspective. In addition, we have highlighted that the geometric formulation of quantum speed limits can be combined with optimal control techniques to characterise a particular dynamics; such an approach could be employed to find achievable minimal times for a given process [20, 55, 98]. Our results may also be relevant to recent proposals employing optimal control in dynamical quantum estimation schemes [127–129, 140]. Furthermore, our framework can naturally be extended to recently proposed resource speed limits [75, 141].

The Morozova-Chentzov-Petz metrics have proved to be useful in slow-driving quantum thermodynamics [120, 126, 142], this opens the door for a connection between action QSLs and quantum thermodynamics. It has been shown that when the Hamiltonian is changed in a sequence of quenches followed by full thermalisation of the system the dissipated work can be calculated up

to first order as

$$\langle W_{diss}\rangle = \beta\tau_{\mathsf{eq}}\int_0^\tau dt\sum_{j,k}^{m} g^b_{j,k}\frac{d\theta^j}{dt}\frac{d\theta^k}{dt}. \tag{2.110}$$

We define $\tau = \tau_{\mathsf{eq}}N$, where τ_{eq} is the equilibration time and N is the total number of quenches. Unfortunately, the geodesic distance is not known for the Bogoliubov metric $\mathbf{g}^b$ but it can be lower bounded by the geodesic distance in the WY metric (2.76). We can use this to get an action QSL style bound,

$$\tau \geq 2k_BT\tau_{\mathsf{eq}}\frac{L_b(\rho_0,\rho_\tau)^2}{\langle W_{diss}\rangle} \geq 2k_BT\tau_{\mathsf{eq}}\frac{\arccos\left(\mathrm{Tr}\left[\sqrt{\rho_0}\sqrt{\rho_\tau}\right]\right)^2}{\langle W_{diss}\rangle}. \tag{2.111}$$

The same first order approximation for the dissipated work can be derived [120] by considering the master equation,

$$\dot{\rho}_t = \tau_{\mathsf{eq}}^{-1}(\pi_t - \rho_t), \tag{2.112}$$

where $\pi_t = e^{-\beta H_t}/\,\mathrm{Tr}\left(e^{-\beta H_t}\right)$ is the Gibbs equilibrium state. One further research direction would be to see if other master equations can also give rise to speed limit like approximations.

Chapter 3

Correlated Quantum Metrology

Measurement is an essential part of every area of physics from detecting gravitational waves to calibrating lab equipment. Metrology is the study of estimating unknown parameters of a system through measurement. In Chapter 2 we saw that the quantum Fisher information is a measure of the infinitesimal distance between quantum states. We used that fact to calculate the average speed of a quantum state along its trajectory. The Fisher information is also a central quantity in the field of metrology, here the Fisher information is used as a measure of statistical distinguishability. The Cramér-Rao bound puts an upper limit on accuracy with which an unknown parameter can be estimated in terms of the statistical distinguishability. Performing measurements on a quantum system adds several interesting subtleties to the metrology process. When we perform a quantum measurement the result of the measurement influences the state of the system after the measurement. This means that the result of any subsequent measurement can be correlated with the results of the previous measurements. Additionally, using quantum systems allows for freedom in the measurement basis and more general measurements in the form of positive operator-valued measures (POVMs). In this chapter we once again make use of the generalised amplitude damping channel (GADC) as an example system to demonstrate and characterise the effects of temperature on open system dynamics. The Chapter is split into two main parts, in Secs 3.1 and 3.2 we introduce the necessary mathematical material to understand our sequential measurement metrology scheme presented from Sec. 3.3 to Sec 3.5. In Secs 3.6.1 and 3.6.2 we recapitulate the collisional thermometry scheme presented in Refs [143,144] before expanding their analysis to include the presence of stochasticity at the level of the waiting time between collisions, as well as connecting these results to the sequential measurement scheme presented earlier. The main results, and the calculations that generated them, were predominantly done by me with the assistance of collaborators.

3.1 Introduction

The goal when performing a measurement is to determine the value of an unknown parameter. Often it is not possible to exactly determine the value of this parameter either due to statistical

noise or more fundamental considerations such as Heisenberg's uncertainty principle as discussed in the Chapter 2. The Cramér-Rao bound [102, 103] allows us to put a fundamental limit on the variance σ_θ of any unbiased estimator of the parameter θ in terms of the Fisher information associated with those measurements,

$$\sigma_\theta \geq \frac{1}{F_{1:N}(\theta)}, \tag{3.1}$$

where $F_{1:N}(\theta)$ is the Fisher information associated with the outcomes of N measurements. When the outcomes of these N measurements are independent and identically distributed (iid), the Fisher information reduces to $F_{1:N}(\theta) = NF_1(\theta)$. This would be the case, for example, if N probes were allowed to fully thermalise with a large bath and then each was measured.

There are many ways to approach metrology, in this chapter we consider two distinct but closely related approaches, with a particular focus on the estimation of the temperature of a quantum system. Firstly, a sequential measurement setup, this involves having a probe system that can be coupled to an environment and performing measurements on the system at discrete time intervals. The advantages of this approach over standard, probe-based thermometry include that we only need a single probe that is reused in each measurement as opposed to a fresh probe for each measurement. We are also performing measurements on a small system as opposed to a full energy measurement on the environment. Crucially, the sequential measurement setup generates correlations between the measurements and allows the exploitation of these correlations in order to increase the Fisher information. One potential drawback is that it often does not take advantage of the quantum nature of the problem and when it does, the Fisher information can become impractical to calculate.

Another approach we consider is a collisional metrology approach where the measurement is no longer performed on the system itself, but on an auxiliary system that has previously interacted with the system itself. This approach allows for specific kinds of POVMs to be applied easily. It also allows for entanglement to be built up between a number of auxiliary units before the measurement is performed. The main drawback is that it requires a large degree of control over a collisional bath which may not be realistic in practice. Collision models have been used in a wide range of topics in quantum physics; for an in-depth review see Ref. [145]. This framework has been extended to correlated input states and different kinds of interactions [144], as well as possible estimation schemes for post-processing [146]. We extend this collisional approach to allow for stochasticity in the waiting times between the collisions. We show that introducing this stochasticity leads to a broadening range of parameters in which a meaningful advantage can be gained.

We will apply both approaches to the problem of thermometry. Accurately determining the temperature of a physical system is a ubiquitous task. For quantum systems, measuring the temperature becomes a significantly more involved job, in part due to the inherent fragility of quantum states, and more pointedly, because temperature itself is not a quantum observable. Recently, significant advances in thermometry schemes for quantum systems have been proposed [147–152]

(see Ref. [153] for an extensive review). The thermometric precision of a probe in equilibrium with the sample is limited by the thermal Cramér-Rao bound, which is inversely proportional to the heat capacity, C, of the thermometer: $(\Delta T/T)^2 \geq k_B/NC$. However, quantum systems have the additional freedom to exploit resources such as entanglement [154, 155] and coherence [156–158] to gain an advantage over their classical counterpart [54, 159–166]. By making use of these resources, along with correlations between measurement results, it is possible to surpass the thermal Cramér-Rao bound. Interestingly, we establish that the greatest advantage can be gained using purely classical correlations and, therefore, the demonstrated advantage can be gained by performing simple single-qubit measurements.

The remainder of the Chapter is organized as follows. In the rest of the introduction, we define the Fisher information and its quantum generalisation and show how they bound the precision of parameter estimation. In Secs. 3.2 and 3.3 we introduce the sequential measurement scheme and investigate the effects it has on the Fisher information in the presence of different kinds of correlations. We prove in Sec 3.4 that under certain conditions the Fisher information of the sequential measurement scheme can be related to a coarse-grained measurement on the environment. We also discuss possible benchmarks of the scheme. In Sec 3.5 we use the sequential measurement scheme to estimate the temperature of a thermal bath. Sec. 3.6 gives an outline of the various topics and techniques employed in collisional quantum thermometry. These techniques are then examined more closely to determine the exact role of correlations and the free parameters. In Sec. 3.6.3 we introduce stochasticity at the level of the waiting time between collisions. We analyse how this stochasticity affects the precision of the measurements and the form of the optimal measurements. We also discuss how our results extend to different forms of measurements. Some of the following results are based on the work in Ref. [2]. Finally, our conclusions and some further discussions are presented in Sec. 3.7.

3.1.1 Estimation theory

In Sec. 2.2 we considered a real-valued random variable $X : \Omega \to \mathbb{R}$ with a space of possible outcomes, $\omega \in \Omega$. Each of these outcomes occurs with probability $p(\omega)$. We can generalise this concept to a collection of N random variables $X_{1:N} = X_1, ..., X_N$ which can in principle be correlated. These random variables then have an associated probability distribution $p(\omega_{1:N})$. This probability distribution is parameterized by a vector of real numbers $\theta = (\theta_1, ...\theta_k)$. An estimator T is then a function that maps a set of measurement outcomes $\omega_{1:N} = \{\omega_1, ..., \omega_N\}$ to an estimate for the parameter vector, $\tilde{\theta}$. An estimator T is said to be unbiased if $\langle T(X_{1:N}) - \theta \rangle_{p_\theta} = 0$. Where the inner product is defined in the same way as in Sec. 2.2 as

$$\langle A, B \rangle_p = \sum_{\omega \in \Omega} A(\omega) B(\omega) p(\omega). \tag{3.2}$$

We can also define the notion of a covariance matrix σ_{ij} for the estimator T

$$\sigma_{ij} = \langle(\tilde{\theta}_i - \theta_i), (\tilde{\theta}_j - \theta_j)\rangle_{p_\theta}. \tag{3.3}$$

In complete analogy with Eq.(2.39) we can define the Fisher information matrix as

$$[F_{1:N}]_{ij} = \left\langle \frac{\partial}{\partial\theta_i} \log p_\theta(\omega_{1:N}), \frac{\partial}{\partial\theta_j} \log p_\theta(\omega_{1:N}) \right\rangle_{p_\theta}. \tag{3.4}$$

It is then possible to prove the multi-parameter Cramér-Rao bound [103, 167]

$$\sigma - (F_{1:N})^{-1} \geq 0, \tag{3.5}$$

meaning the difference in the two matrices is positive semi-definite. $F_{1:N}^{-1}$ denotes the matrix inverse of the Fisher information matrix.

3.1.2 Quantum estimation theory

A number of things change when we go from classical probability distributions, p_θ, to quantum density matrices ρ_θ. We can have not just classical correlations between our systems, but also quantum correlations, such as entanglement. This allows for the Fisher information of a quantum system to scale with the number of subsystems squared, as opposed to linearly when no quantum correlations are present. We also have additional choices with respect to our measurements. As we discussed in the Chapter 1, the most general evolution of a quantum state that is initially uncorrelated with its environment is described by a completely positive trace-preserving (CPTP) map,

$$\mathcal{E}(\rho_S) = \mathrm{tr}_E \left\{ U(\rho_S \otimes \rho_E)U^\dagger \right\} = \sum_i K_i \rho_S K_i^\dagger, \tag{3.6}$$

where $\{K_i\}$ are the Kraus operators and satisfy $\sum_i K_i^\dagger K_i = \mathbf{I}$. For quantum systems, the most general measurement that we can perform is a positive operator-valued measure (POVM), $\boldsymbol{E}$, defined as a set of positive-definite Hermitian matrices $\{E_\omega\}$ that satisfy the condition $\sum_\omega E_\omega = \mathbf{I}$, where $\omega \in \Omega$ is the set of possible measurement outcomes. When the result of the measurement is ω, corresponding to M_ω, the resulting state of the system after the measurement is given by,

$$\rho_S^\omega = \frac{M_\omega \rho_S M_\omega^\dagger}{\mathrm{Tr}\left(M_\omega \rho_S M_\omega^\dagger\right)}, \tag{3.7}$$

where $M_\omega^\dagger M_\omega = E_\omega$. This means that the outcome of a POVM is not necessarily a pure quantum state but is instead a mixture. From this definition of M_ω we can see that it is not unique because we can always multiply it by a unitary matrix on the left and satisfy $M_\omega^\dagger U^\dagger U M_\omega = M_\omega^\dagger M_\omega = E_\omega$. Despite this arbitrariness the probability of obtaining the measurement result ω from the POVM

only depends on E_ω,

$$p(\omega) = \mathrm{Tr}\left[\rho_S E_\omega\right]. \tag{3.8}$$

Finally, we must generalise the classical Fisher information to apply to quantum systems. As we saw in Sec. 2.2, there are infinitely many ways that the classical Fisher information can be generalised. The problem for quantum speed limits is that we are dealing with a ratio of two quantities, the path length, and the geodesic length, that both depend on the generalisation of the Fisher information. Luckily, for metrology, the quantum Cramér-Rao bound only has the Fisher information in the denominator, therefore the generalisation of the Fisher information that leads to the tightest bound is the smallest one. This happens to always be the one generated by the symmetric logarithmic derivative inner product, which we will call the quantum Fisher information from now on. We can now define the quantum Cramér-Rao bound as

$$\sigma^2 - (\mathcal{F}_{1:N})^{-1} \geq 0 \tag{3.9}$$

where $\mathcal{F}_{1:N}$ is the quantum Fisher information matrix,

$$[\mathcal{F}_{1:N}]_{i,j} = \frac{1}{2}\,\mathrm{Tr}(\rho\{L_i, L_j\}), \tag{3.10}$$

and L_i is the symmetric logarithmic derivative defined implicitly as

$$\frac{\partial}{\partial\theta_i}\rho = \frac{1}{2}(\rho L_i + L_i\rho). \tag{3.11}$$

The quantum Fisher information can also be defined as the classical Fisher information maximised over all possible POVMs. From this point onwards, for simplicity we will just consider the case of single parameter estimation. More information on multiparameter concepts can be found in Ref. [168].

3.2 The Fisher information of correlated processes

Accurately determining the parameter θ will require multiple measurements to be performed and this can be achieved in a number of ways. As mentioned in the introduction, when the outcomes of our measurements are iid, the Fisher information scales as $F_{1:N} = NF_1$. An example of an iid scheme would be to prepare multiple probes in the same initial state ρ_S^0. Each of these probes then interact with the environment in an identical manner. This will be iid in the limit where the weak coupling, Eq. (1.25), and Markovian approximations hold, such as when the environment is very large and the environment correlation timescale is short compared to the system evolution timescale in the interaction picture. We could relax the identically distributed condition by having probes prepared in different initial states, or by performing a different interaction on each probe. The Fisher information in this case still takes the compact form, $F_{1:N} = \sum_{i=1}^{N} F_i$. When we remove the independence requirement and allow correlation this equality no longer holds. Additionally, we

cannot say anything about their relative sizes in full generality, i.e.

$$F_{1:N} \leqslant \sum_{i=1}^{N} F_i. \tag{3.12}$$

Obviously the Cramér-Rao bound,Eq. (3.1), still holds and it is not possible to achieve higher estimation precision by considering the individual measurement distributions separately but it can be a useful benchmark to compare the Fisher information of a correlated process to that of an equivalent independent process to determine if the correlations provide additional precision.

An alternative approach that allows for correlations to be generated is to employ a sequential measurement scheme, where the probe is reused after each measurement [169–173], i.e. after each measurement is performed the *same* probe is allowed to interact with the environment again. This means that the probe state at the start of each interaction cycle will depend on the result of the previous measurements, therefore the results of the measurements are correlated with each other. We once again assume that the system and environment can be approximated as being in a product state, for example, via the weak coupling approximation, or in a collision model setup. If this assumption fails to hold, the evolution of the system between measurements will no longer be described by a CPTP map. We define the map $\Phi_\omega(\varrho)$ that represents one iteration of the sequential measurement process with a specific measurement outcome,

$$\Phi_\omega(\varrho) = \mathcal{E}^\omega\left(\frac{M_\omega \varrho M_\omega^\dagger}{\mathrm{Tr}\left(M_\omega \varrho M_\omega^\dagger\right)}\right), \tag{3.13}$$

where the superscript on $\mathcal{E}^\omega$ denotes that the map applied can depend on the result of the measurement. This means that the state of the system after N measurements with measurement results $\boldsymbol{\omega}_{1:N} = \{\omega_1, \ldots, \omega_N\}$ is given by

$$\rho_S^{\boldsymbol{\omega}_{1:N}} = \Phi_{\omega_N} \circ \cdots \circ \Phi_{\omega_1}(\rho_S^0). \tag{3.14}$$

The probability of obtaining outcome ω_{N+1} on the next measurement is then

$$p(\omega_{N+1}|\boldsymbol{\omega}_{1:N}) = \mathrm{Tr}(\rho_S^{\boldsymbol{\omega}_{1:N}} E_{\omega_{N+1}}), \tag{3.15}$$

with $E_{\omega_i} = M_{\omega_i}^\dagger M_{\omega_i}$. It follows that the Fisher information of this measurement can be calculated as

$$F(\Omega_{N+1}|\boldsymbol{\Omega_{1:N}} = \boldsymbol{\omega}_{1:N}) = \sum_{\omega_{N+1}\in\Omega_{N+1}} \frac{1}{p(\omega_{N+1}|\boldsymbol{\omega}_{1:N})}\left(\frac{\partial}{\partial\theta} p(\omega_{N+1}|\boldsymbol{\omega}_{1:N})\right)^2. \tag{3.16}$$

The average Fisher information on the $(N+1)$th measurement can be calculated by averaging over all measurement outcomes $\boldsymbol{\omega}_N$ for the first N measurements,

$$F(\Omega_{N+1}|\boldsymbol{\Omega_{1:N}}) = \sum_{\boldsymbol{\omega}_{1:N}\in\boldsymbol{\Omega_{1:N}}} p(\boldsymbol{\omega}_{1:N}) F(\Omega_{N+1}|\boldsymbol{\Omega_{1:N}} = \boldsymbol{\omega}_{1:N}). \tag{3.17}$$

We can calculate $p(\boldsymbol{\omega}_{1:N})$ by combining the fact that

$$p(A|B) = \frac{p(A,B)}{p(B)}, \tag{3.18}$$

with Eq. (3.15) and to get,

$$\begin{aligned} p(\boldsymbol{\omega}_{1:N}) &= p(\omega_N|\boldsymbol{\omega}_{1:N-1})p(\boldsymbol{\omega}_{1:N-1}) \\ &= \prod_{i=1}^{N-1} p(\omega_{i+1}|\boldsymbol{\omega}_{1:i}) \\ &= \prod_{i=1}^{N-1} \mathrm{Tr}(\rho_S^{\boldsymbol{\omega}_{1:i-1}} E_{\omega_i}). \end{aligned} \tag{3.19}$$

Subbing this property into the Fisher information results in the following the additivity relation [174]

$$F(A|B) = F(A,B) - F(B). \tag{3.20}$$

By applying this property iteratively in exact analogy to Eq. (3.19) we get

$$F_{1:N} \equiv F(\boldsymbol{\Omega}_{1:N}) = F(\Omega_1) + \sum_{i=2}^{N} F(\Omega_i|\boldsymbol{\Omega_{1:i-1}}). \tag{3.21}$$

For a general POVM, Eq. (3.21) is clearly a complicated object but we will see that under certain conditions this formula can significantly reduce in complexity.

3.2.1 Markov order

If we look at the individual terms in Eq. (3.21), $F(\Omega_k|\boldsymbol{\Omega_{1:k-1}})$, we could imagine a scenario where the Fisher information does not depend on the result of all previous measurements, but say only $\boldsymbol{M}_k$ previous measurements. We can define $\boldsymbol{M}_k$ by

$$\boldsymbol{M}_k = \min\{\ell \text{ s.t. } p(\Omega_k|\boldsymbol{\Omega}_{k-1-\ell:k-1}) = p(\Omega_k|\boldsymbol{\Omega}_{1:k-1})\}, \tag{3.22}$$

i.e. the number of previous measurements that need to be considered to fully determine the probability distribution of the kth measurement [175]. Then the Markov order of the entire process can be defined as the largest $\boldsymbol{M}_k$: $\boldsymbol{M} = \max_k \boldsymbol{M}_k$. This value can then be thought of as the memory depth of the system. We can then use this property to separate the terms in Eq. (3.21) giving,

$$F_{1:N} = F_{1:\boldsymbol{M}} + \sum_{k=1}^{N-\boldsymbol{M}} F_{\boldsymbol{M}+k|k:\boldsymbol{M}+k-1}, \tag{3.23}$$

where we have defined

$$F_{i+j|j:i+j-1} = F(\Omega_{i+j}|\boldsymbol{\Omega_{j:i+j-1}}). \tag{3.24}$$

Then if the process is a stationary process, i.e. it satisfies

$$p(\boldsymbol{\Omega}_{k:m}) = p(\boldsymbol{\Omega}_{k+\ell:m+\ell}) \tag{3.25}$$

for any integers k, m, l with $m > k$, $k > \boldsymbol{M}$ and $l \geq 0$ we can further simplify [175] Eq. (3.23) to

$$F_{1:N} = F_{1:\boldsymbol{M}} + (N - \boldsymbol{M})F_{\boldsymbol{M}+1|1:\boldsymbol{M}}. \tag{3.26}$$

In the limit of a large number of measurements the Fisher information can be approximated as

$$F_{1:N} \approx NF_{\boldsymbol{M}+1|1:\boldsymbol{M}}, \tag{3.27}$$

or, more precisely, the Fisher information rate tends to

$$F_{\boldsymbol{M}+1|1:\boldsymbol{M}} = \lim_{N\to\infty} \frac{F_{1:N}}{N}. \tag{3.28}$$

This will be, in principle, significantly easier to calculate than the entire Fisher information.

3.3 Sequential measurement metrology

If we perform a POVM on our system but ignore the measurement result we must average over the state of our system for all measurement outcomes

$$\rho_S^{\Omega} = \sum_{\omega} p(\omega)\rho_S^{\omega} = \sum_{\omega} p(\omega)\frac{M_\omega \rho_S M_\omega^\dagger}{p(\omega)} = \sum_{\omega} M_\omega \rho_S M_\omega^\dagger. \tag{3.29}$$

We see that the result of performing a POVM and ignoring the measurement result is a CPTP map. We can apply a similar treatment to the sequential measurement process,

$$\begin{aligned} \Phi_{\Omega_i}(\rho) &= \sum_{\omega_i} p(\omega_i)\Phi_{\omega_i}(\rho) \\ &= \sum_{\omega_i} \mathcal{E}^{\omega_i}\left(M_{\omega_i}\rho M_{\omega_i}^\dagger\right), \end{aligned} \tag{3.30}$$

which results in another CPTP map. The quantum equivalent of a stationary process is a steady state or fixed point, ρ^*, of a CPTP map that satisfies,

$$\Phi_{\Omega_i}(\rho^*) = \rho^*. \tag{3.31}$$

The steady state of Φ can in principle be different from $\mathcal{E}$. In this scenario the steady state of Φ would represent a stroboscopic steady state [143] that is reached periodically after both the measurement map and $\mathcal{E}$ have been applied. If we assume that the map Φ_{Ω_i} is the same for each iteration and the initial state of the process is the steady state of Φ, the Fisher information will

satisfy Eq. (3.26). In general, the process of applying the map, Φ, N times will have a Markov order of N. However, in many cases the correlations between measurements decay exponentially and therefore, a fixed Markov order becomes a great approximation. Such an example would when the map Φ_{Ω_i} is a mixing map [176], i.e. it satisfies

$$\Phi_{\Omega_N} \circ \cdots \circ \Phi_{\Omega_1}(\rho_S^0) \to \rho^* \quad N \to \infty \tag{3.32}$$

for all initial states, ρ_S^0, with a unique steady state ρ^*. In such cases it is also possible to show that in the large N limit, both the measurement results, and the correlations between them satisfy the central limit theorem and become approximately Gaussian [172]. This provides another method of estimating the unknown parameter when the exact probability distribution is too difficult to calculate. From here on, we will restrict our analysis to mixing maps which converge to a unique steady state in large N limit. Mixing maps have the property that they have a single non-degenerate eigenvalue, of unit value, corresponding to the steady state [176]. It could be fruitful to examine other families of CPTP maps with multiple fixed points, particularly if the behaviour of these fixed points exhibit a strong dependence on the unknown parameter.

A particularly elegant and useful instance of fixed Markov order occurs when the POVM is a projective measurement onto some basis $\{|k\rangle\}$. In this case, the Markov order is $\boldsymbol{M} = 1$ since the projection erases all information about the previous state, giving us

$$F_{1:N} = F_1 + (N-1)F_{2|1}, \tag{3.33}$$

with

$$F_{2|1} = \sum_k q_k F_{2|1=k}. \tag{3.34}$$

In exact analogy with Eq. (3.16) we have

$$F_{2|1=k} = \sum_{k'} \frac{1}{P(k'|k)} \left(\frac{\partial}{\partial\theta} P(k'|k)\right)^2, \tag{3.35}$$

and

$$P(k'|k) = \langle k'| \mathcal{E}^k \left(|k\rangle\langle k|\right) |k'\rangle . \tag{3.36}$$

Since we know that our initial state is a steady state of the map Φ this implies that q_k in Eq. (3.34) satisfies the steady state equation,

$$q_k = \sum_{k'} q_{k'} P(k|k'). \tag{3.37}$$

Projective measurements have the additional benefit of leaving the system and environment in a product state after the measurement is performed. This allows us to describe the evolution between measurements via a CPTP map even when strong quantum correleations are generated between the system and environment. Allowing the map $\mathcal{E}$ to depend on the result of the previous

measurement lets us incorporate feedback control [177, 178] into our setup which can allow us to achieve larger amounts of precision. In our sequential measurement setup, the simplest and most realistic way to incorporate measurement feedback would be to have a different waiting time between measurements based on the result of the previous measurement.

3.4 Comparison to other strategies

As we proved in Eq. (3.12), correlations between measurement results does not necessarily provide a boost to the achievable precision as quantified through the Fisher information. In the context of our sequential measurement setup, this implies

$$F_{2|1} \lesseqgtr F_1. \tag{3.38}$$

A trivial example of a scenario where the addition of correlations has a negative effect is to perform two projective measurements in the energy basis on the same closed quantum system. The probability distribution of both of the measurements would be identical and therefore, $F_1 = F_2$, but the result of the second measurement is always exactly the same as the first and therefore contains no additional information about the unknown parameter, i.e. $F_{1:2} = F_1$.

3.4.1 Comparison to F_1

The most natural way to identify if the correlations are having a positive or negative effect on the Fisher information would be to compare $F_{2|1}$ to F_1. Unfortunately, this comparison is not always fair because information about F_1 is not always easily obtainable. One important reason for this is that the steady state of Φ will, in general, not be equal to the steady state of the map $\mathcal{E}$ by itself and can have a complicated dependence on the unknown parameter θ. Even estimating q_k from a series of measurements $\boldsymbol{\omega}_{1:N}$ is not straightforward. This is because even though the Fisher information $F_{2|1}$ depends only on the result of the previous measurement, the probability $p(\omega_{N+1}|\boldsymbol{\omega}_{1:N})$ depends on all previous measurements. Constructing an estimator for q_k from this data could be difficult, this is made even more challenging when q_k depends on the unknown parameter θ as we will discuss later on in Sec. 3.6.2. This problem and possible solutions have been discussed recently in [179]. Even when we can create a reliable estimator for q_k, F_1 is still not a reasonable comparison to $F_{2|1}$ because there is no useful way to reliably generate F_1 worth of Fisher information. The only way to reliably generate the steady state of Φ would be to perform the map many times and forget all the measurement results but this is obviously not a useful strategy.

There are certain edge cases where F_1 is a useful benchmark, specifically when the steady state of Φ is easy to prepare without explicit knowledge of θ. To make this clear we can consider a specific example, the case of a partial swap interaction between two systems A and B. The unitary that generates the partial swap between subsystems A and B is given by $U_S = -i\sqrt{1-a^2}I_{AB}+aS$

where S is the full swap operator between $\mathcal{H}_A$ and $\mathcal{H}_B$, $S(\rho_A \otimes \rho_B)S = (\rho_B \otimes \rho_A)$. The action of this unitary on subsystem A is given by,

$$\begin{aligned}\mathcal{E}(\rho_A) &= \mathrm{Tr}_B[U_S(\rho_A \otimes \rho_B)U_S^\dagger] \\ &= (1-a^2)\rho_A + a^2\rho_B + \mathrm{Tr}_B[i\sqrt{1-a^2}(S(\rho_A \otimes \rho_B) - (\rho_A \otimes \rho_B)S)].\end{aligned} \tag{3.39}$$

For sequential projective measurements we know that the initial state will always be a pure state in the basis $\{k\}$, therefore, the final term in the above equation becomes

$$\begin{aligned}\mathrm{Tr}_B[...] &= \sum_n p_n \,\mathrm{Tr}_B[i\sqrt{1-a^2}(S(|k'\rangle\langle k'| \otimes |n\rangle\langle n|) - (|k'\rangle\langle k'| \otimes |n\rangle\langle n|)S] \\ &= \sum_n p_n i\sqrt{1-a^2}(\langle k'|n\rangle\, |k'\rangle\langle n| - \langle n|k'\rangle\, |n\rangle\langle k'|).\end{aligned} \tag{3.40}$$

The only contribution of this term to $P(k|k')$ is,

$$\begin{aligned}\langle k|\mathrm{Tr}_B[...]|k\rangle &= \sum_n p_n i\sqrt{1-a^2}(\langle n|k'\rangle \langle k|n\rangle \langle k'|k\rangle - \langle k'|n\rangle \langle k|k'\rangle \langle n|k\rangle) \\ &= \sum_n p_n i\sqrt{1-a^2}(\langle n|k'\rangle \langle k|n\rangle - \langle k'|n\rangle \langle n|k\rangle)\delta_{k,k'} = 0.\end{aligned} \tag{3.41}$$

The final term has no contribution, meaning that,

$$P(k|k') = \langle k|\mathcal{E}(|k'\rangle\langle k'|)|k\rangle = (1-a^2)\delta_{k,k'} + a^2 \langle k|\rho_B|k\rangle\,. \tag{3.42}$$

Knowledge of $P(k|k')$ is sufficient to evaluate the steady state equation Eq. (3.37),

$$\begin{aligned}q_k &= \sum_{k'} q_{k'} P(k|k') \\ &= \sum_{k'} q_{k'} \left((1-a^2)\delta_{k,k'} + a^2 \langle k|\rho_B|k\rangle\right) \\ &= q_k(1-a^2) + a^2 \langle k|\rho_B|k\rangle\,.\end{aligned} \tag{3.43}$$

Rearranging and solving this gives us the steady state,

$$q_k = \langle k|\rho_B|k\rangle\,. \tag{3.44}$$

We can even calculate the Fisher information assuming that a is independent of θ

$$F_{2|1} \leq \sum_{k'} q_{k'} \sum_k \frac{a^4(\langle k|\partial_\theta \rho_B|k\rangle)^2}{(1-a^2)\delta_{k,k'} + a^2\langle k|\rho_B|k\rangle} \leq a^2 F_1 \leq F_1. \tag{3.45}$$

This tells us that, for the partial swap, the addition of correlations is not advantageous when the interaction strength, a, is independent of θ. When the interaction strength depends on θ this will generate additional terms in the Fisher information that can be positive or negative.

This is a very specific example where the steady state has a nice, closed form, and can be prepared reliably without knowledge of θ, in general this is not possible. When the map $\mathcal{E}$ has a unique steady state, it could be reasonable to compare $F_{2|1}$ to the quantum Fisher information of that steady state as was done in, e.g. Refs. [2, 143, 144].

3.4.2 Comparison to F_{iid}

Perhaps a fairer, more meaningful comparison for $F_{2|1}$ would be to prepare N different probes in the same state and perform one iteration of the map $\mathcal{E}$ on each probe [173], followed by a measurement. If we choose the initial state to be an element of the measurement basis, $|k\rangle$, the Fisher information of each probe, F_{iid}, will be exactly equal to $F_{2|1=k}$. Then, it is clear from the form of Eq. (3.34) that we can always choose the initial state, $|k\rangle$, for which this Fisher information is largest which means that $F_{\text{iid}} \geq F_{2|1}$. An obvious drawback of this setup is that it requires the preparation of N probes in a specific initial state, and the best initial state might depend on the unknown parameter of interest making choosing the optimal initial state problematic. Another strategy would be to reset a single probe to the initial state after every measurement, but this could take a long time, especially when the initial state is a pure state. Furthermore, this comparison sheds no light on whether the correlations between the measurements have a positive or negative effect on the achievable precision. In contrast, the sequential measurement setup needs only one probe and with the relevance of the initial state being significantly diminished since all the information about it is erased after the first measurement.

3.4.3 Comparison to coarse-grained measurements

Another interesting comparison is to a coarse-grained measurement on the environment with the same number of outcomes as the dimension of our probe system. In Ref. [180] the authors proved that when the environment is in a thermal state, the maximal information about the temperature of the environment that can be obtained from a d dimensional probe is always less than or equal to the information gained from the optimal coarse-grained measurement with d outcomes. We can prove a more general result by considering the setup from Eq (3.6) of a general system-environment evolution with U and ρ_S independent of θ and $\rho_S = \sum_i s_i \, |s_i\rangle\langle s_i|$. When this is not the case, it is possible to violate the following bound. The addition of an auxiliary system such as was considered in Ref. [180], has no effect on the following proof as long as the auxiliary system also has no θ dependence. Our first step is to derive the map $\mathcal{E}'(\rho_E) = \mathcal{E}(\rho_S)$,

$$
\begin{aligned}
\mathcal{E}(\rho_S) &= Tr_E[U(\rho_S \otimes \rho_E)U^\dagger] \\
&= \sum_i (\mathbf{I}_S \otimes \langle b_i|)[U(\sum_i s_i \, |s_i\rangle\langle s_i| \otimes \rho_E)U^\dagger](\mathbf{I}_S \otimes |b_i\rangle) \\
&= \sum_{i,j} s_j (\mathbf{I}_S \otimes \langle b_i|)[U(|s_j\rangle \otimes \mathbf{I}_E)(\mathbf{I}_S \otimes \rho_E)(\langle s_j| \otimes \mathbf{I}_E)U^\dagger](\mathbf{I}_S \otimes |b_i\rangle) \\
&= \sum_{i,j} s_j [(\mathbf{I}_S \otimes \langle b_i|)U(|s_j\rangle \otimes \mathbf{I}_E)]\rho_E[(\langle s_j| \otimes \mathbf{I}_E)U^\dagger(\mathbf{I}_S \otimes |b_i\rangle)] \\
&= \sum_{i,j} L_{i,j}\rho_E L_{i,j}^\dagger \\
&= \mathcal{E}'(\rho_E),
\end{aligned}
\tag{3.46}
$$

where $\{|b_i\rangle\}$ is an arbitrary basis of $\mathcal{H}_E$ and $L_{i,j} = \sqrt{s_j}(\mathbf{I}_S \otimes \langle b_i|)U(|s_j\rangle \otimes \mathbf{I}_E)$. It is clear the $L_{i,j}$ is independent of θ as long as U is independent of θ. The quantum Fisher information of $\mathcal{E}(\rho_S)$ is given by the Fisher information of the probabilities $p_i(\mathcal{E}(\rho_S), E_i) = \mathrm{Tr}[\mathcal{E}(\rho_S)E_i]$ maximised over all possible POVMs $\{E_i\}$. Where $\{E_i\}$ is a set of Hermitian, positive semi-definite matrices that sum to the identity. Let us now look at the quantum Fisher information of $\mathcal{E}(\rho_S) = \mathcal{E}'(\rho_E) = \sum_{i,j} L_{i,j}\rho_E L_{i,j}^\dagger$. We will label the optimal POVM as $\{F_i\}$,

$$
\begin{aligned}
p_i(\mathcal{E}(\rho_S), F_i) &= p_i(\mathcal{E}'(\rho_E), F_i) \\
&= \mathrm{Tr}[\mathcal{E}'(\rho_E)F_i] = \mathrm{Tr}\left[\sum_{j,k} L_{j,k}\rho_E L_{j,k}^\dagger F_i\right] \\
&= \sum_{j,k} \mathrm{Tr}\Big[L_{j,k}\rho_E L_{j,k}^\dagger F_i\Big] = \sum_{j,k} \mathrm{Tr}\Big[\rho_E L_{j,k}^\dagger F_i L_{j,k}\Big] \\
&= \mathrm{Tr}\left[\rho_E \left(\sum_{j,k} L_{j,k}^\dagger F_i L_{j,k}\right)\right].
\end{aligned}
\tag{3.47}
$$

We can now define a new set of matrices $G_i = \sum_{j,k} L_{j,k}^\dagger F_i L_{j,k}$, it is important to note that $\{G_i\}$ has the same number of elements as $\{F_i\}$. Now we need to prove that $\{G_i\}$ is a valid POVM on $\mathcal{H}_E$. Since F_i is Hermitian, G_i clearly is too. A matrix is positive semi-definite if and only if it can be decomposed into a product $F_i = M_i^\dagger M_i$. Since $\{F_i\}$ is a POVM we know that it can be decomposed. Therefore we can write $G_i = \sum_{j,k} L_{j,k}^\dagger M_i^\dagger M_i L_{j,k} = \sum_{j,k} K_{i,j,k}^\dagger K_{i,j,k}$ with $K_{i,j,k} = M_i L_{j,k}$. This means G_i is the sum of positive semi-definite matrices and is therefore also

positive semi-definite. The last thing to show is that $\{G_i\}$ sums to the identity,

$$\sum_i G_i = \sum_i \sum_{j,k} L_{j,k}^\dagger F_i L_{j,k} \tag{3.48}$$

$$= \sum_{j,k} L_{j,k}^\dagger \left(\sum_i F_i \right) L_{j,k} = \sum_{j,k} L_{j,k}^\dagger L_{j,k} \tag{3.49}$$

$$= \sum_{j,k} s_k (\langle s_k| \otimes \mathbf{I}_E) U^\dagger (\mathbf{I}_S \otimes |b_j\rangle)(\mathbf{I}_S \otimes \langle b_j|) U (|s_k\rangle \otimes \mathbf{I}_E)$$

$$= \sum_k s_k (\langle s_k| \otimes \mathbf{I}_E) U^\dagger (\mathbf{I}_S \otimes \sum_j |b_j\rangle\langle b_j|) U (|s_k\rangle \otimes \mathbf{I}_E)$$

$$= \sum_k s_k (\langle s_k| \otimes \mathbf{I}_E) U^\dagger U (|s_k\rangle \otimes \mathbf{I}_E)$$

$$= \sum_k s_k \mathbf{I}_E = \mathbf{I}_E$$

This implies that the quantum Fisher information of $\mathcal{E}(\rho_S)$, $\mathcal{F}(\mathcal{E}(\rho_S))$ is upper bounded by the optimal coarse-grained measurement on ρ_E with the same number of outcomes as the dimension on ρ_S which we will denote by $F(\rho_E, G_i^*)$. Finally, we know that $F_{2|1=k} = F(\mathcal{E}^{k'}(|k'\rangle\langle k'|), |k\rangle\langle k|)$ which implies

$$F_{2|1} = \sum_{k'} q_{k'} F_{2|1=k} \leq \sum_{k'} q_{k'} \mathcal{F}\left(\mathcal{E}^{k'}\left(|k'\rangle\langle k'|\right)\right) \tag{3.50}$$

$$\leq \sum_{k'} q_{k'} F(\rho_E, G_i^*) = F(\rho_E, G_i^*). \tag{3.51}$$

This gives us a final chain of inequalities when U and ρ_S in Eq. (3.6) are independent of θ

$$F_{2|1} \leq F_{\text{iid}} \leq F(\rho_E, G_i^*) \tag{3.52}$$

where $\{G_i^*\}$ is the optimal coarse-grained measurement with the same dimension as ρ_S. This result is also interesting when the environment has a smaller dimension than the system, such as might be the case in a collision model setup. In this scenario, the Fisher information we can obtain from measuring the system is bounded by the quantum Fisher information of the environment, therefore larger probes are not necessarily more informative.

3.5 Sequential measurement thermometry

While Eq. (3.52) bounds how large the Fisher information of a sequential measurement process can be when the interaction between probe and environment is *independent* of the parameter of interest, θ, there are many relevant scenarios where U explicitly depends on θ. Such examples include when θ is a property of the system Hamiltonian, such as the Rabi oscillation frequency [171] or, as we will focus on in this Chapater, thermometry where the thermalisation rate of the system depends on the temperature of the environment [143, 173]. In these cases, it is possible for

the sequential measurement process to achieve a higher sensitivity over the alternative methods discussed in the previous section.

We choose to focus on the problem of measuring the temperature of a bath that is coupled to our probe system. The natural benchmark for any thermometry protocol is the quantum Fisher information of a probe in thermal equilibrium. We are assuming that we do not have access to measuring the bath itself so we will compare the sequential measurement scheme to a number of thermal probes of the same dimension as the system. Once the probes have fully thermalised they are in a state commonly referred to as the Gibbs state,

$$\rho_{th} = \frac{e^{-\beta H_S}}{\mathrm{Tr}\left[e^{-\beta H_S}\right]}, \tag{3.53}$$

where $\beta = \frac{1}{k_B T}$ is the inverse temperature. The optimal measurement basis for such a system is simply the energy basis which allows us to define the thermal Fisher information,

$$\mathcal{F}_{th} = \frac{C}{k_B T^2}, \qquad C = \frac{\langle H_S^2\rangle - \langle H_S\rangle^2}{k_B T^2}, \tag{3.54}$$

where C is the heat capacity of the probe, H_S is the probe Hamiltonian. From here on out we will use units of $k_B = 1$. We consider the optimal N-level probes for estimating temperature in the Gibbs state, derived by Correa *et. al.* [4], that consist of a non-degenerate ground state and a single, $(N-1)$ degenerate excited state described by the Hamiltonian,

$$H_S = e_0 \left|e_0\right\rangle\!\left\langle e_0\right| + \sum_{i=1}^{N-1} e_1 \left|e_i\right\rangle\!\left\langle e_i\right|, \tag{3.55}$$

with energy spacing $e_0 - e_1 = \Omega$. To find C, we need to calculate $\langle H_S^2\rangle$ and $\langle H_S\rangle$ with the expectation value taken with respect to

$$\begin{aligned} \rho_{th} &= \frac{e^{-\beta H_S}}{\mathrm{Tr}\left[e^{-\beta H_S}\right]} \\ &= \frac{1}{e^{-\beta e_0} + (N-1)e^{-\beta e_1}} \left(e^{-\beta e_0} \left|e_0\right\rangle\!\left\langle e_0\right| + \sum_{i=1}^{N-1} e^{-\beta e_1} \left|e_i\right\rangle\!\left\langle e_i\right| \right) \\ &= \frac{1}{1 + (N-1)e^{\beta\Omega}} \left|e_0\right\rangle\!\left\langle e_0\right| + \sum_{i=1}^{N-1} \frac{1}{e^{-\beta\Omega} + (N-1)} \left|e_i\right\rangle\!\left\langle e_i\right|. \end{aligned} \tag{3.56}$$

Then using this to calculate the two expectation values gives,

$$\begin{aligned} \langle H_S\rangle^2 &= \left(\mathrm{Tr}[H_S \rho_{th}]\right)^2 \\ &= \frac{1}{\left(e^{-\beta e_0} + (N-1)e^{-\beta e_1}\right)^2} \left(e_0 e^{-\beta e_0} + (N-1) e_1 e^{-\beta e_1} \right)^2 \\ &= \frac{1}{\left(1 + (N-1)e^{\beta\Omega}\right)^2} \left(e_0 + (N-1) e_1 e^{\beta\Omega} \right)^2, \end{aligned} \tag{3.57}$$

and

$$\begin{aligned}\langle H_S^2\rangle &= \mathrm{Tr}\Big[H_S^2\rho_{th}\Big] \\ &= \frac{1}{e^{-\beta e_0}+(N-1)e^{-\beta e_1}}\left(e_0^2e^{-\beta e_0}+(N-1)e_1^2e^{-\beta e_1}\right) \\ &= \frac{1}{1+(N-1)e^{\beta\Omega}}\left(e_0^2+(N-1)e_1^2e^{\beta\Omega}\right).\end{aligned} \tag{3.58}$$

Finally, subbing this into the thermal Fisher information we have

$$\begin{aligned}F_{th} &= \beta^4(\langle H_S^2\rangle - \langle H_S\rangle^2) \\ &= \beta^4\frac{\left(1+(N-1)e^{\beta\Omega}\right)\left(e_0^2+(N-1)e_1^2e^{\beta\Omega}\right)-\left(e_0+(N-1)e_1e^{\beta\Omega}\right)^2}{\left(1+(N-1)e^{\beta\Omega}\right)^2} \\ &= \beta^4\frac{(N-1)\Omega^2e^{\beta\Omega}}{\left(1+(N-1)e^{\beta\Omega}\right)^2}.\end{aligned} \tag{3.59}$$

One further step we can take is to make the substitution $\bar{n} = 1/(e^{\hbar\Omega/k_BT}-1)$, $\bar{n}$ is commonly known as the mean occupation number. In terms of $\bar{n}$ the thermal Fisher information is,

$$\begin{aligned}F_{th} &= \beta^4\frac{(N-1)\Omega^2\bar{n}(1+\bar{n})}{(1+N\bar{n})^2} \\ &= \frac{(N-1)}{\bar{n}(1+\bar{n})(1+N\bar{n})^2}\left(\frac{\partial\bar{n}}{\partial T}\right)^2.\end{aligned} \tag{3.60}$$

This substitution is useful because when we are comparing our sequential measurement scheme to the thermal Fisher information, the derivative will cancel and we can get results that only depend on the ratio Ω/T.

Following Ref. [4], we model the environment as a bosonic heat bath. Our total Hamiltonian is therefore

$$H_{\text{tot}} = H_S + \sum_\mu \omega_\mu b_\mu^\dagger b_\mu + X\otimes\omega_\mu g_\mu(b_\mu+b_\mu^\dagger), \tag{3.61}$$

where $X = \sum_{i\neq 0}|e_0\rangle\langle e_i| + |e_i\rangle\langle e_1|$ is a generalisation of σ_x to high dimensional probes. We choose the coupling constant to be $g_\mu = \sqrt{\gamma\omega_\mu}$, implying a flat spectral density [151],

$$J(\omega) \propto \sum_\mu \frac{g_\mu^2}{\omega_\mu}\delta(\omega-\omega_\mu) = \gamma. \tag{3.62}$$

Under the assumptions used in Chapter 1 a Lindblad master equation, Eq. (1.35), can be derived that leads to the following evolution,

$$\dot{\rho} = \gamma(1+\bar{n})\mathcal{D}(\rho) + \gamma\bar{n}\mathcal{D}^\dagger(\rho). \tag{3.63}$$

The dissipator,

$$\mathcal{D}(\varrho) = \sum_{i=1}^{N-1} L_i \rho L_i^\dagger - \frac{1}{2}\{L_i^\dagger L_i, \rho\}, \tag{3.64}$$

with $L_i = |e_0\rangle\langle e_i|$ describes the transitions from excited to ground states. The steady state of this master equation is the Gibbs thermal state. Although the choice of a flat spectral density may seem restrictive, Correa *et al.* [151] show that changing the spectral density is equivalent to a re-scaling of the time parameter for the purpose of estimating the temperature. This implies that the following analysis will hold for any spectral density as long as the environment correlation timescale is sufficiently short (we refer the interested reader to Ref. [10] Section 3.4 for a more detailed discussion of when the master equation formalism holds for different spectral densities). For a two-level system this setup is a form of the spin-boson model [10, 181] and is also often referred to as the generalised amplitude damping channel introduced in Chapter 2.

In the sequential measurement scheme, the state of the system before the measurement will generally depend on the unknown temperature, but we can still say something about the steady state, $\Phi_{\Omega_i}(\rho^*) = \rho^*$ from Eq. (3.31) under certain conditions. We will choose to measure in the energy basis of the system Hamiltonian and apply the same map regardless of the result of the previous measurement. The energy basis is the optimal measurement basis for both the thermal probes and the sequential measurement scheme, although we remark that the maximum Fisher information is not significantly smaller for other measurement bases. By applying this map to the Gibbs state,

$$\begin{aligned}
\Phi_{\Omega_i}(\rho_{th}) &= \sum_{\omega_i} \mathcal{E}\left(M_{\omega_i}\rho_{th}M_{\omega_i}^\dagger\right) \\
&= \mathcal{E}\left(|e_0\rangle\langle e_0|\,\rho_{th}\,|e_0\rangle\langle e_0|\right) + \sum_{i=1}^{N-1} \mathcal{E}\left(|e_i\rangle\langle e_i|\,\rho_{th}\,|e_i\rangle\langle e_i|\right) \\
&= \mathcal{E}(\rho_{th}) \\
&= \rho_{th},
\end{aligned} \tag{3.65}$$

we can see that the Gibbs state is a steady state of the sequential measurement protocol. This means that the steady state probabilities are given by the Boltzmann distribution, which for the ground state gives,

$$\begin{aligned}
p_0 &= \frac{e^{-\beta e_0}}{e^{-\beta e_0} + (N-1)e^{-\beta e_1}} \\
&= \frac{1}{1 + (N-1)e^{\beta\Omega}} \\
&= \frac{1}{1 + (N-1)\frac{\bar{n}}{1+\bar{n}}} \\
&= \frac{1+\bar{n}}{1+N\bar{n}}.
\end{aligned} \tag{3.66}$$

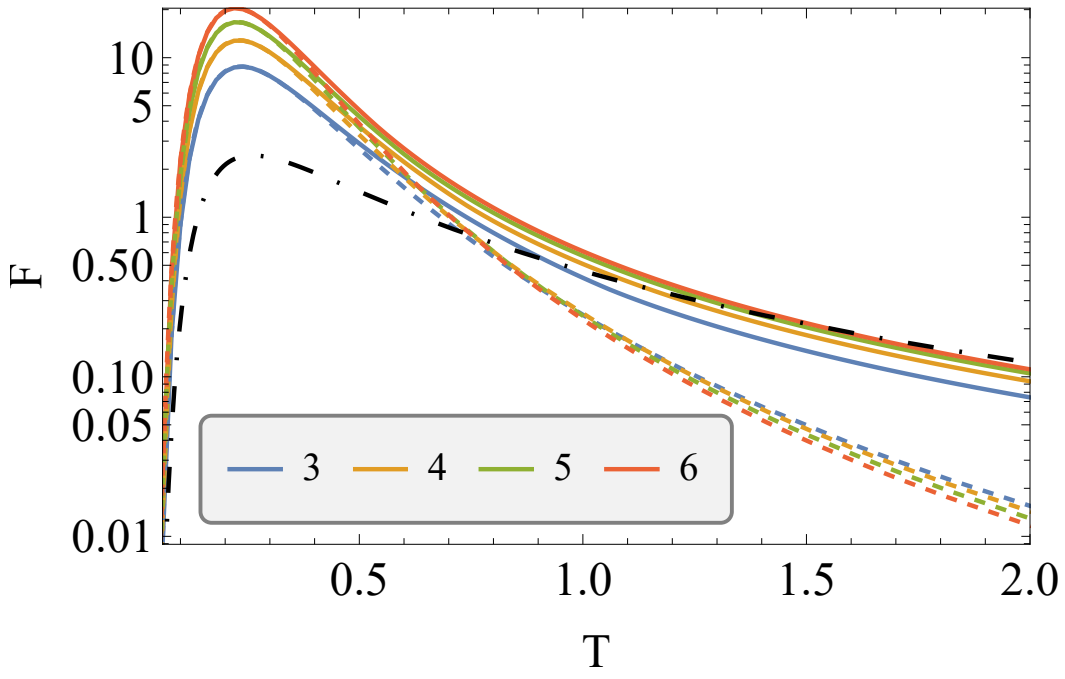

Figure 3.1: Log plot of the Fisher information as a function of temperature of optimal N dimensional probes [4] in their Gibbs state (dashed lines) and in the sequential measurement setup (solid lines). The black dashed, dotted line represents the Fisher information of a harmonic oscillator in the Gibbs state. We fix $\Omega = 1$.

Given that the probabilities sum to 1 and all excited state probabilities are equal we get $p_i = \frac{\bar{n}}{1+N\bar{n}}$ for all $i \neq 0$. This result applies to the behaviour of the system averaged over all measurement results, for each individual measurement result the system is not in the Gibbs state when measured because the state has not fully thermalised. This state can contain additional information about the temperature in the form of the thermalisation rate [143], we can see that the master equation depends on the temperature due to the presence of $\bar{n}$. If the thermalisation rate was temperature independent then the bound from Eq. (3.52) would apply and no advantage could be gained from correlations. Another area that we can find advantage over the thermal Fisher information is in the freedom to apply different quantum maps to our system depending on the result of the previous measurement. In practice this could be quite difficult but one adjustment that we can definitely make is to change the waiting time between measurements based on the result of the previous measurement. This will change the map $\mathcal{E}^k$, resulting in a different $P(k|k')$ and consequently $F_{2|1=k}$. Giving this additional freedom to the map means that our assumptions for deriving Eq. (3.65) no longer hold and therefore, the steady state of this map is not necessarily the Gibbs state. Still, in most cases repeated applications of the map Φ_{Ω_i} will lead to the steady state.

Correa *et. al.* [4] showed that these highly degenerate probes achieve the highest Fisher information possible when optimised over the energy splitting, Ω. This means that there is a

specific value of $\bar{n}$ where the probes give the largest Fisher information. In general, since the temperature is the unknown parameter that we are trying to estimate it is not always going to be possible to select the frequency, Ω, such that $\bar{n}$ is optimal. The optimal value of $\bar{n}$ also depends on the dimension of the probe, getting smaller as the number of degenerate excited states increases. We can see these properties more explicitly when looking at Fig 3.1. The coloured, dashed lines represent the Fisher information of the thermalised probes, $\mathcal{F}_{th}^{N}$, this peaks around $T = 0.2$ and falls off very quickly with increasing temperature. Even though the Gibbs states of these probes give the largest Fisher information when maximised over all values of Ω, they are not necessarily optimal for a different value of $\bar{n}$. If we look closely we can see that around $T = 1$, the Fisher information of the thermal probes all cross and at $T = 2$, the $N = 3$ probe now has the largest Fisher information and $N = 6$ the smallest. This is clear evidence that, these highly degenerate probes are not optimal for all values of $\bar{n}$. The solid lines correspond to the Fisher information of the sequential measurement scheme where the measurement times have been optimized to provide the largest possible Fisher information. In contrast to the thermal Fisher information, $F_{2|1}$ continues to increase as the dimension of the probes increases for all values of $\bar{n}$. For small values of $\bar{n}$ the $\mathcal{F}_{th}^{N}$ is very similar to $F_{2|1}$ but the scaling of $F_{2|1}$ is significantly better in the large T limit. Although the sequential measurement scheme provides no advantage at the optimal value of Ω, the fact remains that this optimal value is itself temperature dependent. Thus, ensuring a higher Fisher information in across a broader parameter range is still important when no prior information about the temperature is available since it provides a more accurate means to identify the most relevant parameter region, where more refined estimation techniques can then be applied. Additionally, the sequential measurement scheme can allow for a shorter time between measurements because the system does not need to fully thermalise after each measurement. Finally, the black dashed line represents the Fisher information of a thermalised Harmonic oscillator which is fully determined by the covariance matrix [151]

$$\boldsymbol{\sigma}_T = \coth\left(\frac{\Omega}{2T}\right)\mathbf{I}_2. \tag{3.67}$$

The quantum Fisher information can then be calculated from the following expression [168],

$$\mathcal{F}_{\mathsf{ho}} = \mathrm{Tr}\left[G_\theta \frac{\partial}{\partial\theta}\boldsymbol{\sigma}_T\right]. \tag{3.68}$$

G_θ can be expressed as

$$G_\theta = -\frac{4c^2-1}{4c^2+1}\sigma_y\left(\frac{\partial}{\partial\theta}J\right)\sigma_y, \tag{3.69}$$

where $c = \sqrt{\det\boldsymbol{\sigma}_T}$ and

$$J = \frac{\boldsymbol{\sigma}_T}{4c^2-1}. \tag{3.70}$$

Subbing Eq. (3.67) into this we get,

$$\mathcal{F}_{\mathsf{ho}} = \frac{\Omega^2\,\mathrm{csch}\left(\frac{\Omega}{2T}\right)^2}{8T^4}. \tag{3.71}$$

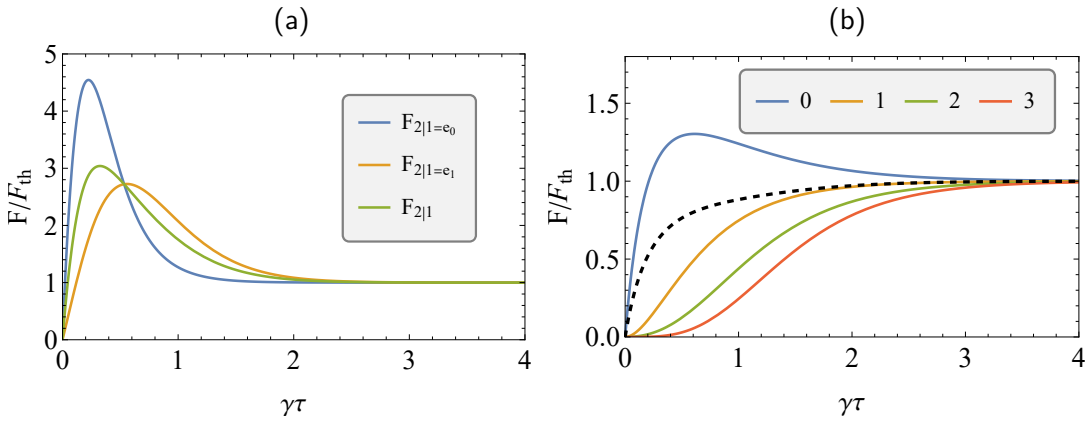

Figure 3.2: **(a)** The blue (orange) line shows the value of the Fisher information when the result of the previous measurement was the ground (excited) state. The green line is the average Fisher information, $F_{2|1}$ that is obtained in each measurement of the sequential measurement process. We (arbitrarily) fix $N = 4$. **(b)** The Fisher information of the Harmonic oscillator for various outcomes of the energy measurement. The black dashed line shows the Fisher information averaged over all measurement outcomes. In each of the above plots we have set $\bar{n} = 1$.

The optimal measurement is a projective measurement in the energy basis [180]. We see that it has the smallest peak but also has the best scaling in the large T limit.

In Fig. 3.2(a), we (arbitrarily) fix $N = 4$ and demonstrate that the sequential measurement scheme can achieve a significant advantage over $\mathcal{F}_{th}$ for $\bar{n} = 1$. These results are qualitatively similar for all sufficiently large values of $\bar{n}$ and in fact the advantage gets larger as $\bar{n}$ gets larger at the cost of the absolute value of the Fisher information getting smaller. Examining the positions of the peaks in Fig. 3.2(a), it is evident that the optimal measurement time depends on the result of the previous measurement. This also highlights the fact that the optimal waiting time for F_{iid} will depend not only on the unknown parameter but also on the initial state chosen. The difference in optimal measurement times opens up the possibility to achieve a higher precision by varying the waiting time based on the previous measurement outcome. It is important to remark that changing the measurement times also affects the steady state probabilities and, therefore, we must optimise $F_{2|1}$ over all possible waiting times between measurements. Since the excited states are all degenerate in our system we need only consider two different waiting times, one for when the previous measurement was e_0 and one for e_1.

We can consider a similar scenario for the harmonic oscillator. We use the same master equation, Eq. (3.63), as the degenerate probes with system Hamiltonian

$$H_S = \Omega \left(\hat{a}^\dagger \hat{a} + \frac{1}{2} \right) \tag{3.72}$$

and jump operators, $L = \{\hat{a}, \hat{a}^\dagger\}$. Since the total evolution is quadratic in both position and momentum, Gaussianity will be preserved during the evolution [151,182]. As long as the first order moments of the initial state are zero, the covariance matrix alone is still sufficient to determine

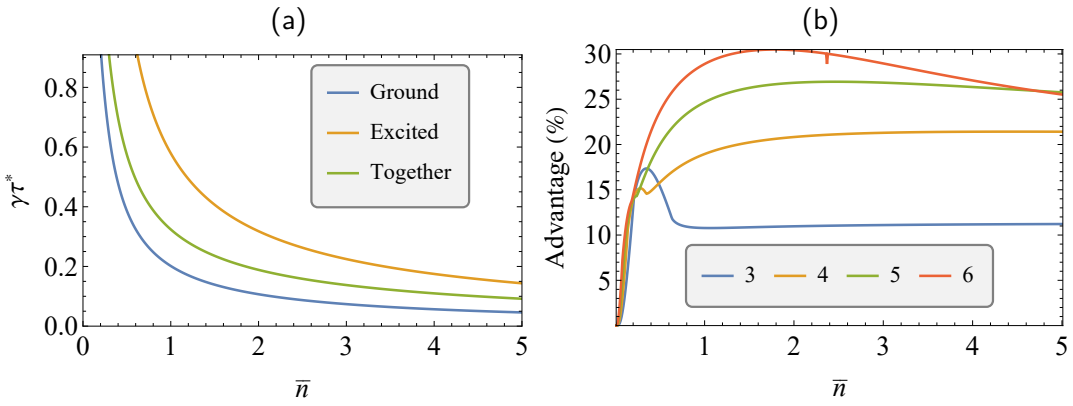

Figure 3.3: **(a)** The blue (orange) line shows the optimal measurement time if the result of the previous measurement was e_0 (e_1). The green line is the optimal measurement time if it is not possible to choose a different measurement time based on the result of the previous measurement. We (arbitrarily) fix $N = 4$. **(b)** The percentage increase in the quantum Fisher information if we allow different measurement times based on the result of the previous measurement.

the Fisher information. Performing a projective measurement in the energy basis ensures that we maximise the Fisher information and start in a pure state with zero first order moments of position and momentum. The evolution of the covariance matrix over time is [151]

$$\begin{aligned}\boldsymbol{\sigma}_k(t) &= e^{-\gamma t(1+\bar{n})}\boldsymbol{\sigma}_k(0) + \left(1 - e^{-\gamma t(1+\bar{n})}\right)\boldsymbol{\sigma}_T \\ &= \left(e^{-\Gamma_{\text{ho}}}\left(k+\frac{1}{2}\right) + \left(1-e^{-\Gamma_{\text{ho}}}\right)\left(\bar{n}+\frac{1}{2}\right)\right)\mathbf{I}_2,\end{aligned} \tag{3.73}$$

with $\Gamma_{\text{ho}} = \gamma t(1+\bar{n})$. This allows us to calculate the Fisher information from a specific measurement outcome,

$$F_{2|1=k} = \frac{1}{2}\frac{\left(1 - e^{\Gamma_{\text{ho}}} + \gamma t(k-\bar{n})\right)^2}{(k-\bar{n}^2) + e^{2\Gamma_{\text{ho}}}\bar{n}(1+\bar{n}) + e^{-\Gamma_{\text{ho}}}(k-\bar{n})(1+2\bar{n})}\left(\frac{\partial\bar{n}}{\partial T}\right)^2. \tag{3.74}$$

If the measurement time is the same for each measurement outcome then the steady state of the map is the thermal state giving

$$q_k = \bar{n}^k(1+\bar{n})^{-(1+k)}. \tag{3.75}$$

The full Fisher information can then, in principle, be calculated as

$$F_{2|1} = \sum_{k=0}^{\infty} q_k F_{2|1=k}. \tag{3.76}$$

The black, dashed line in Fig. 3.2(b) shows this Fisher information as a function of $\gamma\tau$ at $\bar{n}$. It seems to be impossible to beat the thermal Fisher information on average with a fixed measurement time. However, we can clearly see that when the previous measurement is the ground state, i.e. $k = 0$, the Fisher information can be larger than the thermal Fisher information. This means that one

simple strategy to surpass the thermal Fisher information would be to measure at the optimal time when the previous measurement was the ground state and allow all other measurement outcomes to fully thermalise. This will affect the steady state and therefore this strategy is not necessarily optimal, but it is guaranteed to outperform the thermal Fisher information. For larger values of $\bar{n}$, states other than the ground state can also surpass the thermal Fisher information.

In Fig. 3.3(a) we shift back to the degenerate probes and calculate the optimal waiting times between measurements, depending on the previous measurement outcome. We see that the optimal waiting time is shorter if the previous measurement was the ground state, this makes sense given the location of the peaks in Fig 3.2(a). The green "Together" line represents the Fisher information that is obtainable when the measurement time is the same for both previous measurement outcomes. The optimal measurements tend to scale as $\tau \propto \frac{1}{\bar{n}}$ as $\bar{n}$ gets large. If we now allowed different waiting times for different measurement outcomes, one might expect that the waiting times that maximise the Fisher information are going to be equal to the location of the peaks of the "ground" and "excited" curves respectively. While this is a good guess and will perform well in most cases, these are not necessarily the optimal waiting times. This is because changing the relative waiting times has the effect of changing the steady state distribution. So, for example, in Fig. 3.3(a) we see that the maximum possible Fisher information achievable is larger when the previous measurement was "ground", therefore increasing the probability of measuring the ground state has a positive effect on the Fisher information. This full optimisation is significantly more difficult and has to be done numerically. In Fig. 3.3(b) we show the increase in Fisher information that is possible if we allow this additional control over the waiting times. We see a significant increase of $10 - 30\%$ for different values of N. This scheme has the advantage that the increase in Fisher information will only get larger as the number of measurement outcomes increases although for projective measurements $F_{2|1}$ is still always bounded by the Fisher information of a probe initialised in the best measurement state.

We have demonstrated that the sequential measurement approach is not only more realistically implementable than many probe-based schemes but can also provide better measurement accuracy by exploiting correlations between measurement outcomes. These results bear a striking resemblance to the work on collisional quantum metrology [143, 144]. There it is shown that the Fisher information of certain collisional schemes can be expressed in the form [144]

$$F = F_{th} + (N-1)\Delta. \tag{3.77}$$

This is exactly the same form as Eq. (3.33), we will explore this curious connection more concretely in the remainder of this chapter. We will show that collisional metrology can be thought of as method of implementing sequential measurement thermometry with specific POVMs. We find that collisional metrology gives us some additional freedoms that could be exploited to increase the Fisher information. Finally, we explore concepts such as multi-parameter dependence and stochastic waiting times and the effect that they have on the Fisher information.

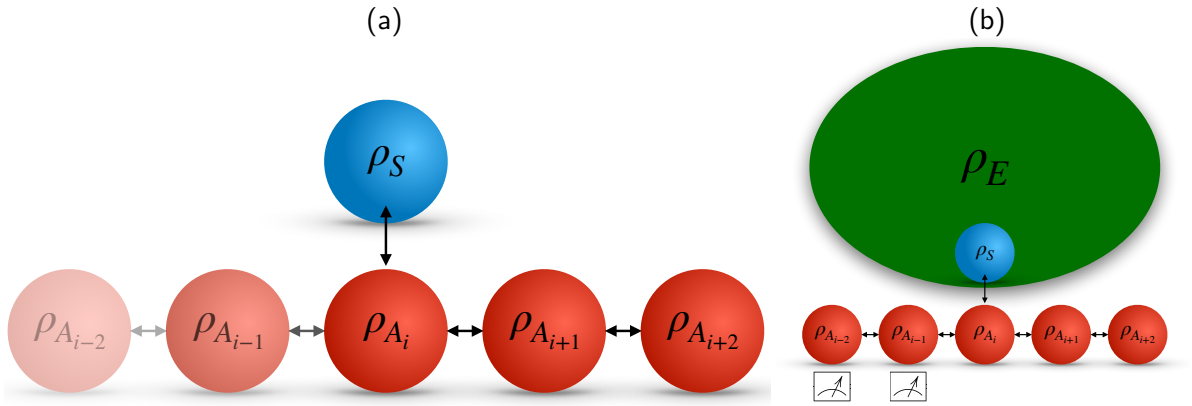

Figure 3.4: **(a)** Collision model diagram. **(b)** Schematic of the collisional thermometry scheme.

3.6 Collisional metrology

3.6.1 Introduction to collision models

Collision models are a method of simulating quantum systems that involves repeated, pairwise, unitary interactions between the system and a collection of auxiliary units. Collision models have applicability in a wide range of fields such quantum optics [183,184], non-Markovian dynamics [185, 186] and quantum thermodynamics [187]. The most common usage of collision models is in the simulation of (possibly complicated) system-bath dynamics by decomposing it into a set of repeated collisions with individual parts of the bath. This is both a useful tool for simplifying the simulation of system-environment dynamics but also a realistic model of what is actually occurring, since environments are made up of many individual particles. There are still limitations on the kinds of environments that collision models can model relaistically simulate because we usually assume that the environment correlations decay before the next collision happens, i.e. the Markov approximation considered in Chapter 1 applies or we assume that the correlations take a very specific form given by interactions between subsequent auxiliary units [186]. Although the most common usage of collision models is in simulating system-environment dynamics, the collision model framework is much more general in scope. In fact, some of the original works involving collision model setups involved classifying weak measurements [188] and describing the micromaser [189]. The micromaser features atoms interacting one at a time with a lossy cavity mode and so is modeled quite literally by a collision model [190]. In this Chapter we will consider a more general repeated interaction scheme that is not necessarily modeling an environment as was considered in the case of collisional quantum thermometry in Ref. [143], where measurements are performed on the auxiliary units after they have interacted with system itself in order to learn something about that system, in this case, the temperature. Depending on the degree of control over the auxiliary units and the system-auxiliary interaction this could look like a weak measurement process [188] or a highly controllable interaction between the system and a number of identically prepared auxiliary systems.

A diagram illustrating the usual setup for a collision model is seen in Fig. 3.4(a), the system

repeatedly interacts with a stream of auxiliary units via a unitary interaction. The auxiliary units may also interact with each other between collisions, this allows non-Markovianity to enter the system dynamics [145] but for now we will consider only interactions between the system and the auxiliary units. After the auxiliary unit has interacted with the system itself we can completely forget about it because it no longer has any effect on the system dynamics. We start with an uncorrelated system-bath state,

$$\rho^0 = \rho_S^0 \otimes \rho_{A_1} \otimes \rho_{A_2} \otimes \cdots \tag{3.78}$$

The unitary evolution of the entire system-bath

$$U_i = e^{-i(H_S + H_{A_i} + V_i)} \tag{3.79}$$

is described by the system Hamiltonian, H_S, the auxiliary Hamiltonian, H_{A_i} and the interaction Hamiltonian, V_i. It is usually assumed that the collision happens quickly and with sufficient strength that we can ignore the system and auxiliary Hamiltonian during the collision. We define the super-operator $\mathscr{U}_i(\rho) = U_i \rho U_i^\dagger$, the system-bath state after N collisions can then be described by,

$$\rho^N = \mathscr{U}_N(\cdots(\mathscr{U}_2(\mathscr{U}_1(\rho_S^0 \otimes \rho_{A_1}) \otimes \rho_{A_2}) \otimes \cdots \otimes \rho_{A_N}). \tag{3.80}$$

We write it this way to highlight the fact that the evolution is a composition of maps and U_i acts only on the system and the i-th auxiliary. Consequently, the state of the system after the i-th collision is described by,

$$\rho_S^i = \mathcal{E}^i(\rho_S^{i-1}) \tag{3.81}$$

where $\mathcal{E}^i$ is a CPTP map defined as

$$\mathcal{E}^i(\sigma) = \mathrm{Tr}_{A_i}\left\{\mathscr{U}_i(\sigma \otimes \rho_{A_i})\right\} \tag{3.82}$$

This tells us that the dynamics of the system after i collisions depends only on the state of the system after $i-1$ collisions and the map $\mathcal{E}_i$. Therefore, the evolution of the system is Markovian at the level of collisions. This fact is what makes collision models so powerful, because we only need to keep track of the system and a handful of auxiliary units at any one time instead of the entire system-bath state which will, in general, be some big, entangled mess after many collisions. Even when we break the Markovianity by adding correlations or collisions between the auxiliary units the number of auxiliary units we need to keep track of is usually very small [191]. We can calculate the reduced state of each auxiliary in an equivalent manner,

$$\rho'_{A_i} = \mathrm{Tr}_S\left\{\mathscr{U}_i(\rho_S^{i-1} \otimes \rho_{A_i})\right\}. \tag{3.83}$$

A state ρ^* is said to be a steady state of the map $\mathcal{E}$ if it is a fixed point of the map i.e.

$$\mathcal{E}(\rho^*) = \rho^*. \tag{3.84}$$

Maps can in principle have more than one fixed point. Often a map will have the stronger property that in the limit of a large number of collisions, every initial state will end up in a unique steady state, this is known as a mixing channel [176]. For example, this could occur if we had a thermalising interaction between the system and the bath then every initial state would end up in the Gibbs state in the long time/large number of collisions limit. In the correct limits of small collision times, it is possible to derive Lindblad master equations from collisional maps [145].

We can immediately see a similarity between the notation used to describe the system evolution coupled to the environment in Eq. (3.6) and the system evolution of the collisional setup in Eq. (3.82). This begs the question, is it possible to recreate the sequential measurement scheme using collision models? In the Introduction chapter, 1, we showed in Eq. (1.14) that performing a projective measurement on the environment is equivalent to performing a specific POVM on the system itself. We also know that according to Neumark's theorem [12], any POVM on the system can be realised as a projective measurement on a separate Hilbert space. Therefore, a collisional interaction followed by a projective measurement on the outgoing auxiliary unit can implement any POVM we want on the system itself. This may be a useful practical technique for employing complicated POVMs in a sequential measurement process. Using this we can recreate the measurement part of the map, Φ_{Ω_i}. For the second part of Φ_{Ω_i} we can take a number of approaches, we could imagine that the system is weakly coupled to a bath, resulting in a master equation like we considered above. Another approach would be to model the system-environment interaction using another collision model. In the remainder of this section, we will consider the first approach and analyse how various kinds of collisional interactions relate to the sequential measurement scheme.

3.6.2 Collisional Thermometry

Now we will apply this collisional metrology approach to the thermometry problem from Sec 3.5. This kind of approach was first proposed in Refs. [143, 144]. The basic ingredients, shown in in Fig. 3.4(b), consist of a (large) bosonic environment, E, with a flat spectral density at fixed temperature T, that we wish to estimate. The environment is coupled to an intermediary system, S, that undergoes the thermalising interaction described by Eq. (3.63). This intermediary system is in turn coupled to a stream of independent and identically prepared auxiliary units, A_i, which form the collisional bath. In what follows, we will assume both S and all A_i's are qubits and that the S-A_i interaction is unitary. Information about the temperature is then gained by performing measurements on the A_i's, either individually or in batches. This is in contrast to standard probe-based thermometry, where the intermediary system is the one that is measured. We assume that the S-A_i interaction time, τ_{SA}, is negligible compared to the system-environment coupling

time, τ_{SE} allowing us to neglect the system-environment coupling during the collisions. After N collisions the system and auxiliaries are given by the combined state

$$\rho_{S,A_1,...,A_N} = \mathscr{U}_{SA_N} \circ \mathcal{E} \circ \mathscr{U}_{SA_{N-1}} \circ ... \circ \mathcal{E} \circ \mathscr{U}_{SA_1}(\rho_S \otimes \rho_{A_1} \otimes ... \otimes \rho_{A_N}) \tag{3.85}$$

where $\mathscr{U}_{SA_i}(\circ) = U_{SA_i} \circ U_{SA_i}^\dagger$ and $\mathcal{E}$ corresponds to the map induced by Eq. (3.63) describing the S-E interaction acting on the intermediary system in between the collisions.

We will consider the specific case of a qubit system with non-degenerate energy levels, the energy spacing is still given by Ω. We choose the intermediary system and auxiliaries to be resonant, i.e. $H_S = H_A = \hbar\Omega\sigma_z/2$. The system, S, therefore experiences the stroboscopic map,

$$\rho_S^i = \mathcal{E}\left(\mathrm{tr}_{A_i}\{\mathscr{U}_{SA_i} \circ (\rho_S^{i-1} \otimes \rho_{A_i})\}\right) := \Phi(\rho_S^{i-1}). \tag{3.86}$$

For equally spaced collision times and a fixed initial state of the auxiliary units, this map has a unique steady state $\rho_S^* = \Phi(\rho_S^*)$, which is not necessarily the Gibbs state, with the notable exception of a pure dephasing interaction between S and A_i as outlined in the following section.

Dephasing Interactions

A number of different interactions have been employed for the collision models in this setup including a partial swap type interaction [143] and a ZZ dephasing interaction [144]. We begin by focusing on the ZZ interaction between the collisional bath and the system,

$$H_{SA_i}^{ZZ} = \frac{\hbar g}{2}\sigma_S^Z\sigma_{A_i}^Z, \tag{3.87}$$

which leads to a dephasing in the energy eigenbasis and is also referred to as an indirect measurement interaction. We tune the effective system-environment coupling, $\gamma\tau_{SE}$, and the effective S-A_i coupling, $g\tau_{SA}$. Since Eq. (3.87) only affects the off-diagonal elements (i.e. coherences), and assuming that S begins in thermal equilibrium with E before any interactions with the auxiliaries occur, the reduced state of S will remain in the Gibbs state. We can also see this by calculating the Kraus operators that are applied to ρ_S when a projective measurement is performed on the auxiliary unit. The unitary generated by $H_{SA_i}^{ZZ}$ is,

$$U_{SA_i} = \begin{pmatrix} e^{-ig\tau_{SA}/2} & 0 & 0 & 0 \\ 0 & e^{ig\tau_{SA}/2} & 0 & 0 \\ 0 & 0 & e^{ig\tau_{SA}/2} & 0 \\ 0 & 0 & 0 & e^{-ig\tau_{SA}/2} \end{pmatrix} \tag{3.88}$$

The Fisher information of this measurement is maximised when the initial state of the auxiliary unit is perpendicular to the Z-axis, e.g. $|+_x\rangle = (|0\rangle + |1\rangle)/\sqrt{2}$, and the measurement is performed

in the basis,

$$|\pm_g\rangle = \frac{1}{\sqrt{2}}(|0\rangle \pm e^{ig\tau_{SA}/2}\,|1\rangle). \tag{3.89}$$

This leads to a maximum possible Fisher information without correlations of

$$F_1 = \frac{1-\cos(2g\tau_{SA})}{2}\mathcal{F}^{th}, \tag{3.90}$$

which is strictly smaller than the thermal Fisher information as we would expect. If the basis had to be independent of $g\tau_{SA}$ then the best measurement basis would be $|\pm_y\rangle = (|0\rangle \pm i\,|1\rangle)/\sqrt{2}$. We can calculate the Kraus operators applied to the system in this basis

$$\begin{aligned} K_\pm &= \left(\mathbf{I}_S \otimes \langle\pm_y|_{A_i}\right) U_{SA} \left(\mathbf{I}_S \otimes |+_x\rangle_{A_i}\right) \\ &= \cos\left(\frac{g\tau_{SA}}{2} \pm \frac{\pi}{4}\right)|0\rangle\langle 0| + \sin\left(\frac{g\tau_{SA}}{2} \pm \frac{\pi}{4}\right)|1\rangle\langle 1| \end{aligned} \tag{3.91}$$

This kind of POVM has been looked at in the context of a sequential measurement scheme [172, 173]. It can be shown that the Fisher information of such a sequential measurement protocol can surpass the Fisher information of identically prepared probes, F_{iid}, when the measurement performed on these probes is identical to the sequential measurement POVM [173]. It is still not possible to beat the quantum Fisher information of the independently prepared probes, only the Fisher information given by the same POVM used in sequential measurement scheme. This POVM can also be prepared by using CNOT gates [192,193]. We can see that for the specific case of $g\tau_{SA} = \frac{\pi}{2}$ the Kraus operators just become the projectors onto the energy basis. Therefore, this kind of collisional setup should provide exactly the same Fisher information as the sequential measurement protocol used in Sec. 3.5. This can also be performed in the collisional setting by making use of the CNOT gate,

$$U_{SA_i} = \text{CNOT} = \begin{pmatrix} 1 & 0 & 0 & 0 \\ 0 & 1 & 0 & 0 \\ 0 & 0 & 0 & 1 \\ 0 & 0 & 1 & 0 \end{pmatrix}. \tag{3.92}$$

with an initial auxiliary state of $|0\rangle$ and measuring the auxiliary unit in the energy basis.

From now on we will maximise the Fisher information by setting $g\tau_{SA} = \pi/2$. The resulting Fisher information can be written in the form [144]

$$\mathcal{F}_N^{|+_x\rangle} = F_{th} + (N-1)\Delta, \qquad \text{with,} \tag{3.93}$$

$$\Delta = \frac{(1+\bar{n})^2\left[1-e^{\Gamma}(1+2\bar{n}\Gamma)\right]}{(1-e^{\Gamma})\left(1-\frac{(1-e^{\Gamma})\bar{n}}{1+2\bar{n}}\right)} + \frac{\bar{n}^2\left[-1+e^{\Gamma}(1-2(1+\bar{n})\Gamma)\right]}{(1-e^{\Gamma})\left(1-\frac{(1-e^{\Gamma})(1+\bar{n})}{1+2\bar{n}}\right)} \tag{3.94}$$

where $\Gamma = \gamma(2\bar{n}+1)\tau_{SE}$ is the effective thermalisation rate of the system and we have redefined N

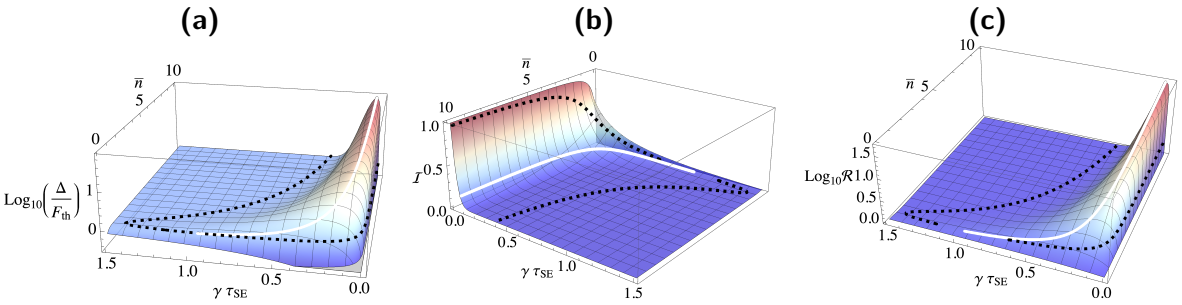

Figure 3.5: **(a)** Plot of the (log of the) ratio between Δ, Eq. (3.94), and $\mathcal{F}_{th}$. Positive regions indicate parameter regimes where a thermometric advantage is achievable via the collisional scheme.**(b)** Mutual information between two adjacent auxiliary units after each has interacted with the system via a ZZ interaction for a deterministic collisional thermometry protocol. **(c)** Measure of the interdependence between γ and $\bar{n}$ captured by Eq. (3.97) for a deterministic protocol with $N=2$ (arbitrary choice). In all panels, the area captured by the dashed black line represents the region in parameter space where the scheme achieves an advantage over the thermal QFI. The white line corresponds to the value of $\bar{n}$ where the QFI is maximal.

to be the number of collisions instead of the number of measurements, but in all of our examples they are equivalent. This makes sense as it should be equivalent to the sequential projective measurement protocol and therefore $\Delta = F_{2|1}$. From Eq. (3.93) we find that the condition for beating the thermal Cramér-Rao bound corresponds to $\Delta/\mathcal{F}_{th} > 1$, shown in Fig. 3.5(a) [144]. We see that we get a large peak in the Fisher information for certain values of $\gamma\tau_{SE}$ that increases with temperature. The location of this peak is highlighted by the solid white line and it is clear that the location of the peak is temperature dependent. This could cause issues when attempting to select the waiting time between collisions. The dashed black line encloses the area in which an advantage of more than 1% can be gained from this setup. We can see that after sufficiently long time the system has re-thermalised and therefore no significant advantage can be gained over the thermal Fisher information. There is also a minimum temperature below which it is not possible to gain any meaningful advantage over $\mathcal{F}^{th}$. Furthermore, the expression for Δ demonstrates that knowledge of the S-E coupling parameter, $\gamma\tau_{SE}$, is essential to achieve any boost in thermometric performance. For the remainder of this section, we will assume a deterministic collisional scheme, namely the system and the environment interaction time is identical between each of the collisional events, i.e. $\gamma\tau_{SE}$ is the same between each collision. Thus, we consider the same setting as Refs. [143, 144] of equally distributed collisions and in Sec. 3.6.3 we introduce stochasticity.

Role of correlations

Given that, for the ZZ interaction, measuring a single auxiliary cannot outperform the thermal Cramér-Rao bound it is natural to ask what allows for the enhancement when multiple units are measured. There are multiple ways to think about this question. We could explicitly consider the state of the system when the SA interaction occurs, that state now has additional dependence on

the temperature that comes in the form of the effective thermalisation rate, Γ. Another way is to consider the correlations that are generated between successive auxiliary units. We can quantify these correlations via the bipartite mutual information,

$$\mathcal{I} = S(\rho_A) + S(\rho_B) - S(\rho_{AB}), \tag{3.95}$$

where $S(\cdot)$ is the von Neumann entropy. This quantity captures all correlations, both quantum and classical, present in the state. In Fig. 3.5(b) we show the mutual information shared between two successive auxiliaries, i.e. $\rho_{A_i A_{i+1}}$ where it clearly appears that significant correlations are established which depend on the time between each collision and the temperature of the environment. The dashed black line indicates that while there appears to be a qualitative relationship between the magnitude of the mutual information shared between the auxiliaries and the corresponding thermometric performance, with some amount of mutual information clearly being necessary in order to gain an advantage, remarkably too much correlation actually results in the QFI being lower than the thermal Fisher information. The boundary is delineated by the white line which tracks the peak QFI for each value of $\bar{n}$. The value of the mutual information along the white line is quite consistently around $\mathcal{I} \approx 0.1$, but does increase slowly with temperature. This poses some interesting questions related to whether there is an optimal amount of correlation between measurement results. We can further characterise the type of correlations present by determining the quantum discord [194, 195] which captures the genuine quantum nature of the correlations present, and in this case turns out to be identically zero. This implies that the correlations contributing to the increased metrological performance are purely classical. This is initially confusing given the fact that we are dealing with a dephasing interaction, but it can be explained by fact that it can be mapped exactly onto a CNOT interaction and onto a sequential measurement protocol in the energy basis.

Parameter Dependence

We see from Eq. (3.94) that the advantage gained from this collisional approach depends on the effective thermal relaxation parameter $\Gamma = \gamma(2\bar{n}+1)\tau_{SE}$. Consequently, in order to maximise this advantage, *both* γ and τ_{SE} must be known with certainty. While τ_{SE} corresponds to the time between collisions, which can usually be known or measured with high accuracy, the parameter γ which corresponds to the coupling strength between the system and the environment is more delicate. In certain circumstances it may be that, prior to any measurements, γ is known for the setup. However, when this is not the case, or if the bath is prone to some other disturbance, determining it precisely is essential [196].

We can demonstrate the importance of knowing γ through the total variance of a measurement in multi-parameter estimation by summing the variances of all parameters. When estimating m

unknown parameters we get the following chain of inequalities [168]

$$\sum_{a}^{m} \mathsf{var}(x_a) \geq \frac{1}{m} \operatorname{Tr}\left\{\mathcal{F}^{-1}\right\} \geq \sum_{a} \frac{1}{m\mathcal{F}_{aa}}, \tag{3.96}$$

where $\mathcal{F}$ is the QFI matrix as defined in Eq. (3.10). In our case $m = 2$ and $x_a \in \{\bar{n}, \gamma\}$. The second inequality is only saturated when all the parameters are independent of each other and therefore by comparing the ratio between the second and third terms, which we denote as

$$\mathcal{R} = \frac{\operatorname{Tr}\{\mathcal{F}^{-1}\}}{\sum_a \frac{1}{\mathcal{F}_{aa}}}, \tag{3.97}$$

allows us to identify the areas in which knowledge of γ is necessary in order to estimate the temperature. Figure 3.5(c) shows the peaks of this ratio line up perfectly with the peaks of the QFI. Additionally, if one has no knowledge of γ it is impossible to gain any advantage over the thermal Fisher information. In fact, the QFI is smaller than the thermal Fisher information in this case when the time between collisions is small. It is clear from looking at the Fisher information that any advantage of the thermal Fisher information had to come from the term, $\Gamma = \gamma(2\bar{n}+1)\tau_{SE}$, in which γ and $\bar{n}$ clearly depend on each other. This gives us some intuition as to why maximising this interdependence corresponds to the maximum of the Fisher information. What is not so clear is why this interdependence falls off again for very short collision times when the system state has the most dependence on Γ. Understanding $\mathcal{R}$ better could help distinguish between situations when correlations have a positive or negative effect on the Fisher information.

3.6.3 Stochastic Approach

The previous section outlined the basic ingredients of the collisional thermometry scheme for the deterministic case introduced in Refs. [143, 144]. We now turn our attention to introducing stochasticity at the level of the time between collisions, τ_{SE}, while keeping the average collision time consistent with the previous section.

In nature, interactions will not generally occur in fixed intervals or at deterministic times. Rather, processes are typically random with the time between interactions captured by a suitable probability distribution, the waiting time distribution (WTD). Within the framework of open quantum systems, collision models allow us to introduce such randomness either in the intervals between successive collisions or in the collision time itself and are referred to as stochastic collision models [197–199]. We will focus on randomness in the intervals between collisions.

Collision models, in their usual form, are useful tools for modelling system dynamics but often seem artificial. Employing WTDs in this sense clearly brings collision models closer to modelling real physical systems [200–202], where there is randomness involved. Here we look at how introducing such randomness affects the Fisher information obtained from the collisional thermometry scheme. As we shall demonstrate, stochastic collision models allow us to achieve a greater parameter range of advantage over deterministic collision models without significantly

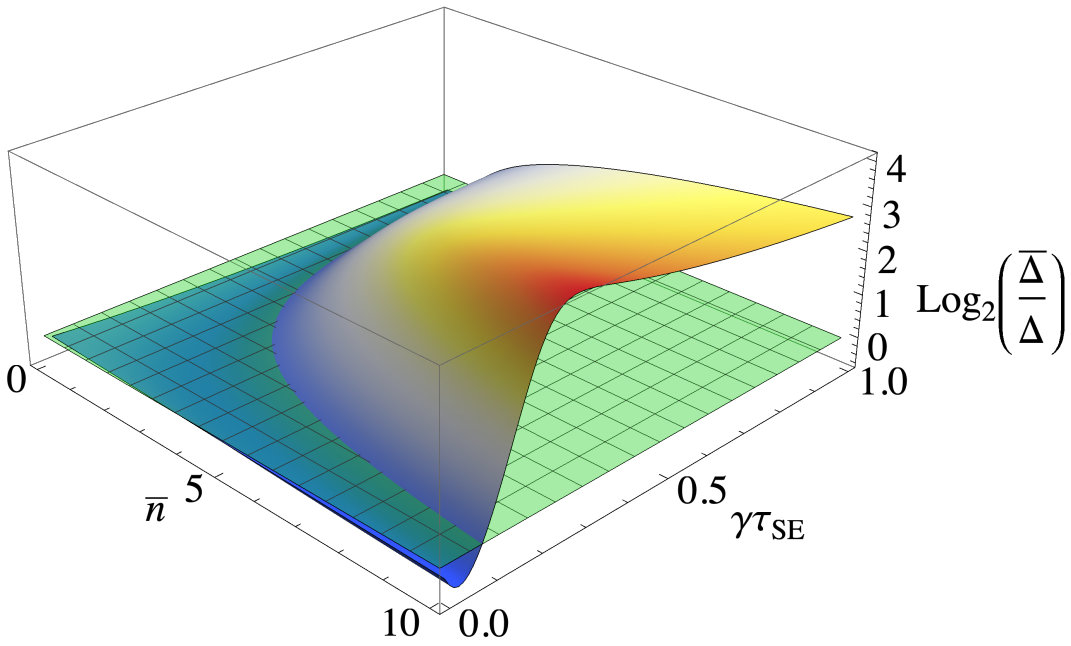

Figure 3.6: Comparison of the ratio between Δ and $\overline{\Delta}$ for a Weibull distribution with $k=1$, and a deterministic equally spaced waiting time distribution. The green plane represents the crossing point where one term becomes larger than the other. $\gamma\tau_{SE}$ is the average time between collisions.

sacrificing the maximal achievable precision. For concreteness, we shall focus on the Weibull renewal distribution, but our results remain qualitatively unaffected for other families of WTD, e.g. Erlang distributions. The Weibull renewal distribution can be expressed as

$$p(t) = \frac{k}{\lambda}\left(\frac{t}{\lambda}\right)^{k-1} e^{-(t/\lambda)^k}, \tag{3.98}$$

where λ is the average time between collisions and k determines the shape of the distribution. Some examples of such distributions can be seen in the inset of Fig. 3.7. In particular, large k tends to produce regular intervals between collisions with small, Gaussian like deviations from the mean and, in the limit $k \to \infty$, the collisions are deterministic and equally spaced as considered in Refs. [143, 144] and previous sections. Whereas, small k is characterised by bursts of collisions followed by long breaks [199]. For $k=1$, the WTD corresponds to the exponential distribution characterising a Poisson point process.

As we see from Eq. (3.93) and Fig 3.5, when the waiting time between subsequent collisions is deterministic and constant, it is possible to obtain a QFI that is orders of magnitude higher than the thermal Fisher information for specific values of the coupling parameters and temperature [143, 144]. However, a drawback of this is that such high precision is restricted to a narrow parameter range, delicately dependent on the temperature of the environment. Such a situation is clearly not ideal given that the temperature is the very quantity which we wish to estimate [143, 144]. This is a well-known issue in metrology, specifically in local estimation schemes making use of

the Fisher information. Approaches to address this issue include introducing global estimation schemes [54, 203–206] and biased estimators [146]. Here, we demonstrate that if the interactions are random, governed by a particular WTD, this randomness will affect the Fisher information obtainable from the measurements even when the average collision time is still the same. It is straightforward to extend our proof of Eq. (3.33) to account for random waiting time distributions under certain conditions. It is important that the steady state equation does not depend on the waiting time. If this were not the case, the Fisher information of each measurement would once again depend on the results of all previous measurements. For the ZZ interaction, the reduced state of the system still satisfies the steady state equation (3.65). This means that we can still write the Fisher information in the form,

$$\mathcal{F}_N^{|+_x\rangle} = \mathcal{F}^{th} + \sum_{i=1}^{N-1} \Delta_i, \tag{3.99}$$

where Δ_i takes an identical form as given in Eq. (3.94) except with τ_{SE} now replaced with a variable time τ_{SE}^i which is randomly determined from the waiting time distribution. To determine the average performance of a particular WTD, $p(t)$, we now average over each collision time,

$$\mathscr{F}_N^{|+_x\rangle} = \int_0^\infty \cdots \int_0^\infty \prod_{i=1}^{N-1} d\tau_{SE}^i \, p(\tau_{SE}^i) \, \mathcal{F}_N^{|+_x\rangle} = \mathcal{F}^{th} + (N-1)\overline{\Delta}, \tag{3.100}$$

where $\overline{\Delta} = \int_0^\infty d\tau_{SE} \, p(\tau_{SE}) \, \Delta$ with the WTD, $p(t)$ being any positive function that satisfies $\int_0^\infty dt \, p(t) = 1$. In Fig. 3.6 we show the (log of the) ratio between $\overline{\Delta}$ for an exponential distribution, i.e. $k = 1$ (arbitrary choice) and the deterministic Δ. We can see that the randomness allows for a significant performance boost (up to ten times larger) over a wide range of parameters at the cost of a slight sensitivity loss when the deterministic QFI is maximal.

While we have established that an advantage over the regularly spaced collisions can be achieved for a particular choice of WTD, we now turn our attention to how the particular form of the distribution affects the performance. As mentioned previously, varying k in the Weibull distribution, Eq. (3.98), interpolates between distributions with regularly space collisions for $k \to \infty$ to collisions in batches followed by long pauses as $k \to 0$. We compare the QFI for various values of k at a fixed (arbitrarily chosen) value of temperature, corresponding to $\bar{n} = 2$, in Fig. 3.7. For larger values of k, we find the behaviour tends to the deterministic case which is characterised by a QFI with a large peak that is narrow in the parameter range. However, for smaller values of k, leading to a more random sequence of collisions, we find the range over which an advantage can be demonstrated is significantly broadened, albeit at the expense of reducing the "maximum" achievable precision. Thus, by introducing stochasticity to the process we are able to alleviate the need for precise knowledge of the optimal system-environment coupling. Interestingly there is a limit to how small k can be and still retain an advantage, with very small k leading to collisions happening so close together that no additional information can be gained. This can be related back to the fact that when the time between collisions is very small, the correlations between measurements

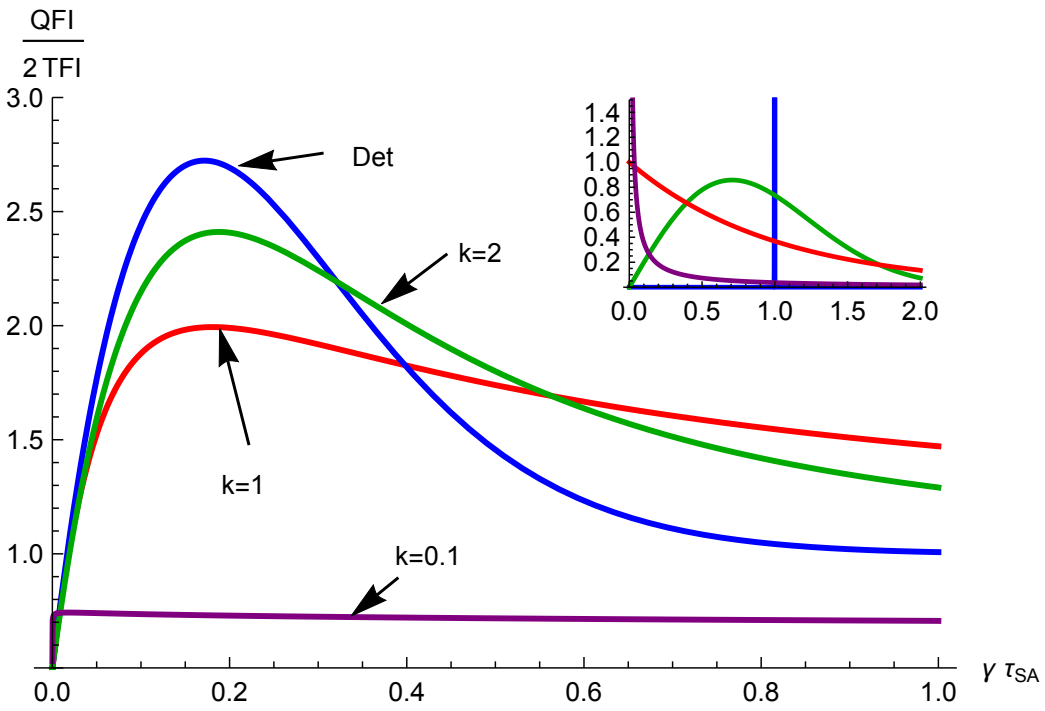

Figure 3.7: Comparison of the value of the quantum Fisher information for various Weibull distributions of the collision time interval (see Eq. (3.98)), with the deterministic case, for $\bar{n} = 2$. Similar behaviour is seen for other values of temperature above $\bar{n} = 1.5$. *Inset:* Distributions for various values of k shown in the main panel.

are so large that very little additional information is gained from subsequent measurements.

3.6.4 Optimal Measurements

While the QFI places an asymptotic bound on the accuracy of parameter estimation it does not provide details on precisely what POVM should be implemented in order to saturate the bound. Therefore, identifying the measurements that must be performed on the auxiliary units is important for assessing the implementability of the scheme, something which is particularly relevant for our stochastic collisional approach, in order to assess whether optimal measurements depend on the waiting time between collisions. To find the optimal measurement we need the symmetric logarithmic derivative (SLD) operator L_a for parameter x_a. In terms of the eigen-decomposition of $\rho = \sum_i \lambda_i \left|\lambda_i\right\rangle\!\left\langle\lambda_i\right|$, the SLD operator is [168],

$$\left\langle\lambda_i\right| L_a \left|\lambda_j\right\rangle = \delta_{ij} \frac{\partial_a \lambda_i}{\lambda_i} + \frac{2(\lambda_j - \lambda_i)}{\lambda_i + \lambda_j} \left\langle\lambda_i\right| \partial_a \lambda_j \rangle.$$

For our scheme we find that the eigenvectors $\{|l_i\rangle\}$ of L_a are independent of x_a and the Fisher information is

$$\begin{aligned} F_{aa} &= \sum_i \frac{\langle l_i| \partial_a \rho |l_i\rangle^2}{\langle l_i| \rho |l_i\rangle} = \sum_i \frac{\langle l_i| \rho L_a + L_a \rho |l_i\rangle^2}{\langle l_i| \rho |l_i\rangle} \\ &= \mathrm{Tr}\Big\{\rho L_a^2\Big\} = \mathcal{F}_{aa} \end{aligned}$$

where $\mathcal{F}_{aa}$ is the quantum Fisher information for parameter x_a. This implies that the optimal measurement corresponds to one performed over the $\{|l_i\rangle\}$ basis. For the ZZ interaction considered with $g\tau_{SA} = \pi/2$, the eigenvectors $|\lambda_i\rangle$ of ρ are independent of T and γ meaning that the optimal measurement is precisely the measurement in the $\{|\lambda_i\rangle\}$ basis and is the same for both T and γ. One advantage that the collisional setup has over the sequential measurement protocol is that the measurement on the auxiliary units does not have to be performed immediately after interacting with the system. We can wait for a large number of collisions to occur and then perform a measurement on many auxiliary units at the same time. This would allow us to make use of entanglement generated between the systems. In the thermometry case we considered, there are no quantum correlations between the auxiliary units and therefore, the optimal measurement can be done using single-qubit measurements. For the auxiliary units initialised in the $|x_+\rangle$ state considered here, there is some ambiguity in the measurement basis due to degeneracy in the eigenvalues. However, the simplest basis is $|\pm_y\rangle_1 \ldots |\pm_y\rangle_{1M}$ for M collisions. The optimal measurements involve only product states and therefore can be performed using only single-qubit projective measurements.

3.6.5 Partial Swap Interactions

We conclude our analysis by considering an alternative form of the S-A_i interaction that has been considered frequently in collisional thermometry [143, 144, 146]. This is a partial swap (also referred to as an exchange) style interaction given by

$$H_{SA}^{\mathsf{Swap}} = \hbar g(\sigma_S^+ \sigma_A^- + \sigma_S^- \sigma_A^+). \tag{3.101}$$

where similarly to the previous case we can tune the effective couplings, $\gamma\tau_{SE}$ and $g\tau_{SA}$. This results in the unitary,

$$U_{SA_i}^{\mathsf{Swap}} = \begin{pmatrix} 1 & 0 & 0 & 0 \\ 0 & \cos(g\tau_{SA_i}) & -i\sin(g\tau_{SA_i}) & 0 \\ 0 & -i\sin(g\tau_{SA_i}) & \cos(g\tau_{SA_i}) & 0 \\ 0 & 0 & 0 & 1 \end{pmatrix}. \tag{3.102}$$

The Fisher information is maximised by choosing the initial state of the auxiliary units to be the energy ground state and measuring in the energy basis [144]. This results in the following POVM

being applied to the probe itself,

$$K_0 = \left(\mathbf{I}_S \otimes \langle 0|_{A_i}\right) U_{SA_i}^{\mathsf{Swap}} \left(\mathbf{I}_S \otimes |0\rangle_{A_i}\right) \tag{3.103}$$
$$= |0\rangle\langle 0| + \cos\left(g\tau_{SA}\right)|1\rangle\langle 1|\,,$$

$$K_1 = \left(\mathbf{I}_S \otimes \langle 1|_{A_i}\right) U_{SA_i}^{\mathsf{Swap}} \left(\mathbf{I}_S \otimes |0\rangle_{A_i}\right) \tag{3.104}$$
$$= \sin\left(g\tau_{SA}\right)|0\rangle\langle 1|\,.$$

We can see that this becomes a full swap when $g\tau_{SA} = \pi/2$. One interesting consequence of this kind of POVM (in the full swap limit) is that the state of the probe system after the interaction is independent of the temperature. Therefore, the sequential measurement scheme has Markov order 1, even though the POVM is not a projective measurement. In fact, this specific POVM gives us the Fisher information in the form of Eq. (3.93) with $\Delta = F_{2|1=e_0}$. This explains why it is possible to obtain slightly higher precision with this kind of interaction over the ZZ interaction [143] because the ground state is the optimal initial state for an iid scheme [173]. In contrast to the ZZ interaction, now the system and auxiliaries will exchange energy as well as coherences and thus the system will not remain in the Gibbs state throughout the dynamics. The steady state of the map Φ can be calculated as

$$\rho_{SS} = \frac{1+\bar{n}+e^{-\Gamma}\bar{n}}{1+2\bar{n}}|0\rangle\langle 0| + \frac{\bar{n}-e^{-\Gamma}\bar{n}}{1+2\bar{n}}|0\rangle\langle 0|\,. \tag{3.105}$$

We see that this interaction does not preserve the thermal steady state, instead we get additional temperature dependence entering the state through the effective thermalisation rate Γ. This interaction is significantly more disruptive to the thermal bath itself because the probe remains in a non-equilibrium state. This may cause some issues if the bath was sufficiently small, the temperature was very low, or a large number of measurements are performed. While clearly there are some differences due to the change in interaction, we find that introducing different waiting time distributions has a qualitatively identical effect in this case, i.e. the introduction of stochasticity allows to significantly extend the range over which a thermometric advantage can be gained from the collisional thermometry scheme.

3.7 Conclusions

Correlations in the Fisher information are a double-edged sword. They can lead to large increases in the precision of measurements while also dramatically increasing the complexity of estimating the unknown parameter. The sequential projective measurement scheme provides a powerful and practical metrology method that can achieve higher precision than many of the traditional metrology strategies, while still being simple to implement and calculate. The Fisher information takes on a simple form but still leaves plenty of room for optimisation. We showed that this

scheme is equivalent to averaging over the Fisher information of individual, iid probes, initialised in the measurement basis states. We were also able to show that when the unitary that governs the system-environment evolution is independent of the parameter to be estimated, the Fisher information obtainable from the system is bounded above by the Fisher information of a coarse-grained measurement on the environment. More precisely, this applies when the Kraus operators of the map $\mathcal{E}'(\rho_E)$ are independent of the unknown parameter. We also demonstrated that any sequential measurement protocol can be simulated using a collision model setup. This collisional setup has some additional benefits of allowing for entanglement between the auxiliary units and even correlations between the auxiliary units before interacting with the probe [144].

In the case of thermometry, we found that for specific waiting times between measurements it was possible to obtain a large advantage over the thermal Fisher information. We showed that allowing for different waiting times between measurements based on the result of the previous measurement resulted in an increase in the average Fisher information of each measurement. This increase tended to get larger as the dimension of the probe increased. We also saw that larger probes tended to give higher precision, even when that property was not reflected in the thermal Fisher information. Although large advantages were possible, we ran into the common issue that gaining maximum advantage requires *a priori* knowledge of the unknown parameter. Introducing stochasticity in the waiting time between measurements allows us to blunt this problem by achieving significant advantage over the Fisher information over a larger range of temperatures.

There is plenty of room to build on the framework and results from this Chapter. Some avenues of further research include using different kinds of POVMs instead of projective measurements such as weak measurements or any POVM with finite Markov order. It would also be interesting to look at system environment interactions beyond the weak coupling limit, possibly with the use of non-Markovian collision models in order to see what effect this can have on the Fisher information. As we discussed in Sec. 3.4 it is not always easy to know what uncorrelated process to compare our correlated process to, let alone identifying the conditions under which those correlations provide an advantage over said uncorrelated process. Nevertheless, we were able to prove that additional information about the unknown parameter must be present in the system-environment interaction in order for the Fisher information of the sequential measurement scheme to perform better than any coarse-grained measurement of the environment. Additionally, this coarse-grained environment measurement coincides with other notions of the uncorrelated Fisher information, such as F_1, in the case of thermometry. All this does is rule out certain cases where it is not possible for the correlations to lead to a larger Fisher information without helping us identify what kinds of correlations lead to advantages. It can be shown that when using estimators based on the sample mean that the Fisher information of the sample mean is larger when individual measurements are negatively correlated [175]. We can understand this intuitively because fluctuations in the individual measurements will tend to cancel out when they are negatively correlated [175]. This analysis does not hold for our thermometry example because our measurement results are positively correlated. Another approach that could be taken would be to ignore the concept of

correlations and focus on the Fisher information of specific measurement results, i.e. specific initial states, and attempting to identify when and why we see Fisher information increases in these scenarios. Further inquiry is warranted into the nature of the correlations and how these relate to the multiparameter dependence that we looked at in Sec. 3.6.2. In the collisional setup it would be interesting to investigate whether generating entanglement between the auxiliary units would allow for Heisenberg scaling to apply in addition to the advantages that are gained from correlations [207].

Chapter 4

Entropy of the Quantum Work Distribution

When it comes to manipulating quantum states, there is no such thing as a free lunch. Even a unitary evolution can have associated costs when control is involved [113]. One area in which these costs appear is in thermodynamic quantities. In this Chapter we will focus on the notion of thermodynamic work, which is a tricky concept to define for quantum systems. Just as discussed in Chapter 2 where we found that it is not possible to define a time operator in quantum mechanics the same can be true for the thermodynamic work. In fact, for work the problem is even more pronounced, this is because it is not a property of a quantum state but of a process. This is obvious from the point of view of classical thermodynamics because work does not have an exact differential and therefore, is not a state variable [208]. One clear difference that the quantum scenario possesses is the presence of coherence. We will analyse the effect that this coherence has on the work for both pure states and Gibbs equilibrium states, Eq. (3.53). We discover that there are important contributions to the work from both the classical and quantum components and establish that the work probability distribution is a useful tool, encoding information about both the micoscopic properties of the system, e.g. its critical nature for many-body system, and relevant information about the dynamics the system is undergoing. Section 4.1 introduces the relevant concepts from the existing literature. The remainder of the Chapter is adapted from Ref. [3] which is a collaboration between with several authors, with the bulk of the theoretical and computational work performed by myself and Anthony Kiely. Secs. 4.4.1, 4.4.2 and 4.4.4 represent additional original work done by me after the publication of the original paper.

4.1 Introduction

Since work is property of a process, it makes sense to make two different measurements of the system, one at the start, and one at the end of the process. This definition of the work is known as the two-point measurement (TPM) approach [209] because it involves performing energy basis measurements at the start and end of the process [210, 211]. The TPM approach has

proved to be fruitful for developing connections between thermodynamics and other areas of quantum physics including, out-of-time-order correlators [212], information scrambling [213, 214] and Kibble-Zurek scaling [215, 216]. The main drawback of the TPM approach is that the initial measurement destroys any coherence that the initial state had. Coherence can play a significant role in the thermodynamics of quantum systems [217–220]. In particular, it is possible to use quantum coherence to extract useful work from a system [221] and, therefore, there must be a thermodynamic cost associated with their creation [222, 223]. Although the coherence is destroyed in the first measurement, coherence can still be generated between the two measurements. A potential downside of generating a lot of coherence in non-equilibrium systems is that it can lead to large fluctuations [224].

When a measurement is performed in quantum mechanics the results are not deterministic, therefore, the work done in any single iteration of the TPM scheme is also not deterministic. This means that there is a probability distribution associated with each of the measurements and with the work done itself. In the TPM approach, we start with our system prepared in an arbitrary initial state, ρ, and perform a measurement in the energy basis of the initial system Hamiltonian, $\mathcal{H}_i = \sum_n E_n^i \left|n_i\right\rangle\!\left\langle n_i\right|$. The system Hamiltonian is then varied over time until it reaches the final Hamiltonian $\mathcal{H}_f = \sum_m E_m^f \left|m_f\right\rangle\!\left\langle m_f\right|$. Another measurement is then performed in energy basis of $\mathcal{H}_f$. The evolution of the system during this process is described by a unitary evolution, which changes the state to $\rho' = U\rho U^\dagger$. The probability of the first measurement being the state $\left|n_i\right\rangle$ is given by $p_n = \left\langle n_i\right| \rho \left|n_i\right\rangle$. Since the initial measurement changes the state of the system, the probability distribution of the second measurement depends on the result of the first measurement, in analogy with the sequential measurement scheme in Chapter 3. We can therefore define the probability of measuring the state $\left|m_f\right\rangle$ in the second measurement as $p_{m|n} = \left|\left\langle m_f\right| U \left|n_i\right\rangle\right|^2$, which can also be thought of as the transition probability. The work of a single iteration of the TPM protocol is just the difference in the energy eigenvalues of the two measurements, $E_m^f - E_n^i$, this is also known as the *Bohr (transition) frequency* between the initial and final energy level. The probability that a certain amount of work, W, is injected or extracted can then be calculated by grouping together all the measurement outcomes with the same amount of work,

$$P(W) = \sum_{n,m} p_n p_{m|n} \delta_{W, E_m^f - E_n^i} \,. \tag{4.1}$$

We assume these form a discrete (possibly infinite) set.

The work distribution can be incredibly complicated and therefore it is often useful to focus on summary statistics such as the moments of the work distribution, $\langle W^n \rangle = \sum_W W^n P(W)$, and their cumulants. This is particularly useful when the work distribution is Gaussian [225] but for more complicated distributions the first few cumulants might not be enough to capture all the interesting features of the full distribution [225, 226]. We aim to tackle some of these shortcomings by looking at a different summary statistic of the work distribution, namely the entropy of the distribution. The entropy of a distribution can be thought of as a measure of its complexity. We

derive a general and saturable bound on H_W, that consists of two distinct contributions: one is the entropy of the initial measurement in the TPM protocol and is therefore a property of the initial state and initial Hamiltonian only, in suitable limits, this corresponds simply to the Gibbs equilibrium entropy; and a second term which is purely quantum in nature, related to the coherence established between the initial and final Hamiltonian bases by the driving protocol, and given by the relative entropy of coherence.

The chapter is organised as follows. First we detail how thermodynamics can be generalised to include features of quantum systems, in particular coherence. Secondly, we introduce the entropy of the work distribution and derive a number of upper and lower bounds that shed some light on its structure. Next, we illustrate the utility of our results in the Landau-Zener model which reveals that the entropy of the work distribution clearly highlights the avoided crossing, whereas the moments show little to no evidence of this feature. We then conduct a detailed analysis of work fluctuations in the Aubry-André-Harper (AAH) model, a paradigmatic model for studying localization. We show that H_W is related to a modified inverse participation ratio and provides a remarkably sensitive indicator of the localization transition.

4.1.1 Quantum Coherence

Although it is a fundamental part of what distinguishes quantum systems from classical systems, it can be hard to pin down exactly what coherence is in a quantum system. The coherence must be defined relative to a specific basis which we will denote $\{|i\rangle\}$. Then, there is the problem of quantifying the coherence of a quantum system for which many different approaches exist [227]. We will focus on one family of approaches, distance-based quantifiers of coherence. A distance-based coherence quantifier can be defined as [228]

$$\mathcal{C}_D(\rho) = \inf_{\sigma \in \mathcal{I}} D(\rho, \sigma), \tag{4.2}$$

where $\mathcal{I}$ is the set of incoherent states, i.e. the states of the form $\sigma = \sum_i p_i \, |i\rangle\langle i|$. Immediately we can see a problem in that there are infinitely many ways to define a distance measure between quantum states and each of these can give a different measure of coherence. Nevertheless, different quantifiers of coherence can be useful in different contexts. We will focus of a specific distance-based coherence measure known as the relative entropy of coherence (REC) [228]. This can be obtained by choosing the quantum relative entropy or quantum Kullback-Leibler divergence,

$$S(\rho \| \sigma) = -S(\rho) - \mathrm{Tr}\left[\rho \ln \sigma\right], \tag{4.3}$$

as our distance measure, where $S(\rho) = \mathrm{Tr}\left[\rho \ln \rho\right]$ is the Von-Neumann entropy. If we analyse the second term in this equation we see that

$$\begin{aligned} \mathrm{Tr}\left[\rho \sum_i \ln p_i \left|i\right\rangle\!\left\langle i\right|\right] &= \sum_i \left\langle i\right| \rho \left|i\right\rangle \ln p_i \\ &= \mathrm{Tr}\left[\sum_j \left\langle j\right| \rho \left|j\right\rangle \left|j\right\rangle\!\left\langle j\right| \sum_i \ln p_i \left|i\right\rangle\!\left\langle i\right|\right] \\ &= \mathrm{Tr}\left[D(\rho) \ln \sigma\right] \end{aligned} \tag{4.4}$$

where $D(\rho) = \sum_i \left\langle i\right| \rho \left|i\right\rangle \left|i\right\rangle\!\left\langle i\right|$ is the full dephasing operation in the coherence basis. This means that we can rewrite the relative entropy as

$$S(\rho \| \sigma) = -S(\rho) + S(D(\rho) \| \sigma) + S(D(\rho)). \tag{4.5}$$

This is clearly minimised when $\sigma = D(\rho)$ giving us a closed form for the REC [228]

$$\mathcal{C}_r(\rho) = S(D(\rho)) - S(\rho). \tag{4.6}$$

It can be shown that the REC corresponds to the distillable coherence for incoherent operations [229]. The distillable coherence is the maximum rate at which maximally coherent two-qubit states, $\left|\psi\right\rangle_2 = \frac{1}{2} \sum_{i,j=0}^{1} \left|i\right\rangle\!\left\langle j\right|$, can be generated from ρ using incoherent operations. So explicitly, n copies of ρ can generate, at most, $n\mathcal{C}_r(\rho)$ copies of $\left|\psi\right\rangle_2$ via incoherent operations when the REC is measured in units of bits, i.e. the logarithm is taken to base 2.

4.1.2 Thermodynamics of Gibbs equilibrium states

One scenario where the work is much easier to define in quantum systems is when the system is initially in a Gibbs equilibrium state. This can occur when our system is coupled to a heat reservoir at inverse temperature β in the weak coupling limit. It is easier to make comparisons to classical thermodynamics in this limit because our initial state has no coherence in the basis of the initial Hamiltonian and therefore the initial measurement has no effect, on average, on thermodynamic quantities. We allow the system Hamiltonian $H(\lambda)$ to be controlled by an external work parameter, λ. Therefore, the initial state of our system is

$$\rho_\beta(\lambda_0) = \frac{e^{-\beta H(\lambda_0)}}{\mathcal{Z}(\lambda_0)}, \tag{4.7}$$

where $\mathcal{Z}(\lambda) = \mathrm{Tr}\left[e^{-\beta H(\lambda)}\right]$ [220]. The external work parameter is ramped from $\lambda_0 \to \lambda_\tau$, this causes the system to evolve under the unitary dynamics,

$$U(0, \tau) = T_{\leftarrow} \exp\left[-i \int_0^\tau ds H(\lambda_t)\right] \tag{4.8}$$

A measurement is then performed at time τ in the energy basis of the Hamiltonian,

$$H(\lambda_\tau) = \sum_m E_m^f(\lambda_\tau) \left|m_f\right\rangle\!\left\langle m_f\right| . \tag{4.9}$$

This gives us a work distribution as defined in Eq. (4.1). The average work, $\langle W \rangle$, of such a process can is just the difference in the average energy of the system at the start and end of the process, i.e.

$$\langle W \rangle = \mathrm{Tr}\left[H(\lambda_\tau)\rho_\tau\right] - \mathrm{Tr}\left[H(\lambda_0)\rho_\beta(\lambda_0)\right] . \tag{4.10}$$

The final state of the system before measurement is $\rho_\tau = U(0,\tau)\rho_\beta(\lambda_0)U(0,\tau)^\dagger$, which is not equal to the Gibbs state $\rho_\beta(\lambda_\tau)$ because, in general, it is not possible to transform one Gibbs state to another via unitary evolution. As we will prove below, the process that minimises the entropy is the quasi-static, isothermal process where the work done is just the change in free energy,

$$\Delta F = \frac{1}{\beta}\left(\ln \mathcal{Z}(\lambda_0) - \ln \mathcal{Z}(\lambda_\tau)\right) . \tag{4.11}$$

This means that we can define the irreversible work and subsequently the irreversible entropy change by subtracting the actual average work from the free energy,

$$\langle S_{irr} \rangle = \beta \langle W_{irr} \rangle = \beta(\langle W \rangle - \Delta F). \tag{4.12}$$

In order to prove that $\beta\Delta F$ is the minimum entropy production we must derive a quantum version of the Jarzynski equality [230] for the TPM scheme. For an initial Gibbs state, we have $p_n = \frac{e^{-\beta E_n^i}}{\mathcal{Z}(\lambda_0)}$ so we can write the average exponential work as

$$\begin{aligned}
\left\langle e^{-\beta W} \right\rangle &= \sum_W P(W) e^{-\beta W} \\
&= \sum_{n,m} p_n p_{m|n} \delta_{W, E_m^f - E_n^i} e^{-\beta W} \\
&= \sum_{n,m} \frac{e^{-\beta E_n^i}}{\mathcal{Z}(\lambda_0)} |\left\langle m_f\right| U \left|n_i\right\rangle|^2 e^{-\beta(E_m^f - E_n^i)} \\
&= \frac{1}{\mathcal{Z}(\lambda_0)} \sum_n \left\langle n_i\right| U^\dagger \left(\sum_m e^{-\beta E_m^f} \left|m_f\right\rangle\!\left\langle m_f\right| \right) U \left|n_i\right\rangle \\
&= \frac{\mathcal{Z}(\lambda_\tau)}{\mathcal{Z}(\lambda_0)} \mathrm{Tr}\left(U^\dagger \rho_\beta(\lambda_\tau) U \right) \\
&= \frac{\mathcal{Z}(\lambda_\tau)}{\mathcal{Z}(\lambda_0)} = e^{-\beta \Delta F} .
\end{aligned} \tag{4.13}$$

This tells us that the definition of the work based on the TPM scheme provides a quantum equivalent of the Jarzynski equality of the exact same form. Rearranging this we get, $\langle e^{-S_{irr}} \rangle = 1$, then we can apply Jensen's inequality we get, $\langle S_{irr} \rangle \geq 0$, thus proving that $\beta\Delta F$ is the minimum

possible entropy production. Another way to prove this is to look directly at $\langle S_{irr} \rangle$,

$$\begin{aligned}
\langle S_{irr} \rangle &= \beta(\langle W \rangle - \Delta F) \\
&= \beta \left(\mathrm{Tr} \left[H(\lambda_\tau) \rho_\tau \right] - \mathrm{Tr} \left[H(\lambda_0) \rho_\beta(\lambda_0) \right] \right) - \left(\ln \mathcal{Z}(\lambda_0) + \ln \mathcal{Z}(\lambda_\tau) \right) \\
&= - \mathrm{Tr} \left[\ln \left(\frac{e^{-\beta H(\lambda_\tau)}}{\mathcal{Z}(\lambda_\tau)} \right) \rho_\tau \right] + \mathrm{Tr} \left[\ln \left(\frac{e^{-\beta H(\lambda_0)}}{\mathcal{Z}(\lambda_0)} \right) \rho_\beta(\lambda_0) \right] \\
&= - \mathrm{Tr} \left[\rho_\tau \ln \rho_\beta(\lambda_\tau) \right] - S(\rho_\beta(\lambda_0)) \\
&= S(\rho_\tau \| \rho_\beta(\lambda_\tau)).
\end{aligned} \tag{4.14}$$

This result holds when the system evolution is unitary, when we have a more general evolution described by a master equation, calculating the excess entropy production is much trickier as we discussed at the end of Chapter 2. We showed in Eq. (2.110) that the minimum excess entropy production for a series of sudden quenches can be calculated using action quantum speed limits.

Another important quantity is the characteristic function of the work,

$$G(u) = \int dW e^{iuW} P(W) = \mathrm{Tr} \left[U^\dagger e^{iuH(\lambda_\tau)} U e^{-iuH(\lambda_0)} \bar{\rho} \right] \tag{4.15}$$

where $\bar{\rho} = \sum_n \langle n_i | \rho | n_i \rangle | n_i \rangle\langle n_i |$ is the initial state, dephased in the basis of $\mathcal{H}_i$. The characteristic function can be used to derive many important quantities and relations. For example, we can see that $G(i\beta) = \int dW e^{-\beta W} P(W) = \left\langle e^{-\beta W} \right\rangle$. Talkner and Hänggi [231] use the characteristic function to derive a quantum version of the Crooks relation [232],

$$\frac{P_{\mathsf{F}}(W)}{P_{\mathsf{B}}(-W)} = e^{-\beta(W - \Delta F)}. \tag{4.16}$$

$P_{\mathsf{F}}(W)$ is just the work distribution in Eq. (4.1) with an initial thermal state $\rho_\beta(\lambda_0)$ ramped from $H(\lambda_0)$ to $H(\lambda_\tau)$, then the reverse process that gives $P_{\mathsf{B}}(W)$ is just an initial state $\rho_\beta(\lambda_\tau)$ undergoing the time-reversed ramp from $H(\lambda_\tau)$ to $H(\lambda_0)$. The quantum Crooks relation implies that a quantum TPM process is exponentially more likely to lead to a positive $\langle S_{irr} \rangle$. This sheds some light on how we obtain a thermodynamic arrow of time from an underlying time-reversible unitary evolution combined with the TPM protocol. The Jarzynski equality can be derived from the Crooks relation by rearranging and integrating over W. If instead, we take the log of both sides of Eq. (4.16) first and integrate over $P_{\mathsf{F}}(W)$ we get [233],

$$\begin{aligned}
\langle S_{irr} \rangle = \beta(\langle W \rangle - \Delta F) &= \int dW P_{\mathsf{F}}(W) (\log P_{\mathsf{F}}(W) - \log P_{\mathsf{B}}(-W)) \\
&= K(P_{\mathsf{F}}(W) \| P_{\mathsf{B}}(-W)),
\end{aligned} \tag{4.17}$$

where $K(P\|Q)$ is the classical Kullback–Leibler divergence. Comparing this to Eq. (4.14) we get an interesting relation between a classical and a quantum Kullback–Leibler divergence,

$$K(P_{\mathsf{F}}(W) \| P_{\mathsf{B}}(-W)) = S(\rho_\tau \| \rho_\beta(\lambda_\tau)). \tag{4.18}$$

By definition, the characteristic function is the generating function of the work distribution $P(W)$. Therefore, we can expand $G(u)$ around $u = 0$ to get,

$$G(u) = \sum_n^\infty \frac{(iu)^n}{n!} \langle W^n \rangle \,, \tag{4.19}$$

this means that the nth statistical moment can be calculated as

$$\langle W^n \rangle = (-i)^n \partial_u^n G(u)|_{u=0}. \tag{4.20}$$

The cumulants K_n can also be defined by expanding $\log G(u)$ in the same manner [234],

$$C_n = (-i)^n \partial_u^n \log G(u)|_{u=0}. \tag{4.21}$$

Combining the fact that $G(i\beta) = \left\langle e^{-\beta W} \right\rangle$ with the Jarzynski equality we get

$$\log G(i\beta) = -\beta \Delta F = \langle S_{irr} \rangle - \beta \langle W \rangle. \tag{4.22}$$

Then since $C_1 = \langle W \rangle$ we can write the irreversible entropy production solely in terms of the cumulants

$$\langle S_{irr} \rangle = \sum_{n=2}^\infty (-1)^n \frac{\beta^n}{n!} C_n. \tag{4.23}$$

This is particularly useful when the work distribution is a Gaussian, reducing the irreversible entropy production to $\langle S_{irr} \rangle = \beta^2 \, \mathrm{Var}(W)/2$.

4.1.3 Sudden Quench

A sudden quench is a protocol where the ramp from $\lambda_0 \to \lambda_\tau$ occurs in a very short time, such that the unitary, $U(0, \tau)$, can be approximated by the identity. This kind of quench is realisable experimentally in ultra cold atom experiments. Theoretically, sudden quenches have been particularly useful in the study of phase transitions through a quantum critical point [235–238].

It is worth digging more deeply into the idea of a sudden quench in order to identify just how fast the quench needs to be for the assumption of $U(0, \tau) = \mathbf{I}$ to hold and why it is useful to use this approximation. As we know from classical thermodynamics, the final state of our system depends not just on the total time of the ramp from $\lambda_0 \to \lambda_\tau$, but also on how the ramp is performed, i.e. it can depend on the value of λ_t at intermediate times. This is part of the motivation that we had in Chapter 2 to derive a quantum speed limit that depends on the instantaneous speed of the system evolution rather than just the average speed. There are infinitely many ways to ramp the system from $\lambda_0 \to \lambda_\tau$ and each of these can give different work distributions, therefore it is difficult to make any general claims about the work distribution without specifying the exact ramp protocol.

For the sudden quench we will assume that at time $t \leq 0$, the Hamiltonian of the system is

given by $\mathcal{H}_i = \sum_n E_n^i |n_i\rangle\langle n_i|$, and at time $t \geq \tau$, the Hamiltonian is $\mathcal{H}_f = \sum_m E_m^f |m_f\rangle\langle m_f|$. Then for times $0 \leq t \leq \tau$, it is useful to write the Hamiltonian in the form,

$$\mathcal{H}(t) = \mathcal{H}_f + V(t). \tag{4.24}$$

If we assume an initial pure state, then we can decompose the time dependent state in the final Hamiltonian basis,

$$|\psi_t\rangle = \sum_m c_m(t) |m_f\rangle \tag{4.25}$$

By applying the Schrödinger equation we can get a differential equation for the time evolution of $c_m(t)$,

$$i\hbar \frac{d}{dt} c_n(t) = \sum_m \langle n_f| V(t) |m_f\rangle e^{-i(E_m^f - E_n^f)t} c_m(t). \tag{4.26}$$

Then we can integrate this expression to get an explicit formula for the time dependent coefficients,

$$c_n(t) = c_n(0) - \frac{i}{\hbar} \sum_m \int_0^t \langle n_f| V(t') |m_f\rangle e^{-i(E_m^f - E_n^f)t'} c_m(t') dt'. \tag{4.27}$$

Now we want to consider the scenario where the quench is fast enough so that we can perturbatively expand $c_n(t)$. This means that we need $\langle n_f| V(t) |m_f\rangle \ll 1$ for all n, m. We will also assume that $(E_m^f - E_n^f)t' \ll 1$ so that we can approximate the exponential as 1. To first order we get [234] $c_n(t) \approx c_n(0) + c_n^{(1)}(t)$ with

$$c_n^{(1)}(t) = -\frac{i}{\hbar} \sum_m \int_0^t \langle n_f| V(t') |m_f\rangle c_m(0) dt'. \tag{4.28}$$

If our sudden quench assumption is to hold true then we expect that the change in the system state to be negligible, i.e. $|c_n^{(1)}(t)|^2 \ll 1$ for all n. If we assume that the initial state of our system is an eigenstate of initial Hamiltonian, which is always the case in the TPM protocol, we can decompose it in the final basis as $|k_i\rangle = \sum_m c_m(0) |m_f\rangle$ and we get the following condition [234]

$$|c_n^{(1)}(t)|^2 = \frac{1}{\hbar^2} \left| \int_0^t \langle n_f| V(t') |k_i\rangle \right|^2 \ll 1. \tag{4.29}$$

This term still depends on the specific quench but as we will see later, under some reasonable assumptions we can determine how fast the quench needs to be.

When it is not possible perform the quench fast enough for the sudden quench approximation to be valid, it may be possible to calculate the entropy of the work distribution by applying a control Hamiltonian, $H_c(t)$, to the system. The system Hamiltonian would be kept fixed leading to the unitary

$$U(\tau) = T_{\leftarrow} \exp\left[-\frac{i}{\hbar} \int_0^\tau dt \left(\mathcal{H}_i + \mathcal{H}_c(t) \right) \right]. \tag{4.30}$$

If we could choose $H_c(t)$ such that $U(\tau)$ is the unitary that transforms the eigenbasis of $\mathcal{H}_i$ to

that of $\mathcal{H}_f$ then the transition frequency between eigenstates would be identical to that of the sudden quench, allowing us to recreate H_u.

4.2 Entropy of the Work Distribution

In the previous section we defined the work distribution, $P(W)$, in Eq. (4.1). Using this definition, we can simply define the entropy of the work distribution as,

$$H_W = -\sum_W P(W) \ln P(W), \tag{4.31}$$

which characterizes the complexity of $P(W)$. It is zero when the work is deterministic, and can range up to $\ln N^2$ when $P(W)$ is uniform and all the Bohr frequencies are non-degenerate.

H_W is in general different from

$$H_{\mathrm{u}} = -\sum_{n,m} p_n p_{m|n} \ln p_n p_{m|n}, \tag{4.32}$$

which is the entropy of the distribution $p_n p_{m|n}$ when we do not collect probabilities that have equal values of work. We can define these sets of equal work as, $\Gamma_W = \{(n,m) : E_m^f - E_n^i = W\}$, and we can rewrite Eqs. (4.31) and (4.32) as

$$H_W = -\sum_W \sum_{(n,m)\in\Gamma_W} p_n p_{m|n} \ln P(W), \tag{4.33}$$

$$H_{\mathrm{u}} = -\sum_W \sum_{(n,m)\in\Gamma_W} p_n p_{m|n} \ln p_n p_{m|n}. \tag{4.34}$$

Their difference is then given by,

$$H_{\mathrm{u}} - H_W = -\sum_W \sum_{(n,m)\in\Gamma_W} p_n p_{m|n} \ln\left(\frac{p_n p_{m|n}}{P(W)}\right) \geq 0, \tag{4.35}$$

where the inequality follows from the fact that $\frac{p_n p_{m|n}}{P(W)} \leq 1$ for any $(n,m) \in \Gamma_W$. This immediately tells us that $H_{\mathrm{u}} \geq H_W$.

To provide a lower bound on H_W, we can also use Eq. (4.35). The entropy of each Γ_W on the right-hand side is maximal when all $p_n p_{m|n}$ in Γ_W are equal. So, if there are $|\Gamma_W|$ elements in Γ_W, we get

$$-\sum_{(n,m)\in\Gamma_W} p_n p_{m|n} \ln\left(\frac{p_n p_{m|n}}{P(W)}\right) \leq -\sum_{(n,m)\in\Gamma_W} p_n p_{m|n} \ln\left(\frac{1}{|\Gamma_W|}\right) = P(W) \ln|\Gamma_W|.$$

Hence

$$H_{\mathrm{u}} - H_W \leq \sum_W P(W) \ln|\Gamma_W| \leq \ln \gamma_{\max}. \tag{4.36}$$

Where $\gamma_{\max}$ is the size of the largest set Γ_W or equivalently can be thought of as the maximal degeneracy of the Bohr frequencies ($\gamma_{\max} \geq g_i g_f$, where $g_{i(f)}$ are the degeneracies of $\mathcal{H}_{i(f)}$). Now we can finally bound H_W above and below by

$$H_{\mathrm{u}} - \ln \gamma_{\max} \leq H_W \leq H_{\mathrm{u}}, \tag{4.37}$$

with equality if the values of work are all non-degenerate.

H_{u} is a much easier quantity to work with compared to H_W because, as we can see from Eq. (4.1), the properties of H_W can depend very sensitively on the specific structure of the initial and final Hamiltonians and their relation to each other. Although, as we will see, in practice, their behaviour is very closely related. H_{u} can be interpreted more straightforwardly, as we will see below.

We will now show that H_{u} can be split up into two contributions, the first is related to the entropy of the diagonal ensemble of the initial state, i.e. the initial state projected onto the basis of the initial Hamiltonian. Therefore, this is the contribution that comes from the first measurement in the TPM protocol. The second contribution is related to the transition frequencies between different states of the initial and final Hamiltonians and directly quantifies the degree of quantum coherence generated in the process. We start by separating the uncollected work,

$$\begin{aligned} H_{\mathrm{u}} &= -\sum_{n,m} p_n p_{m|n} \ln p_n p_{m|n} \\ &= -\sum_{n,m} p_n p_{m|n} \ln p_n - \sum_{n,m} p_n p_{m|n} \ln p_{m|n} \\ &= -\sum_{n} p_n \left(\sum_{m} p_{m|n} \right) \ln p_n - \sum_{n} p_n \sum_{m} p_{m|n} \ln p_{m|n} \\ &= -\sum_{n} p_n \ln p_n - \sum_{n} p_n \sum_{m} p_{m|n} \ln p_{m|n}. \end{aligned} \tag{4.38}$$

If we consider the basis $\left|m'_f\right\rangle = U^\dagger \left|m_f\right\rangle$ to be the coherent basis we can calculate the REC of an eigenstate of the initial Hamiltonian giving,

$$\mathcal{C}_r \left(|n_i\rangle\langle n_i| \right) = S(D_f(|n_i\rangle\langle n_i|)) - S(|n_i\rangle\langle n_i|) \tag{4.39}$$

$$= S\left(\sum_m \left\langle m'_f \middle| n_i \right\rangle \left\langle n_i \middle| m'_f \right\rangle \left| m'_f \middle\rangle\middle\langle m'_f \right| \right) \tag{4.40}$$

$$= S\left(\sum_m \langle m_f | U | n_i \rangle \ \langle n_i | U^\dagger | m_f \rangle \left| m'_f \middle\rangle\middle\langle m'_f \right| \right) \tag{4.41}$$

$$= -\sum_m p_{m|n} \ln p_{m|n}, \tag{4.42}$$

where the last line follows from the definition of $p_{m|n} = |\left\langle m_f \right| U \left| n_i \right\rangle|^2$. Thus, taking all this

together, Eq. (4.38) can be written as

$$H_{\mathrm{u}} = S(\bar{\rho}) + \sum_n p_n \mathcal{C}_r\left(|n_i\rangle\langle n_i|\right), \tag{4.43}$$

where $\bar{\rho} = \sum_n \langle n_i|\,\rho\,|n_i\rangle\,|n_i\rangle\langle n_i|$ is the initial state dephased in the basis of $\mathcal{H}_i$. Equivalently we could have considered the REC in the basis $|m_f\rangle$, which we will denote by $\mathcal{C}_r^*(\sigma)$, then we have the relation,

$$\mathcal{C}_r\left(|n_i\rangle\langle n_i|\right) = \mathcal{C}_r^*\left(U\,|n_i\rangle\langle n_i|\,U^\dagger\right), \tag{4.44}$$

this form is less concise, but it emphasises the fact that what matters is the coherence between the eigenstates of the final Hamiltonian and actual system state after the unitary evolution.

Equation (4.43) summarizes the rich physics behind the entropy of the work distribution. The first term is the entropy of the initial outcomes, p_n, of the TPM, i.e. the entropy of the so-called diagonal ensemble [239–243]. If $[\rho, \mathcal{H}_i] = 0$, it reduces to the von Neumann entropy of ρ, and if $\rho = e^{-\beta\mathcal{H}_i}/\mathcal{Z}_i$ is a thermal state, it reduces to the Gibbs thermal entropy. If $\rho = |k_i\rangle\langle k_i|$ is any eigenstate of $\mathcal{H}_i$, $S(\bar{\rho})$ vanishes and Eq. (4.43) reduces to $H_{\mathrm{u}} = \mathcal{C}(\,|k_i\rangle\langle k_i|\,)$. The second term in Eq. (4.43) establishes that the relevant coherences are those of each $|n_i\rangle$ in the eigenbasis $|m_f'\rangle$. Therefore, this term contains information on both the dynamics (work protocol) and of how $\mathcal{H}_f$ differs from $\mathcal{H}_i$. The process is incoherent if $p_{m|n} = |\langle m_f|U|n_i\rangle|^2 = \delta_{m,n}$, which occurs when $[\mathcal{H}_i, U^\dagger\mathcal{H}_f U] = 0$. In this case, Eq. (4.43) reduces to $H_{\mathrm{u}} = S(\bar{\rho})$.

We can take this a step further,

$$\begin{aligned}
\sum_n p_n \mathcal{C}\left(|n_i\rangle\langle n_i|\right) &= \sum_n p_n S\left(D_f(|n_i\rangle\langle n_i|)\right) && (4.45)\\
&\leq S\left(\sum_n p_n D_f(|n_i\rangle\langle n_i|)\right) && (4.46)\\
&= S\left(D_f(\bar{\rho})\right) && (4.47)\\
&= \mathcal{C}(\bar{\rho}) + S(\bar{\rho}) && (4.48)
\end{aligned}$$

where the inequality is a consequence of the concavity of the von Neumann entropy. Subbing this into our equation for H_{u} we get

$$H_{\mathrm{u}} \leq 2S(\bar{\rho}) + \mathcal{C}(\bar{\rho}). \tag{4.49}$$

The tightness of this bound is related to the purity of $\bar{\rho}$, being saturated when ρ is an eigenstate of $\mathcal{H}_i$ or for thermal states in the zero-temperature limit.

Combining Eqs. (4.37), (4.43) and (4.49), we can place a series of bounds on the entropy of the work distribution,

$$H_W \leq S(\bar{\rho}) + \sum_n p_n \mathcal{C}(\,|n_i\rangle\langle n_i|\,) \leq 2S(\bar{\rho}) + \mathcal{C}(\bar{\rho}). \tag{4.50}$$

The first inequality is often quite tight and relates H_W to the coherences of each individual

transition $\mathcal{C}(\,|n_i\rangle\langle n_i|\,)$. The second inequality bounds H_W to the full REC of $\bar{\rho}$ and its tightness is related to the purity of $\bar{\rho}$. Eq. (4.50) also allows us to estimate the dependence of H_W with temperature T, in the case of an initial thermal state. Both $S(\bar{\rho})$ and the p_n depend on T. However, by convexity

$$H_W \leq S(\bar{\rho}) + \mathcal{C}_{\max}, \tag{4.51}$$

where $\mathcal{C}_{\max} = \max_n \mathcal{C}(\,|n_i\rangle\langle n_i|\,)$. The last term is now T independent, pushing the temperature dependence solely to the Gibbs thermal entropy. The temperature dependence of the coherence terms is therefore simple and bounded, while $S(\bar{\rho})$ is the Gibbs entropy and remains temperature dependent. We next turn to the study of H_W in different models and show that it conveys crucial information about the work statistics.

4.3 Landau-Zener Model

Consider a qubit with local Hamiltonian,

$$\mathcal{H}_{\mathrm{LZ}}(\omega) = \hbar\Delta\sigma_x + \hbar\omega\sigma_z, \tag{4.52}$$

where σ_i are the Pauli matrices. This is known as the Landau-Zener (LZ) model, it simulates a two-level quantum system interacting with a time-dependent external field, $\omega(t)$. Although this is an incredibly simple system, it captures the physics of a wide range of phenomena over many orders of magnitude of length scales. Some examples of these phenomena include superconducting circuits with Josephson junctions [244] which can perhaps, most famously, be used to encode physical qubits in quantum computers; quantum dots can also behave as effective two-level systems under the right conditions [245]. Another candidate for quantum computing that can be modelled by the LZ model are atomic impurities, such as nitrogen-vacancy centers in diamond [246]. At larger length scales, graphene connected to two gold electrodes can display the avoided crossing and non-adiabatic transitions that are found in the LZ model [247]. Surprisingly, the physics of the LZ model also appears in classical physics, one example of this can be found in the study of nanomechanical resonators [248]. More detail and many more examples of LZ physics can be found in the review by Ivakhnenko *et. al.* [249].

The eigenenergies are $E_- = -\sqrt{\omega^2 + \Delta^2}\hbar$ and $E_+ = \sqrt{\omega^2 + \Delta^2}\hbar$. This tells us that the energy gap between the ground and excited state is $\Delta E = 2\sqrt{\omega^2 + \Delta^2}\hbar$. In the usual setup of the LZ model, Δ is fixed and ω is an externally controlled parameter that is varied from an initial to a final value. We can see from Fig. 4.1 that the minimum energy gap, which is equal to 2Δ, is obtained when $\omega = \omega_c \equiv 0$. The energy levels never cross, this is often referred to as an avoided crossing at ω_c. The instantaneous eigenstates of the model can also be calculated as

$$|E_\pm\rangle = \epsilon_\mp\,|0\rangle + \epsilon_\pm\,|1\rangle \tag{4.53}$$

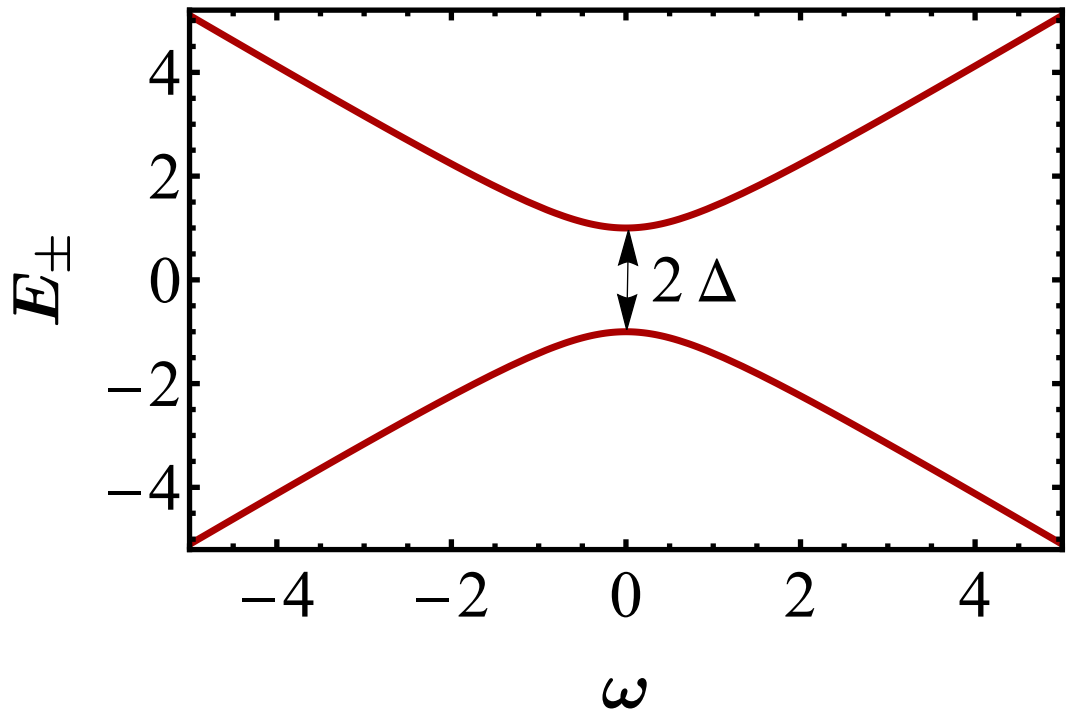

Figure 4.1: The Landau-Zener energy spectrum as a function of ω with $\Delta = 1$, highlighting the avoided crossing at $\omega = 0$.

where

$$\epsilon_\pm = \frac{1}{\sqrt{2}}\sqrt{1 \pm \frac{\omega}{\sqrt{\omega^2 + \Delta^2}}}. \tag{4.54}$$

Perhaps the most common use case of the LZ model is to calculate the probability of a non-adiabatic transition happening between the ground state and the excited state when the field is varied at a finite speed. If we assume a linear ramp, $\omega(t) = \nu t$, and start in the ground state at $t \to -\infty$ and ramp through the avoided crossing to $t \to +\infty$, the probability of finding the system in the excited state can be calculated as [249]

$$P_+ = e^{-\frac{\pi\Delta^2}{2\hbar\nu}}. \tag{4.55}$$

We see that the probability of obtaining a non-adiabatic transition scales exponentially with the speed of the ramp. This analysis is related to the so-called adiabatic theorem [250] which says that if a system initially in an eigenstate of the Hamiltonian and the Hamiltonian is varied slowly enough then the system will remain in that instantaneous eigenstate. So, for the LZ model with a linear ramp, the condition for the adiabatic theorem to hold is [234], $\hbar\nu/\Delta^2 \ll 1$. We will be working in the sudden quench regime where the adiabatic theorem definitely does not hold.

We assume the system starts in a thermal state at inverse temperature β, and consider a sudden quench ($U = \mathbf{I}$) from $\mathcal{H}_i = \mathcal{H}_{\rm LZ}(\omega_i)$, with $\omega_i < 0$, to $\mathcal{H}_f = \mathcal{H}_{\rm LZ}(\omega_f)$. There are four allowed values of W, given by $E_\pm(\omega_f) - E_\pm(\omega_i)$. For $\omega_f \neq \pm\omega_i$ and fixed Δ, these will always be

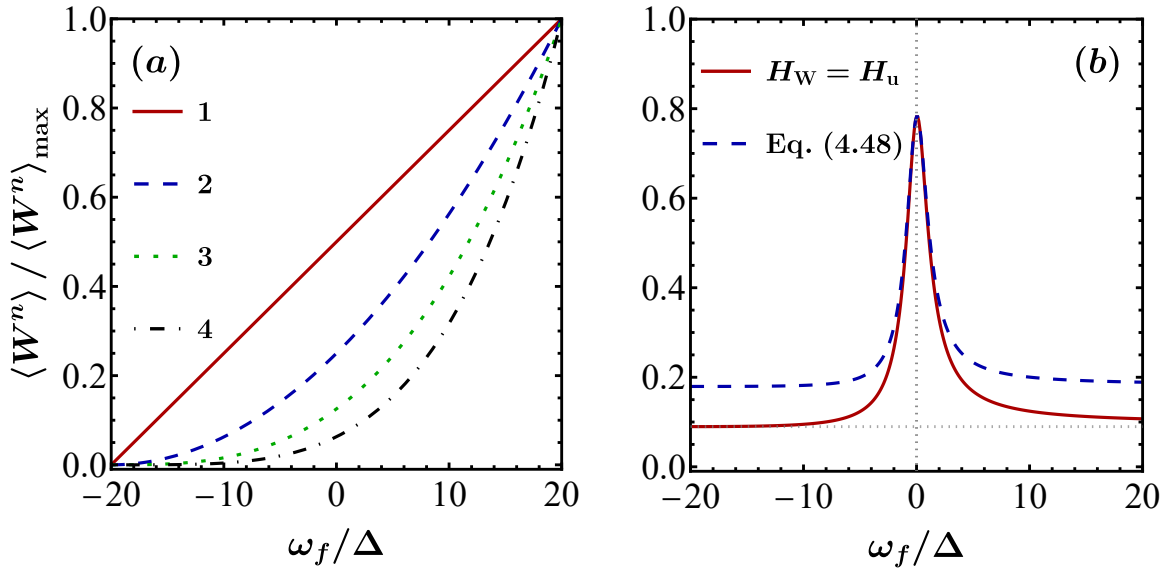

Figure 4.2: Work fluctuations in the Landau-Zener model under a sudden quench. (a) First four moments $\langle W^n \rangle$ of $P(W)$ as a function of ω_f/Δ (normalized by their maximum value, at $\omega_f = \Delta$). (b) Entropy of the work distribution, Eq. (4.31) (red-solid), and the corresponding bound, Eq. (4.49) (blue-dashed). Parameters: $\beta = 0.1(\hbar\Delta)^{-1}$ and $\omega_i = -20\Delta$.

non-degenerate and thus $H_W = H_u$. Figure 4.2(a) shows the first four moments $\langle W^n \rangle$ of $P(W)$, as a function of ω_f/Δ. We can explicitly calculate these moments and we get,

$$\langle W \rangle = \frac{\omega_i(\omega_i - \omega_f)\tanh\left(\beta\sqrt{1+\omega_i^2}\right)}{\sqrt{1+\omega_i^2}} \tag{4.56}$$
$$\langle W^2 \rangle = (\omega_i - \omega_f)^2$$

for the first two moments. This explains why we see linear scaling for $\langle W \rangle$ as a function of ω_f. Even when we fix the ω_f and allow ω_i to vary, there is no evidence of an avoided crossing in the first few moments. Although knowledge of all the moments is sufficient to recover the entire probability distribution, this is not feasible in practise. The cumulants also show no evidence of the avoided crossing. In Fig. 4.2(b) we see a clear peak in H_W around $\omega_f = 0$. The first term in (4.43), $S(\bar{\rho})$, yields a constant base value, as it depends only on the initial condition, this value is displayed as the horizontal grey line in Fig. 4.2(b). The second term, on the other hand, presents a peak at $\omega_f = \omega_c$. This term is a sum of coherence measures, highlighting that the interesting features of the LZ model occur due to the generation of coherence between the Hamiltonian bases. This also explains why we see the majority of non-adiabatic transitions occurring near the avoided crossing where the coherence is largest [113]. By probing H_W we can therefore highlight the avoided crossing, which is the most important feature of the LZ model, and which is masked in the moments. In Fig. 4.2(b) we also plot the bound. Eq. (4.49), which displays evidence of the

avoided crossing and becomes tight around $\omega_f = 0$. The Landau-Zener model has proved to be important when dealing with a number of quantum critical models including the XY and Ising models [251] and the Kitaev model [252, 253]. These models can all be expressed as the sum of non-interacting Landau-Zener models. This fact can be used to traverse the quantum critical point adiabatically by applying a counter-diabatic control Hamiltonian [254]. Furthermore, the entropy of the work distribution could be used to identify systems in which Landau-Zener physics may be playing an important role.

4.4 Aubry-André-Harper Model

The localisation phenomenon is a major area of interest in condensed matter physics. An electron in a lattice is said to be localised if its wave function has little to no overlap with neighbouring sites. There are two main toy models that exhibit a transition from de-localised to localised, known as the metal-insulator transition, as disorder is increased. One is the Anderson tight-binding model [255]. For non-interacting systems this model is described by the time-dependent Schrödinger equation where the Hamiltonian acts on the state like

$$H\psi_j = E_j\psi_j + \sum_{k\neq j} V_{jk}\psi_k \tag{4.57}$$

where E_j are independent random variables and $V(r)$ is symmetric in all dimensions and falls off faster than r^{-3} at infinity. Anderson showed that localisation occurs in this model in any dimension when the disorder, produced by the random energy amplitudes, is sufficiently large. Additionally, he showed that in one and two dimensions localisation occurs in the thermodynamic limit no matter how small the disorder is [255]. The other main toy model used is the Aubry-André-Harper Model (AAH) model, in this model the disorder is caused by the existence of two lattice potentials where the ratio between their wavelengths is irrational. Unlike the Anderson model, the disorder here is correlated rather than random [256], the irrational ratio of wavelengths ensures that the lattice potential is aperiodic. For finite lattices, a rational ratio P/Q is sufficient but both P and Q must be prime numbers larger than the size of the lattice [256] such that the potential is aperiodic within the lattice. We chose to study the AAH model because there is a localisation transition in one dimension whereas for the Anderson model there must be at least three dimensions for a transition to be present [257]. Additionally, the AAH model requires no random disorder, and it is therefore easier to examine analytically and finite dimensional properties.

We consider a single particle AAH model in the extreme tight binding limit on a lattice with N sites, labelled by states $|i\rangle$. The Hamiltonian is [256, 258, 259]

$$\mathcal{H}_{\mathrm{AAH}}(\Delta) = \hbar\sum_{j=1}^{N}\Big[\Delta\cos\left(2\pi\gamma j+\eta\right)|j\rangle\langle j| - J(\,|j\rangle\langle j+1| + |j+1\rangle\langle j|\,)\Big], \tag{4.58}$$

with periodic boundary conditions. The first term denotes the on-site potentials, with overall

magnitude Δ, phase η, and γ modulation or ratio between the lattice potential wavelengths. One interesting property of the AAH Hamiltonian can be seen in its representation in the momentum basis,

$$|k\rangle_m = \frac{1}{\sqrt{N}} \sum_j e^{-2\pi i \gamma k j} \, |j\rangle \, . \tag{4.59}$$

if we sub this into Eq. (4.58) the first term becomes

$$\begin{aligned} \Delta \sum_{j=1}^{N} \cos\left(2\pi\gamma j + \eta\right) |j\rangle\langle j| &= \frac{\Delta}{N} \sum_{j,k,l=1}^{N} \cos\left(2\pi\gamma j + \eta\right) e^{2\pi i \gamma j (l-k)} \, {}_m|k\rangle\langle l|_m \\ &= \frac{\Delta}{2N} \sum_{j,k,l=1}^{N} \left(e^{i\eta} e^{2\pi i \gamma j (1+l-k)} + e^{-i\eta} e^{2\pi i \gamma j (l-k-1)} \right) \, {}_m|k\rangle\langle l|_m \, , \end{aligned} \tag{4.60}$$

where we applied Euler's identity between the first and second lines. From here we can apply the geometric series formula over j to obtain

$$\sum_{j=1}^{N} e^{2\pi i \gamma j n} = \frac{e^{2\pi i \gamma N n} - 1}{1 - e^{2\pi i \gamma n}}. \tag{4.61}$$

If γN is an integer, which we will assume, and $n \neq \{0, N\}$ this is just 0. Therefore, the only non-zero terms left are for $n = 0$, i.e. $k = l - 1$ and $k = l + 1$, and periodic boundary conditions. These terms all sum to N, subbing this back into Eq. (4.60) gives,

$$\Delta \sum_{j=1}^{N} \cos\left(2\pi\gamma j + \eta\right) |j\rangle\langle j| = \frac{\Delta}{2} \sum_{k=1}^{N} \left(e^{i\eta} \, {}_m|k\rangle\langle k-1|_m + e^{-i\eta} \, {}_m|k\rangle\langle k+1|_m \right) . \tag{4.62}$$

Now we can look at the second term in Eq. (4.58),

$$\begin{aligned} J \sum_{j=1}^{N} \left(|j\rangle\langle j+1| + |j+1\rangle\langle j| \right) &= J \sum_{j=1}^{N} \left(|j\rangle\langle j+1| + |j\rangle\langle j-1| \right) \\ &= \frac{J}{N} \sum_{j,k,l=1}^{N} \left(e^{2\pi i \gamma [(j+1)l - jk]} + e^{2\pi i \gamma [(j-1)l - jk]} \right) \, {}_m|k\rangle\langle l|_m \\ &= \frac{2J}{N} \sum_{l=1}^{N} \cos\left(2\pi\gamma l\right) \sum_{j,k=1}^{N} \left(e^{2\pi i \gamma j (l-k)} \right) \, {}_m|k\rangle\langle l|_m \\ &= 2J \sum_{l=1}^{N} \cos\left(2\pi\gamma l\right) \, {}_m|l\rangle\langle l|_m \, , \end{aligned} \tag{4.63}$$

where we once again applied the summation trick over j. So, if we set $\eta = 0$ we find that the Hamiltonian in the momentum basis is

$$\mathcal{H}_{\mathrm{AAH}}(\Delta) = \hbar \sum_{j=1}^{N} \left[2J \cos\left(2\pi\gamma j\right) \, {}_m|j\rangle\langle j|_m - \frac{\Delta}{2} \left(\, {}_m|j\rangle\langle j+1|_m + \, {}_m|j+1\rangle\langle j|_m \right) \right]. \tag{4.64}$$

We see that the on-site energy term has changed from $\Delta \to 2J$ and the hopping rate has changed from $J \to \Delta/2$. This tells us that when $J = 2\Delta$, the Hamiltonian is equivalent in the position and momentum bases. The Heisenberg uncertainty principle for position and momentum as in Eq. (2.6) tells us that if the AAH Hamiltonian has an exponentially localised eigenstate in the position basis, this eigenstate must be exponentially delocalised or extended in the momentum basis. Therefore, if there is a sharp localisation transition in this model it must occur at $J = 2\Delta$. Indeed, we do find a sharp localisation transition in this model in the thermodynamic limit, for $\Delta < 2J$ all eigenvectors are delocalized in space, in particular, for $\Delta = 0$, they are all plane waves, while for $\Delta > 2J$, they become localized around the sites in the lattice.

We focus on the work distribution associated with turning the quasiperiodic potential off/on, i.e. in going from $\mathcal{H}_{\mathrm{AAH}}(\Delta) \to \mathcal{H}_{\mathrm{AAH}}(0)$, and vice-versa. We refer to these as $\Delta \to 0$ and $0 \to \Delta$, respectively. Following [256, 260, 261], we choose the lattice size, N, to be a Fibonacci number, F_n and $\gamma = F_{n-1}/F_n$ to be a rational approximation to the inverse golden ratio. This ensures that while the periodic boundary conditions are fulfilled, the potential is aperiodic within the lattice as in experimental realizations in optical lattices. We also get an integer value for $N\gamma$ which allows for nice analytic properties such as the momentum basis transformation in Eq. (4.64)

4.4.1 Sudden Quench

We also choose to focus on sudden quenches ($U = \mathbf{I}$). Following on from our discussion in Sec. 4.1.3, we can look more closely at Eq. (4.29) in order to see in how fast our quench needs to be for the sudden quench approximation to hold. Since our Hamiltonian is of the form

$$\mathcal{H}(t) = A + \lambda(t)B \tag{4.65}$$

where our quench parameter is $\Delta(t)$, giving

$$B = -\frac{\hbar}{2}\sum_{i=1}^{N}\left(|i\rangle\langle i+1| + |i+1\rangle\langle i|\right)\Bigg]. \tag{4.66}$$

we can write Eq. (4.29) as [234]

$$|c_n^{(1)}(t)|^2 = \frac{1}{\hbar^2}\left|\langle n_f|\, B\, |k_i\rangle\right|^2 \left|\int_0^t (\lambda_\tau - \lambda(t'))dt'\right|^2 \ll 1. \tag{4.67}$$

Then if we assume that our quench is approximately linear from $\lambda_0 \to \lambda_\tau$ we get the following upper bound on the quench time τ

$$\tau \ll \frac{\hbar}{|\lambda_\tau - \lambda_0|}\frac{2}{|\langle n_f|\, B\, |k_i\rangle|}. \tag{4.68}$$

Finally, we need to explicitly calculate this for the AAH model,

$$|\langle n_f|\, B\, |k_i\rangle| = \frac{\hbar}{2}\left|\sum_j \langle n_f|j\rangle\, \langle j+1|k_i\rangle + \langle n_f|j+1\rangle\, \langle j|k_i\rangle\right|. \tag{4.69}$$

By splitting the two terms up into separate sums and applying the triangle inequality we get

$$|\langle n_f|\, B\, |k_i\rangle| \leq \frac{\hbar}{2}\left(\left|\sum_j \langle n_f|j\rangle\, \langle j+1|k_i\rangle\right| + \left|\sum_j \langle n_f|j+1\rangle\, \langle j|k_i\rangle\right|\right). \tag{4.70}$$

Now we can apply the Cauchy-Schwarz inequality to both sums giving

$$|\langle n_f|\, B\, |k_i\rangle| \leq \frac{\hbar}{2}\sqrt{\left(\sum_j \langle n_f|j\rangle\, \langle j|n_f\rangle\right)\left(\sum_j \langle k_i|j+1\rangle\, \langle j+1|k_i\rangle\right)} \tag{4.71}$$

$$+\frac{\hbar}{2}\sqrt{\left(\sum_j \langle n_f|j+1\rangle\, \langle j+1|n_f\rangle\right)\left(\sum_j \langle k_i|j\rangle\, \langle j|k_i\rangle\right)} = \hbar. \tag{4.72}$$

So, when we have a quench from $\Delta \to 0$ or $0 \to \Delta$ the quench time must be much less than

$$\tau \ll \frac{2}{\Delta}. \tag{4.73}$$

These kinds of timescale are achievable in these models when using ultra cold atoms in an optical lattice. In one experiment [261] they had a value of $\hbar J = h \times 150$ Hz, meaning that in order to perform quenches up to $\Delta = 4J$ the quench time would need to be much smaller than $5 \times 10^{-4} s$.

4.4.2 Approximating the Energy Spectrum

Figure 4.3(a,b) shows the work distribution, Eq. (4.1), for the two protocols, assuming the system starts in the ground-state of the initial Hamiltonian. The spectrum of $\mathcal{H}_{\mathrm{AAH}}(\Delta)/\hbar$ is bounded between $\{-2J-\Delta, 2J+\Delta\}$ [262]. This bound is rather loose, however. To obtain a tight bound, we can use the fact that the eigenstates of our Hamiltonian are exponentially localised in position space for $\Delta > 2J$ and exponentially localised in momentum space for $\Delta < 2J$. This means that a perturbative expansion of the Hamiltonian will be particularly effective at capturing the physics of the system. In the $\Delta > 2J$ regime we can factor Δ out of the Hamiltonian to get,

$$\mathcal{H}_{\mathrm{AAH}}(\Delta) = \hbar\Delta \sum_{j=1}^{N}\left[\cos\left(2\pi\gamma j + \eta\right)|j\rangle\langle j| - \frac{J}{\Delta}\left(\,|j\rangle\langle j+1| + |j+1\rangle\langle j|\,\right)\right] \tag{4.74}$$

$$= \hbar\Delta\left[H_0 - \frac{J}{\Delta}V\right],$$

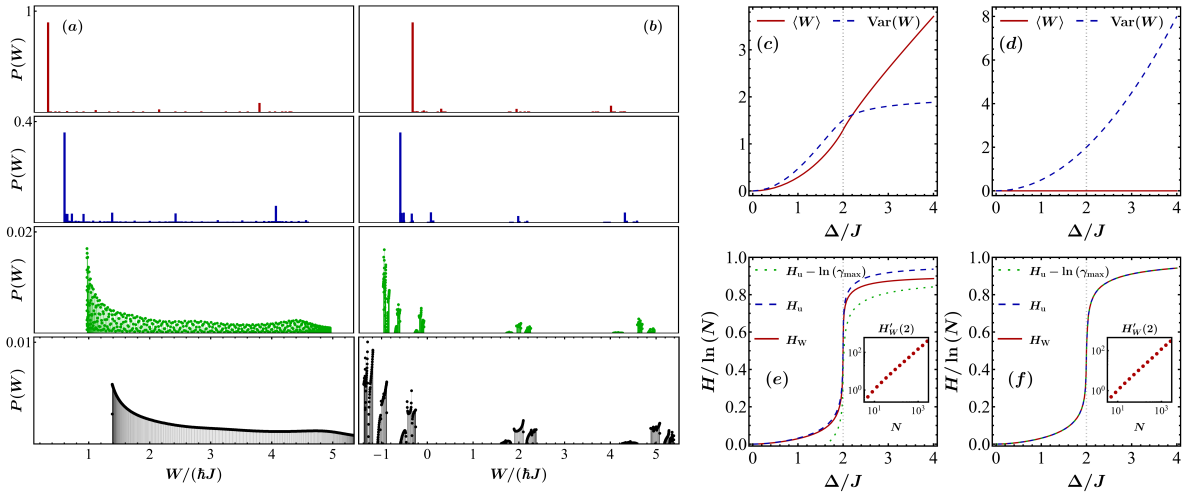

Figure 4.3: Work statistics of the AAH model (4.58). (a) $P(W)$ for the $\Delta \to 0$ protocol, for $\Delta/J = 1.5, 2, 2.5$ and 3. (b) Similar, but for $0 \to \Delta$. (c,d) Corresponding mean and variance vs. Δ/J, for the two protocols. (e,f) H_W vs. Δ/J [Eq. (4.31)] for the two protocols along with the upper and lower bounds derived in Eq. (4.43). (Inset): $dH_W/d\Delta\big|_{\Delta=2J}$ as a function of a Fibonacci number N, showing that in the thermodynamic limit H_W will change discontinuously at $\Delta/J = 2$. In all simulations the system starts in the ground-state, $N = F_{16} = 987$ and $\eta = 1.2$, except in the insets of (e,f), which were averaged over 50 values of η.

the eigenvalues of the unperturbed Hamiltonian are therefore $E_j^{(0)} = \cos(2\pi\gamma j + \eta)$. We can now expand this in powers of $\frac{-J}{\Delta}$. The first order correction to the energies is just $\left\langle j^{(0)}\right| V \left|j^{(0)}\right\rangle$ which is zero for all j. The second order correction is given by

$$E_j^{(2)} = \sum_{k\neq j} \frac{|\langle k^0| V |j^0\rangle|^2}{E_j^{(0)} - E_k^{(0)}} \tag{4.75}$$
$$= \frac{1}{\cos(2\pi\gamma j + \eta) - \cos(2\pi\gamma(j+1) + \eta)} + \frac{1}{\cos(2\pi\gamma j + \eta) - \cos(2\pi\gamma(j-1) + \eta)}.$$

The maximum and minimum eigenvalues occur for $\cos(2\pi\gamma j + \eta) \approx 1$ and -1 respectively. This gives us an approximate estimate of the range of the spectrum between

$$E_\pm^> = \pm\left(\Delta + \frac{2J^2}{\Delta}\frac{1}{1-\cos(2\pi\gamma)}\right) + O\left(\frac{J^4}{\Delta^3}\right), \tag{4.76}$$

in the $\Delta > 2J$ regime. We can perform an equivalent analysis for the momentum basis Hamiltonian in the $\Delta < 2J$ regime to get

$$E_\pm^< = \pm\left(2J + \frac{\Delta^2}{4J}\frac{1}{1-\cos(2\pi\gamma)}\right) + O\left(\frac{\Delta^4}{J^3}\right). \tag{4.77}$$

These approximations are even equal at $\Delta = 2J$ giving a continuous estimate for the maximum and minimum eigenvalues that we can define as

$$E_{\pm}(\Delta) = \begin{cases} E_{\pm}^{<} & 0 \leq \frac{\Delta}{J} \leq 2 \\ E_{\pm}^{>} & \frac{\Delta}{J} > 2 \end{cases}.$$

These results are for Δ and J both positive but changing the signs will only affect the sign in front of the maximum and minimum energies and not on their form or absolute value.

This analysis can help us understand the maximum and minimum work in both protocols. For the $\Delta \to 0$ protocol we know that starting in the ground state $E_i \approx E_-(\Delta) = -E_+(\Delta)$, then the final energy can range between $E_f \in [-2J, 2J]$. We can use this to put an approximate bound on the possible work values, $W \in [E_+ - 2J, E_+ + 2J]$. Since $E_+(\Delta) \geq 2J$ for all Δ, we get $W > 0$ in the $\Delta \to 0$ protocol. On the other hand, for $0 \to \Delta$, we have $E_i = -2J$,and $E_f \in [-E_+(\Delta), E_+(\Delta)]$. This gives a range of works $W \in [2J - E_+, E_+ + 2J]$ meaning that $W \lesseqgtr 0$. Thus, work can be extracted by turning the potential on, but not by turning it off.

The overall behaviour of $P(W)$ clearly reflects the localization transition at $\Delta = 2J$. For both protocols, quenches that keep the system in the delocalized phase, i.e. $\Delta < 2J$ (corresponding to the first two upper panels of Fig. 4.3(a,b)), result in a $P(W)$ with small support, and mostly concentrated around a minimum work value. In this regime, the work cost of turning the potentials on or off is overall small and fluctuates very little. This is also evidenced in Fig. 4.3(c,d), which plots the mean and variance of W, for the two protocols. Conversely, when $\Delta/J > 2$ the support of $P(W)$ increases significantly. For $\Delta \to 0$ (Fig. 4.3(a)) the distribution reflects the smooth energy spectrum, while for $0 \to \Delta$ [Fig. 4.3(b)] it is very irregular due to the fractal nature of the localized spectrum. The corresponding mean and variance of the work are shown in Fig. 4.3(c,d) and, except for $\langle W \rangle$ in the $0 \to \Delta$ protocol which turns out to be identically zero, all grow steadily with Δ/J. To understand why the work is zero in the $0 \to \Delta$ protocol we need to look more closely at how the average work is calculated

$$\langle W \rangle = \mathrm{Tr}\left[\left(\mathcal{H}_f - \mathcal{H}_i \right) |\psi_0\rangle\langle\psi_0| \right], \tag{4.78}$$

where $|\psi_0\rangle$ is the ground state of the initial Hamiltonian. Using Eq. (4.58) we can rewrite this as

$$\langle W \rangle = \Delta \sum_{k=1}^{N} \cos(2\pi\gamma k + \eta) \left| \langle k|\psi_0\rangle \right|^2. \tag{4.79}$$

It is clear from this equation that if $|\psi_0\rangle$ is independent of Δ then the work will scale linearly with Δ, this explains why we only see evidence of the localisation transition when $\mathcal{H}_i$ changes with Δ. When $\mathcal{H}_i = \mathcal{H}_{\mathrm{AAH}}(0)$ we can additionally prove that $\langle W \rangle = 0$. This follows from the fact that

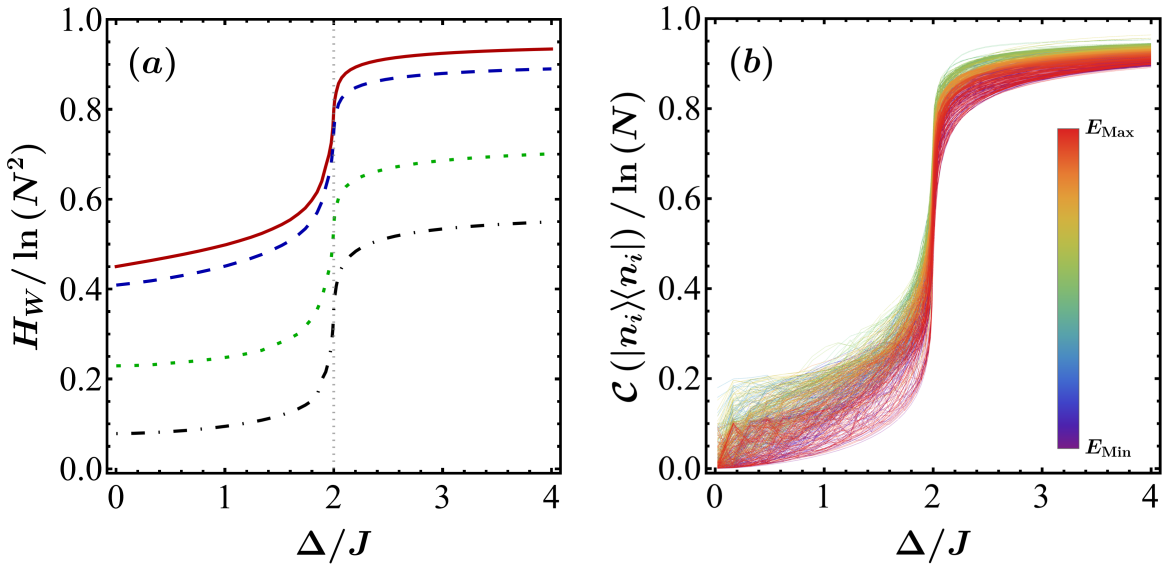

Figure 4.4: The entropy of $P(W)$ for (a) initial thermal states with temperatures $J\beta = \{10^{-2}, 10^{0}, 10^{2}, 10^{4}\}$(red [top], blue, green, black [bottom]) and (b) every eigenstate of the initial Hamiltonian, $\mathcal{H}_{\rm AAH}(0)$. These are all for the $0 \to \Delta$ case but the $\Delta \to 0$ case is very similar. The choice of phase and system size are as in Fig. 4.3.

the ground state is completely delocalised: $|\psi_0\rangle = \frac{1}{\sqrt{N}} \sum_{j=1}^{N} |j\rangle$. Substituting this in we get

$$\langle W \rangle = \frac{\Delta}{N} \sum_{k=1}^{N} \cos[2\pi\gamma k + \eta] \tag{4.80}$$

$$= \frac{\Delta}{N} \mathcal{R}\left[\sum_{k=1}^{N} e^{2\pi i\gamma k + i\eta}\right] \tag{4.81}$$

$$= \frac{\Delta}{N} \mathcal{R}\left[e^{i\eta} \frac{e^{i2\pi\gamma N} - 1}{1 - e^{-i2\pi\gamma}}\right] = 0. \tag{4.82}$$

The last equation comes from the fact that we use a rational approximation for the golden ratio given by the ratio of Fibonacci numbers, $\gamma = F_{n-1}/F_n$, and $N = F_n$. Unlike in the previous example, where due to the simplicity of the LZ model the moments of the distribution showed no signatures of the avoided crossing, here we find that some evidence of the transition is imprinted on the moments for $\Delta \to 0$, albeit in a significantly less striking manner than in the entropy.

4.4.3 Entropy of the quantum work distribution

H_W is plotted in Figs. 4.3(e,f). It shows a jump at $\Delta/J = 2$, the sharpness of which depends on the lattice size N. To illustrate this, the insets of Figs. 4.3(e,f) show the slope $H'_W(2) := dH_W/d\Delta$, evaluated at $\Delta = 2J$, for different system sizes, N. A fit of the data reveals the relation, $H'_W(2) \propto \sqrt{N}$, which implies that, in the thermodynamic limit, H_W will change discontinuously

at the localization transition. The entropy therefore succinctly captures the criticality of the AAH model. The two bounds in Eq. (4.37) are also shown in Figs. 4.3(e,f). For any $\Delta \neq 0$, the spectrum of the AAH model is non-degenerate but for $\Delta = 0$ there is a two-fold degeneracy in all eigenvalues except the minimum and maximum eigenvalues. This explains why for $\Delta \to 0$ (Fig.4.3(e)) the curves differ from H_W, but for $0 \to \Delta$ (Fig.4.3(f)) they coincide: the former depends on the degeneracies of $\mathcal{H}_{\mathrm{AAH}}(0)$, leading to $\gamma_{\max} = 2$, while the latter does not since we start in the (non-degenerate) ground-state. For $\Delta/J > 2$, H_W is close to $H_W - \ln \gamma_{\max}$, tending to it asymptotically as $\Delta/J \to \infty$ because the probability of measuring in either of the degenerate states becomes equal.

It is clear from the above discussion that H_W is an effective quantifier of localisation. To better understand why this is the case, we must first look at the most common quantifier of localisation in the literature, the inverse participation ratio (IPR). The IPR of a state $|\psi\rangle$ is the sum of the squared overlap of $|\psi\rangle$ with the localised states, i.e.

$$\mathrm{IPR}(|\psi\rangle) = \sum_j |\langle j|\psi\rangle|^4. \tag{4.83}$$

When the state is fully localised, we have $\mathrm{IPR}(|\psi\rangle) = 1$ and a fully delocalised state gives $\mathrm{IPR}(|\psi\rangle) = 1/N$. We can define a modified version of the IPR where the localised states are replaced by the eigenstates of the final Hamiltonian,

$$\mathcal{I}_n := \sum_m p_{m|n}^2 = \sum_m |\langle m_f| U |n_i\rangle|^4. \tag{4.84}$$

These two quantities would coincide for a $\Delta \to \infty$ sudden quench but it is unrealistic to perform this as a sudden quench. In fact, due to the position-momentum duality in the model, for the $\Delta \to 0$ protocol $\mathcal{I}$ can be thought of as an IPR measuring localisation in momentum space. This quantity is the inverse of the "effective dimension" [263, 264] which has been used to investigate localisation and quantum scars. Noticing that $-\ln \mathcal{I}_n$ is the Rényi-2 entropy of $p_{m|n}$, it then follows that,

$$\mathcal{C}\left(|n_i\rangle\langle n_i|\right) = -\sum_m p_{m|n} \ln p_{m|n} \geq -\ln \mathcal{I}_n. \tag{4.85}$$

Then subbing this into Eq.(4.43) we can relate the modified IPR to the entropy of the work distribution,

$$H_W \geq H_{\mathrm{u}} \geq S(\bar{\rho}) - \sum_n p_n \ln \mathcal{I}_n. \tag{4.86}$$

While Fig. 4.3 was concerned with the ground state, in the AAH model H_W shows a qualitatively similar behaviour at finite temperatures [Fig. 4.4(a)]. As the temperature increases, H_W tends to grow, but maintains the same overall shape as a function of Δ, and still exhibits strong signatures of the transition. This is due to the fact that in a localization transition *all* eigenvectors undergo a sudden change. This means that all terms $\mathcal{C}(|n_i\rangle\langle n_i|)$ in Eq. (4.43) behave similarly at the localisation transition, resulting in a consistent shape of the H_W curve since $S(\bar{\rho})$ is indepen-

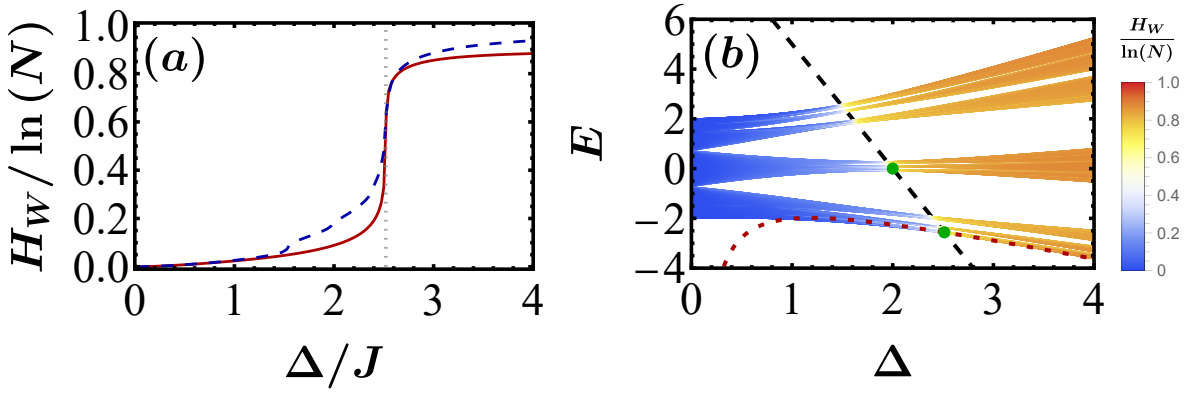

Figure 4.5: **(a)** The entropy of the work distribution for the $\Delta \to 0$ (solid, red) and $0 \to \Delta$ (dashed, blue) ground state quenches for the α model, the grey dotted line corresponds to the location of the mobility edge **(b)** The spectrum of the α model with the mobility edge (dashed, black) shown, the colour is a function of the work distribution for each initial eigenstate in the $\Delta \to 0$ protocol. The red, dotted line represents the perturbative approximation for the ground state energy and the green dots are the estimated location of the mobility edge from the work distribution entropy in (a). Parameters: $\alpha = 0.2$, $J = 1$, $N = 987$.

dent of Δ/J and the second term is just an average over all $\mathcal{C}(|n_i\rangle\langle n_i|)$. Another consequence is that the bound (4.51) is very tight because the difference between the largest and smallest $\mathcal{C}(|n_i\rangle\langle n_i|)$ is small. We confirm this numerically in Fig. 4.4(b), where we plot $\mathcal{C}(|n_i\rangle\langle n_i|)$ for all eigenvectors. We thus reach the conclusion that the monotonic vertical shift in H_W, observed in Fig. 4.4(a), is predominantly due to the Gibbs entropy $S(\bar{\rho})$. Our bounds therefore allow us to pinpoint different physical origins for different effects, namely thermal fluctuations, and the localization transition.

4.4.4 Mobility Edges

In the AAH model the localisation transition occurs at the same value of Δ/J for all energies, this is due to the position-momentum duality in the model. When this duality symmetry is broken in a controlled manner, the model tends to display a mobility edge instead [265–268]. A mobility edge corresponds to a critical value of the energy that demarcates extended eigenstates from local eigenstates for a specific realisation of the Hamiltonian. In the models that we will consider this critical energy will be a function of the disorder parameter Δ and the hopping parameter J. An example of such modification of the AAH Hamiltonian takes the form [266]

$$\mathcal{H}_\alpha(\Delta) = \hbar \sum_{j=1}^{N} \left[\Delta \frac{\cos(2\pi\gamma j + \eta)}{1 - \alpha\cos(2\pi\gamma j + \eta)} |j\rangle\langle j| - J(|j\rangle\langle j+1| + |j+1\rangle\langle j|) \right], \tag{4.87}$$

where $\alpha \in (0,1)$, with $\alpha = 0$ corresponding to the AAH model. In this model the mobility edge can be calculated exactly as [266]

$$\alpha E = \Delta \left(\left| \frac{2J}{\Delta} \right| - 1 \right) \tag{4.88}$$

One interesting question is, can the entropy of the work distribution still capture the localisation transition in the presence of a mobility edge. Figure 4.5(a) shows that both the $\Delta \to 0$ and $0 \to \Delta$ protocol do a good job at highlighting the mobility edge for the ground state, where the grey vertical line represents its location for the ground state energy of our Hamiltonian. We see that both the $\Delta \to 0$ and $0 \to \Delta$ protocol have a sharp uptick at the mobility edge which suggests that the entropy of the work distribution could be a useful tool in identifying its location. This is quite surprising for the $0 \to \Delta$ protocol because the ground state is fully extended, therefore, you would expect the entropy to be approximately proportional to the number of localised states in the basis of the final Hamiltonian. In Fig. 4.5(b) the entire spectrum of $\mathcal{H}_\alpha(\Delta)$ is plotted for $N = 987$ and $\alpha = 0.2$. The colour of each eigenstate depends on the value of $H_W/\ln(N)$ when that eigenstate is the initial state in the $\Delta \to 0$ protocol. It is clear the entropy of the work distribution is able to capture the key physical characteristics at all energies. This means that with enough iterations of the TPM protocol starting with an initial thermal state it should be possible to recreate the entire mobility edge. It has been suggested that mobility edges in AAH style models may be observable via Raman scattering experiments [265] and recently a mobility edge has been observed experimentally in both this model [269] and another generalisation of the AAH model [270]. Mobility edges have also been observed in the Anderson model in three dimensions [271].

Another interesting idea would be to try to estimate α using just a single measurement in the basis of the final Hamiltonian. This is tricky because the value of eigenvalues of the spectrum are not known analytically for $\Delta \neq 0$. One strategy would be to prepare the ground state at $\Delta = 0$ and quench to a finite Δ, we would expect to get an entropy like the blue, dashed line in Fig 4.5(a). We can use this to identify the value of Δ that the ground state mobility edge is at. The ground state energy at the mobility edge can be estimated by taking the minimum energy measured at that value of Δ. Then using the fact that there is a mobility edge at $E = 0$ and $\Delta/J = 2$ for any value of α, we can use Eq. (4.88) to estimate α. For the $\Delta \to 0$ protocol it is a little trickier because we do not know the ground state energy exactly. To get around this we can once again use perturbation theory to get an estimate for the ground state energy. Since, in this model, we do not have the Fourier transform symmetry, only the $\Delta > 2J$ limit can be easily calculated. The Hamiltonian once again has no first order correction, the second order correction to the maximum and minimum eigenvalues is given by

$$E_{\pm}^{>} = \pm \left(\frac{\Delta}{1 \mp \alpha} + \frac{2J^2}{\Delta} \frac{(1 \mp \alpha)(1 \mp \alpha \cos(2\pi\gamma))}{1 - \cos(2\pi\gamma)} \right) + O\left(\frac{J^4}{\Delta^3} \right). \tag{4.89}$$

We can use this to estimate $E(\Delta)$ at the mobility edge. This estimate corresponds to the bottom green point in Fig. 4.5(b). From there we follow a similar process as we did for the $0 \to \Delta$ protocol to estimate α which is just (-1 times) the slope of the line connecting the two points. By applying this method for the $\Delta \to 0$ protocol with $\alpha = 0.2$, we get an estimate of $\alpha = 0.200002$. For larger value of α the estimate is not as good with $\alpha = \{0.4, 0.6\}$ giving estimates of $\alpha = \{0.408, 0.606\}$. Mobility edges are not necessarily linear functions, even for modifications to the AAH model [267], therefore this method has very limited applicability.

4.5 Conclusions

In this chapter we have introduced the entropy of the quantum work distribution and demonstrated that it can be a useful tool for probing the properties of quantum systems under quench dynamics. The entropy captures the complexity of the full work distribution and we have shown that under sudden quench dynamics it is sensitive to key features of the Hamiltonian such as avoided crossings, localization transitions and mobility edges. One possible direction for further research would be to analyse the effect of different kinds of quenches, such as infinitesimal quenches or slow-driving quenches, on the entropy. Our main result, Eq. (4.50), shows that H_W can be understood as stemming from two distinct contributions, one given by the entropy of the initial state, dephased by the TPM, and a second term related to the coherences created by the work protocol. More specifically, what matters are the coherences between the initial states, evolved in time, $U|n_i\rangle$ and the eigenbasis of the final Hamiltonian $|m_i\rangle$. It therefore accounts not only for the change in Hamiltonian, from $\mathcal{H}_i \to \mathcal{H}_f$, but also for the entire work protocol, summarized by U. The contribution of quantum coherence to work has been explored in the past [120, 272, 273], but only for initial thermal states, and with a focus on the first few moments. We have shown that the first few moments and cumulants are not always sufficient to capture the important features of the work distribution and can vary drastically depending on the direction of the quench. We therefore believe that the entropy of the work distribution could serve as a powerful tool for characterizing work statistics away from equilibrium. The entropy of the work distribution may be useful for characterising different critical systems such as the the transverse field Ising model [274] or the Lipkin-Meshkov-Glick model [275]. Although, the localisation phenomenon is particularly suited to this method due to the similarity between the IPR and the entropy of the work distribution. We also demonstrated that the entropy of the work distribution is a candidate for experimentally identifying mobility edges in quasi-periodic models. It would be interesting to see if the work distribution can capture the localisation phenomenon in disordered lattices.

Chapter 5

Conclusions and outlook

The overarching theme of this Thesis has been in examining and characterising the complex dynamics of quantum systems. This involved exploring geometric characteristics of general quantum evolutions, assessing the utility of such evolutions in more practical metrological settings, and probing the thermodynamics of many-body dynamics. Achieving the results necessitated carefully assessing and understanding the associated probability distributions. First, in Chapter 2 we learned that there is a unique contractive Riemannian metric on the space of pure quantum states, the Fubini-Study metric. Probability distributions also have such a unique metric, the Fisher information metric. It can be shown that the Fubini-study metric is just the Fisher information metric extended to complex probability amplitudes. For mixed quantum states we see both of these concepts combined, the fundamental difference now, is that the mixed states can only be represented as a matrix whereas pure states and probability distributions are vectors. This means that the inner product requires matrix multiplication and since matrices do not commute we end up with many possible ways to define the inner product. This results in an infinite family of distance measures, each with their own geodesic path. This ambiguity has led to a lot of confusion in the quantum speed limits (QSL) literature, there are many papers where the authors compare their formulation of the speed limit to other popular versions. We highlight that the precise physical meaning of this kind of analysis is usually difficult to pin-down. We established that the important properties of a QSL are that it is achievable and that saturating the bound corresponds to minimising a useful quantity. Both of these properties have been lacking in the QSL literature, particularly the second point. An example of this is the fact that the vast majority of quantum speed limits are completely insensitive to the instantaneous speed along the path. In an attempt to remedy this, we introduced a new kind of QSL which we call action quantum speed limits. We do not claim that these QSLs are always better than geometric QSLs, but we highlight that even though action QSLs are strictly looser than their geometric counterpart that does not mean that they are useless. In certain scenarios, such as asymptotic dynamics they give much more realistic results for the QSL time.

We hope that this work can inspire new directions in the field of QSLs that focus on applicability of the bound rather than simply on the tightness. The inspiration for action quantum speed limits

came from analysing older work in classical thermodynamics [115, 116]. It would be interesting to explore this connection further and see if there are any other concepts in the geometry of classical thermodynamics that could be investigated further for quantum systems. We point to one place where this connection could occur in slow-driving quantum thermodynamics [120, 126, 142]. Here the action can be related to the irreversible entropy production for certain kinds of processes. It is possible that a more general connection can be drawn between the master equations and different quantum Fisher information metrics. Another area that is often overlooked in the QSL literature is figuring out how to actually achieve the minimum time set by the QSL once it has been calculated. For two of the quantum Fisher information metrics the geodesic path is known, but for all the others we must rely of numerical techniques. Action QSLs are particularly suited to optimal control techniques due to their form as an action. Additionally, it is simple to apply constraints to the system and optimise the action under those constraints.

Whenever measurements are performed, different measurement results occur according to a probability distribution. Metrology is the process of both sampling the probability distribution and using that same distribution to estimate an unknown parameter. The Cramér-Rao bound bounds the variance of that estimate by the inverse of the Fisher information. When it comes to quantum parameter estimation the ambiguity in quantum Fisher information metrics is no longer a problem since there is a strict hierarchy. The smallest inner product is given by the symmetric logarithmic derivative inner product. In fact, this quantum Fisher information can be defined as the Fisher information of the probability distributions obtained from a specific POVM, optimised over all possible POVMs. In the thesis we focused on the topic of sequential measurement metrology, where repeated measurements are performed on the same system. This allows for correlations to be generated between the probability distributions associated with each measurement result. These correlations can have a positive or negative effect on the resulting Fisher information and very little is known about when or why this happens. We were able to prove that when the system-bath interaction is independent of the parameter that you are trying to estimate, it is impossible for the correlations to increase the Fisher information. We additionally showed that the Fisher information is always smaller than the optimal coarse-grained measurement on the environment itself.

When the interaction Hamiltonian does depend on the unknown parameter, significant increases in the Fisher information are possible. We demonstrated this by considering the ubiquitous case of a probe coupled to a thermal bath. By performing sequential projective measurements in the energy basis, the Markov order of the resulting probability distribution is 1. This means that for a large number of measurements the Fisher information can be approximated as $F_{1:N} \approx NF_{2|1}$ where $F_{2|1}$ is the Fisher information attainable when the result of the previous measurement is known. We demonstrated that it is not immediately obvious how to even check if the addition of correlation has a positive or negative effect because there is not always a suitable limit that is experimentally realisable. Luckily, for the case of probe-based thermometry, several of the possible candidates are equivalent and are equal to the thermal Fisher information, which is very much

realisable in practice. We then proved that any sequential metrology scheme could be simulated using a collision model setup with projective measurements performed on the outgoing auxiliary units. When dealing with a collisional setup it is not always possible to have fine grained control over the waiting time between measurements as we had assumed for the sequential measurement scheme. To account for this, we investigated the effect of the waiting time being described by a probability distribution. We were able to prove that as long as the steady state of the process did not depend on the waiting time, the overall process was still Markov order 1 on average. This meant that we could directly compare different waiting time distributions(WTDs). The effect of introducing a WTD was to lower the peak of the Fisher information but allow for an advantage over a larger parameter range. There were certain WTDs where the collisions became so clumped together that the correlations were too strong, and the collision model performed worse than the thermal Fisher information. When we look closer at the actual form of the Fisher information of our thermometry setup, we see that there are two main contributions. One that comes from the fact that the thermal Gibbs state depends on the temperature, this gives rise to the thermal Fisher information. The second contribution is a result of the temperature dependence of the thermalisation rate, Γ. Finally, we showed that it is not only projective measurements that lead to Markov order 1 processes, there are also certain POVMs that can achieve this. In the collisional setup, we could implement such a POVM using a full swap interaction, this allowed us to achieve slightly higher Fisher information than is attainable with projective measurements.

The probes that we considered are the optimal probes for estimating temperature at thermal equilibrium when optimised over all possible Rabi frequencies of the probes, still, it is not clear this means that these are the optimal probes for a sequential measurement scheme. We know that when the Rabi frequency is not tuned correctly, the highly degenerate probes are not even optimal at thermal equilibrium. The addition of variable waiting times depending on the result of the previous measurement could also have an effect of the optimal probes. More research is needed to pin down exactly when correlations have a positive effect on the Fisher information. We proved that for the correlations to be advantageous there needs to be some additional information about the unknown parameter contained in the system-environment interaction. This alone is not enough to guarantee advantage, our analysis of parameter dependence suggests that these effects need to interfere with each other constructively. One tool that is missing from our analysis is the presence of genuinely quantum correlations. The most obvious way to introduce these would be via the collisional setup, quantum correlation could be built up between the auxiliary systems and then they could all be measured at once at the end. It is not clear what the Fisher information would look like in this scenario and if it would still maintain a relatively simple form but nonetheless this would be an interesting direction to explore. Obtaining the Fisher information is one thing, but in order to actually estimate the unknown parameter an estimator is required and that is not always so simple. For our sequential measurement scheme, we have access to the transition probabilities and the frequencies of each measurement result which are both be functions of T. If an estimator could be constructed that approached the Cramér-Rao bound for any sequential

measurement process this would be good evidence of the practicality of this scheme.

Probability in classical thermodynamics comes from a lack of information about the microstate of the system, in quantum mechanics the probabilities are slightly more fundamental and occur as the result of measurements. We have argued in Chapter 1 that in some sense even these probabilities are related to a lack of information (at least until you look at the measurement result) but nonetheless it can give a more solid basis for the appearance of probabilistic laws such as the Crooks relation [232]. In Chapter 4 we considered the two-point measurement scheme where a projective measurement is performed on the system at the start and end of the process in the respective energy bases. Each of these measurements have a probability associated with them, the first measurement depends only on the initial state, but the second measurement depends on the result of the first measurement in a very similar way to the sequential measurement scheme considered in Chapter 3. The difference here is that the final measurement basis is not necessarily the same as the initial measurement basis. The work of a single iteration of this process is the difference between the eigenvalues of the initial and final measurement results. This leads to a probability distribution associated with each value of the work. This work distribution can be tricky to deal with analytically because it involves collecting together transitions with identical work values, this can be very problem specific. Instead, we chose to work with the uncollected work distribution, but provided an upper and lower bound on the work distribution itself. In practice the collected and uncollected work distributions behave very similarly. The work distribution itself can be quite difficult to interpret so usually summary statistics are used such as the moments or cumulants of the distribution. We introduced a new summary statistic, the entropy of the work distribution. We were able to split the uncollected entropy up into a classical component that depends only on the initial state and a quantum component that measured the coherence generated between the initial and final measurement bases.

We proceeded to calculate the entropy of the work distribution for a number of important quantum models. First we looked at the Landau-Zener model, which displays an avoided energy level crossing, a common feature in a wide range of physical phenomena. The entropy showed a clear peak at the avoided crossing that was not present in either the moments or the cumulants. Next we looked at the Aubry-André-Harper Model, an example of a model that displays a localisation transition in the thermodynamic limit. Here we find that the entropy of the work distribution also displays a sharp jump at the critical value that becomes discontinuous in the thermodynamic limit. Here, the moments do show some signals of the localisation transition, but it is not as clear, and is only present in one direction of the quench. Another model that we consider is a generalisation of the Aubry-André-Harper Model that displays a mobility edge. A mobility edge is a localisation transition that is energy dependent. Surprisingly, the entropy of the work distribution is still effective at locating the mobility edge for both directions of the quench.

There is plenty of scope to extend this work by looking at other models and by moving past the sudden quench regime. One idea would be to introduce a linear quench and see if the mobility edge is still visible in the entropy beyond the linear quench regime. Another possibility would be

to consider a different method of obtaining the work distribution as the two-point measurement scheme is not always realistic in practice.

In summary, we have demonstrated the power and flexibility of open quantum systems for exploring a variety of physical phenomena. We used them to explore geometric properties of quantum evolutions, the practical role of these properties in metrology, and the subtleties of quantum thermodynamics. By analysing the interplay between superposition and classical probabilities, we highlighted the cause of ambiguity in quantum speed limits, emphasizing the importance or attainability and meaningful limits. We explored the concept of sequential measurement metrology, shedding some light on the effects of correlation on the Fisher information, and related this scheme to equivalent collisional setups. Finally, we developed a new tool for probing the physics of avoided crossings and localisation transitions in the form of the entropy of the work distribution. This work lays the foundation for continued work, encouraging the consideration of practicality in fundamental bounds, estimation schemes and thermodynamic protocols.

Bibliography

[1] E. O'Connor, G. Guarnieri, and S. Campbell. Action quantum speed limits. *Physical Review A*, 103(2):022210, 2021. URL: https://journals.aps.org/pra/abstract/10.1103/PhysRevA.103.022210, doi:10.1103/PhysRevA.103.022210.

[2] Eoin O'Connor, Bassano Vacchini, and Steve Campbell. Stochastic collisional quantum thermometry. *Entropy*, 23(12):1634, dec 2021. doi:10.3390/e23121634.

[3] Anthony Kiely, Eoin O'Connor, Thomá s Fogarty, Gabriel T. Landi, and Steve Campbell. Entropy of the quantum work distribution. *Physical Review Research*, 5(2), apr 2023. URL: https://doi.org/10.1103%2Fphysrevresearch.5.l022010, doi:10.1103/physrevresearch.5.l022010.

[4] Luis A. Correa, Mohammad Mehboudi, Gerardo Adesso, and Anna Sanpera. Individual quantum probes for optimal thermometry. *Physical Review Letters*, 114(22), jun 2015. doi:10.1103/physrevlett.114.220405.

[5] Philip W Anderson. More is different: Broken symmetry and the nature of the hierarchical structure of science. *Science*, 177(4047):393–396, 1972.

[6] Sebastian Deffner and Steve Campbell. *Quantum Thermodynamics: An introduction to the thermodynamics of quantum information*. Morgan & Claypool Publishers, 2019.

[7] Wojciech Hubert Zurek. Quantum darwinism. *Nature Physics*, 5(3):181–188, mar 2009. doi:10.1038/nphys1202.

[8] William K Wootters and Wojciech H Zurek. A single quantum cannot be cloned. *Nature*, 299(5886):802–803, 1982.

[9] John Preskill. Lecture notes for physics 229: Quantum information and computation. *California Institute of Technology*, 16(1):1–8, 1998.

[10] Heinz-Peter Breuer and Francesco Petruccione. *The theory of open quantum systems*. Oxford University Press, USA, 2002.

[11] Isaac L. Chuang Michael A. Nielsen. *Quantum Computation and Quantum Information*. Cambridge University Press, 2010. URL:

/core/books/quantum-computation-and-quantum-information/01E10196D0A682A6AEFFEA52D53BE9AE, doi:10.1017/cbo9780511976667.

[12] Israel Gelfand and Mark Neumark. On the imbedding of normed rings into the ring of operators in hilbert space. *Rec. Math. [Mat. Sbornik] N.S.*, 12(2):197–217, 1943.

[13] S. Lloyd. Ultimate physical limits to computation. *Nature*, 406:1047, 2000. doi:10.1038/35023282.

[14] N. Pancotti, M. Scandi, M. T. Mitchison, and M. Perarnau-Llobet. Speed-ups to isothermality: Enhanced quantum thermal machines through control of the system-bath coupling. *Phys. Rev. X*, 10:031015, 2020. URL: https://link.aps.org/doi/10.1103/PhysRevX.10.031015, doi:10.1103/PhysRevX.10.031015.

[15] Wojciech H. Zurek, Uwe Dorner, and Peter Zoller. Dynamics of a quantum phase transition. *Physical Review Letters*, 95(10), sep 2005. doi:10.1103/physrevlett.95.105701.

[16] Adolfo del Campo and Wojciech H. Zurek. Universality of phase transition dynamics: Topological defects from symmetry breaking. *International Journal of Modern Physics A*, 29(08):1430018, mar 2014. doi:10.1142/s0217751x1430018x.

[17] Eoin Carolan, Barış Çakmak, and Steve Campbell. Robustness of controlled hamiltonian approaches to unitary quantum gates, 2023. arXiv:2304.14667.

[18] Arpan Das, Anindita Bera, Sagnik Chakraborty, and Dariusz Chruś ciński. Thermodynamics and the quantum speed limit in the non-markovian regime. *Physical Review A*, 104(4), oct 2021. doi:10.1103/physreva.104.042202.

[19] R. Puebla, S. Deffner, and S. Campbell. Kibble-zurek scaling in quantum speed limits for shortcuts to adiabaticity. *Phys. Rev. Research*, 2:032020, 2020. URL: https://link.aps.org/doi/10.1103/PhysRevResearch.2.032020, doi:10.1103/PhysRevResearch.2.032020.

[20] P. M. Poggi. Geometric quantum speed limits and short-time accessibility to unitary operations. *Phys. Rev. A*, 99:042116, 2019. URL: https://link.aps.org/doi/10.1103/PhysRevA.99.042116, doi:10.1103/PhysRevA.99.042116.

[21] S. J. Glaser, U. Boscain, T. Calarco, C. P. Koch, W. Köckenberger, R. Kosloff, I. Kuprov, B. Luy, S. Schirmer, T. Schulte-Herbrüggen, et al. Training schrödinger's cat: quantum optimal control. *The European Physical Journal D*, 69(12):1–24, 2015. doi:10.1140/epjd/e2015-60464-1.

[22] W. Heisenberg. Ueber den anschlanlichen inhalt der quantentheorischen kinematik und mechanik. *Z. Phys.*, 43:172, 1927. URL: https://link.springer.com/article/10.1007/BF01397280, doi:10.1007/BF01397280.

[23] H. P. Robertson. The uncertainty principle. *Physical Review*, 34(1):163, 1929. URL: https://journals.aps.org/pr/abstract/10.1103/PhysRev.34.163, doi:10.1103/PhysRev.34.163.

[24] J. Hilgevoord and J. Uffink. A new view on the uncertainty principle. In *Sixty-two years of uncertainty*, pages 121–137. Springer, 1990. URL: https://link.springer.com/chapter/10.1007/978-1-4684-8771-8_8, doi:10.1007/978-1-4684-8771-8_8.

[25] John Von Neumann. *Mathematical foundations of quantum mechanics: New edition*. Princeton university press, 1932.

[26] A. Lahiri and P.B. Pal. *A First Book of Quantum Field Theory*. Alpha Science International, 2005. URL: https://books.google.ie/books?id=_UmPP8Yr5mYC.

[27] J. Hilgevoord. The uncertainty principle for energy and time. *American Journal of Physics*, 64(12):1451–1456, 1996. URL: https://aapt.scitation.org/doi/10.1119/1.18410, doi:10.1119/1.18410.

[28] J. Hilgevoord. The uncertainty principle for energy and time. ii. *American Journal of Physics*, 66(5):396–402, 1998. URL: https://aapt.scitation.org/doi/10.1119/1.18880, doi:10.1119/1.18880.

[29] J. Hilgevoord. Time in quantum mechanics. *American Journal of Physics*, 70(3):301–306, 2002. URL: https://aapt.scitation.org/doi/10.1119/1.1430697, doi:10.1119/1.1430697.

[30] Theodore Duddell Newton and Eugene P Wigner. Localized states for elementary systems. *Reviews of Modern Physics*, 21(3):400, 1949.

[31] M. Basil Altaie, Daniel Hodgson, and Almut Beige. Time and quantum clocks: A review of recent developments. *Frontiers in Physics*, 10, jun 2022. doi:10.3389/fphy.2022.897305.

[32] Paul Erker, Mark T. Mitchison, Ralph Silva, Mischa P. Woods, Nicolas Brunner, and Marcus Huber. Autonomous quantum clocks: Does thermodynamics limit our ability to measure time? *Physical Review X*, 7(3), aug 2017. doi:10.1103/physrevx.7.031022.

[33] L. Mandelstam and I. Tamm. The uncertainty relation between energy and time in nonrelativistic quantum mechanics. *J. Phys.*, 9:249, 1945.

[34] Jacob D Bekenstein. Energy cost of information transfer. *Physical Review Letters*, 46(10):623, 1981.

[35] Sebastian Deffner and Eric Lutz. Generalized clausius inequality for nonequilibrium quantum processes. *Physical Review Letters*, 105(17), oct 2010. doi:10.1103/physrevlett.105.170402.

[36] Seth Lloyd. Ultimate physical limits to computation. *Nature*, 406(6799):1047–1054, aug 2000. doi:10.1038/35023282.

[37] T. Caneva, M. Murphy, T. Calarco, R. Fazio, S. Montangero, V. Giovannetti, and G. E. Santoro. Optimal control at the quantum speed limit. *Physical Review Letters*, 103(24), dec 2009. doi:10.1103/physrevlett.103.240501.

[38] K. Bhattacharyya. Quantum decay and the Mandelstam-Tamm-energy inequality. *J. Phys. A: Math. Gen.*, 16:2993, 1983. URL: http://stacks.iop.org/0305-4470/16/i=13/a=021.

[39] G. N. Fleming. A unitarity bound on the evolution of nonstationary states. *Il Nuovo Cimento A (1965-1970)*, 16:232, 1973. URL: http://dx.doi.org/10.1007/BF02819419, doi:10.1007/BF02819419.

[40] J. Anandan and Y. Aharonov. Geometry of quantum evolution. *Phys. Rev. Lett.*, 65:1697, 1990. URL: http://link.aps.org/doi/10.1103/PhysRevLett.65.1697, doi:10.1103/PhysRevLett.65.1697.

[41] N. Margolus and L. B. Levitin. The maximum speed of dynamical evolution. *Physica D*, 120:188, 1998. URL: http://dx.doi.org/10.1016/S0167-2789(98)00054-2, doi:10.1016/S0167-2789(98)00054-2.

[42] Vittorio Giovannetti, Seth Lloyd, and Lorenzo Maccone. Quantum limits to dynamical evolution. *Physical Review A*, 67(5):052109, 2003. doi:10.1103/PhysRevA.67.052109.

[43] V. Giovannetti, S. Lloyd, and L. Maccone. The speed limit of quantum unitary evolution. *J. Opt. B*, 6:807, 2004. doi:10.1088/1464-4266/6/8/028.

[44] Niklas Hörnedal and Ole Sönnerborn. The margolus-levitin quantum speed limit for an arbitrary fidelity. *arXiv preprint arXiv:2301.10063*, 2023. doi:10.48550/arXiv.2301.10063.

[45] Gal Ness, Andrea Alberti, and Yoav Sagi. Quantum speed limit for states with a bounded energy spectrum. *Physical Review Letters*, 129(14):140403, 2022. doi:10.1103/PhysRevLett.129.140403.

[46] W. K. Wootters. Statistical distance and Hilbert space. *Phys. Rev. D*, 23:357–362, 1981. URL: https://journals.aps.org/prd/abstract/10.1103/PhysRevD.23.357, doi:10.1103/PhysRevD.23.357.

[47] S. L. Braunstein and C. M. Caves. Statistical distance and the geometry of quantum states. *Phys. Rev. Lett.*, 72:3439–3443, 1994. URL: https://journals.aps.org/prl/abstract/10.1103/PhysRevLett.72.3439, doi:10.1103/PhysRevLett.72.3439.

[48] D. C. Brody and D. W. Hook. On optimum Hamiltonians for state transformations. *J. Phys. A*, 39, 2006. URL: http://dx.doi.org/10.1088/0305-4470/39/11/L02.

[49] A. Mostafazadeh. Hamiltonians generating optimal-speed evolutions. *Phys. Rev. A*, 79:014101, 2009. URL: https://link.aps.org/doi/10.1103/PhysRevA.79.014101, doi:10.1103/PhysRevA.79.014101.

[50] S. Deffner and E. Lutz. Energy-time uncertainty relation for driven quantum systems. *J. Phys. A*, 46:335302, 2013. URL: https://iopscience.iop.org/article/10.1088/1751-8113/46/33/335302https://iopscience.iop.org/article/10.1088/1751-8113/46/33/335302/meta, doi:10.1088/1751-8113/46/33/335302.

[51] F. Campaioli, F. A. Pollock, F. C. Binder, and K. Modi. Tightening quantum speed limits for almost all states. *Phys. Rev. Lett.*, 120:060409, 2018. URL: https://link.aps.org/doi/10.1103/PhysRevLett.120.060409, doi:10.1103/PhysRevLett.120.060409.

[52] D. Mondal and A. K. Pati. Quantum speed limit for mixed states using an experimentally realizable metric. *Phys. Lett. A*, 380:1395, 2016. URL: http://www.sciencedirect.com/science/article/pii/S0375960116001559, doi:http://dx.doi.org/10.1016/j.physleta.2016.02.018.

[53] P. M. Poggi, F. C. Lombardo, and D. A. Wisniacki. Quantum speed limit and optimal evolution time in a two-level system. *EPL*, 104, 2013. URL: http://doi.org/10.1209/0295-5075/104/40005.

[54] S. Campbell and S. Deffner. Trade-off between speed and cost in shortcuts to adiabaticity. *Phys. Rev. Lett.*, 118:100601, 2017. URL: https://link.aps.org/doi/10.1103/PhysRevLett.118.100601, doi:10.1103/PhysRevLett.118.100601.

[55] P. M. Poggi. Analysis of lower bounds for quantum control times and their relation to the quantum speed limit. *arXiv:2002.11147*, 2020. URL: https://arxiv.org/abs/2002.11147.

[56] F. Fröwis. Kind of entanglement that speeds up quantum evolution. *Phys. Rev. A*, 85:052127, May 2012. URL: https://link.aps.org/doi/10.1103/PhysRevA.85.052127, doi:10.1103/PhysRevA.85.052127.

[57] I. Marvian and D. A. Lidar. Quantum speed limits for leakage and decoherence. *Phys. Rev. Lett.*, 115:210402, 2015. URL: http://link.aps.org/doi/10.1103/PhysRevLett.115.210402, doi:10.1103/PhysRevLett.115.210402.

[58] I. Marvian, R. W. Spekkens, and P. Zanardi. Quantum speed limits, coherence, and asymmetry. *Phys. Rev. A*, 93:052331, 2016. URL: http://link.aps.org/doi/10.1103/PhysRevA.93.052331, doi:10.1103/PhysRevA.93.052331.

[59] L. P. García-Pintos and A. del Campo. Quantum speed limits under continuous quantum measurements. *New J. Phys.*, 21:033012, 2019. doi:10.1088/1367-2630/ab099e.

[60] B. Shanahan, A. Chenu, N. Margolus, and A. del Campo. Quantum speed limits across the quantum-to-classical transition. *Phys. Rev. Lett.*, 120:070401, 2018. URL: https://link.aps.org/doi/10.1103/PhysRevLett.120.070401, doi:10.1103/PhysRevLett.120.070401.

[61] T. Fogarty, S. Deffner, T. Busch, and S. Campbell. Orthogonality catastrophe as a consequence of the quantum speed limit. *Phys. Rev. Lett.*, 124:110601, 2020. URL: https://link.aps.org/doi/10.1103/PhysRevLett.124.110601, doi:10.1103/PhysRevLett.124.110601.

[62] O. Lychkovskiy, O. Gamayun, and V. Cheianov. Time scale for adiabaticity breakdown in driven many-body systems and orthogonality catastrophe. *Phys. Rev. Lett.*, 119:200401, 2017. URL: https://link.aps.org/doi/10.1103/PhysRevLett.119.200401, doi:10.1103/PhysRevLett.119.200401.

[63] F. Campaioli, W. Sloan, K. Modi, and F. A. Pollock. Algorithm for solving unconstrained unitary quantum brachistochrone problems. *Phys. Rev. A*, 100:062328, 2019. URL: https://link.aps.org/doi/10.1103/PhysRevA.100.062328, doi:10.1103/PhysRevA.100.062328.

[64] L. B. Levitin and T. Toffoli. Fundamental limit on the rate of quantum dynamics: The unified bound is tight. *Phys. Rev. Lett.*, 103:160502, 2009. URL: http://dx.doi.org/10.1103/PhysRevLett.103.160502, doi:10.1103/PhysRevLett.103.160502.

[65] A. del Campo, I. L. Egusquiza, M. B. Plenio, and S. F. Huelga. Quantum speed limits in open system dynamics. *Phys. Rev. Lett.*, 110:050403, 2013. doi:10.1103/PhysRevLett.110.050403.

[66] S. Deffner and E. Lutz. Quantum speed limit for non-Markovian dynamics. *Phys. Rev. Lett.*, 111:010402, 2013. doi:10.1103/PhysRevLett.111.010402.

[67] Z. Sun, J. Liu, J. Ma, and X. Wang. Quantum speed limits in open systems: Non-Markovian dynamics without rotating-wave approximation. *Sci. Rep.*, 5:8444, 2015. URL: http://doi.org/10.1038/srep08444, doi:10.1038/srep08444.

[68] Y. J. Zhang, W. Han, Y. J. Xia, J. P. Cao, and H. Fan. Quantum speed limit for arbitrary initial states. *Sci. Rep.*, 4, 2014. URL: https://doi.org/10.1038/srep04890.

[69] R. Uzdin and R. Kosloff. Speed limits in Liouville space for open quantum systems. *EPL (Europhysics Letters)*, 115:40003, 2016. URL: http://stacks.iop.org/0295-5075/115/i=4/a=40003.

[70] L. Zhang, Y. Sun, and S. Luo. Quantum speed limit for qubit systems: Exact results. *Phys. Lett. A*, 382:2599–2604, 2018. doi:10.1016/j.physleta.2018.07.030.

[71] A. Ektesabi, N. Behzadi, and E. Faizi. Improved bound for quantum-speed-limit time in open quantum systems by introducing an alternative fidelity. *Phys. Rev. A*, 95:022115, 2017. URL: https://journals.aps.org/pra/abstract/10.1103/PhysRevA.95.022115, doi:10.1103/PhysRevA.95.022115.

[72] X. Cai and Y. Zheng. Quantum dynamical speedup in a nonequilibrium environment. *Phys. Rev. A*, 95:052104, 2017. URL: https://link.aps.org/doi/10.1103/PhysRevA.95.052104, doi:10.1103/PhysRevA.95.052104.

[73] S. Deffner. Geometric quantum speed limits: A case for Wigner phase space. *New J. Phys.*, 19:103018, 2017. URL: http://dx.doi.org/10.1088/1367-2630/aa83dc, doi:10.1088/1367-2630/aa83dc.

[74] S.-X. Wu and C.-S. Yu. Quantum speed limit for a mixed initial state. *Phys. Rev. A*, 98:042132, 2018. URL: https://link.aps.org/doi/10.1103/PhysRevA.98.042132, doi:10.1103/PhysRevA.98.042132.

[75] Francesco Campaioli, Chang shui Yu, Felix A Pollock, and Kavan Modi. Resource speed limits: maximal rate of resource variation. *New Journal of Physics*, 24(6):065001, jun 2022. doi:10.1088/1367-2630/ac7346.

[76] Niklas Hörnedal, Nicoletta Carabba, Kazutaka Takahashi, and Adolfo del Campo. Geometric operator quantum speed limit, wegner hamiltonian flow and operator growth, 2023. arXiv:2301.04372.

[77] M. M. Taddei, B. M. Escher, L. Davidovich, and R. L. De Matos Filho. Quantum speed limit for physical processes. *Phys. Rev. Lett.*, 110, 2013. URL: https://doi.org/10.1103/PhysRevLett.110.050402.

[78] D. P. Pires, M. Cianciaruso, L. C. Céleri, G. Adesso, and D. O. Soares-Pinto. Generalized geometric quantum speed limits. *Phys. Rev. X*, 6:021031, 2016. URL: http://link.aps.org/doi/10.1103/PhysRevX.6.021031, doi:10.1103/PhysRevX.6.021031.

[79] D. Mondal, C. Datta, and S. Sazim. Quantum coherence sets the quantum speed limit for mixed states. *Phys. Lett. A*, 380:689, 2016. URL: http://www.sciencedirect.com/science/article/pii/S0375960115010518, doi:http://dx.doi.org/10.1016/j.physleta.2015.12.015.

[80] P. J. Jones and P. Kok. Geometric derivation of the quantum speed limit. *Phys. Rev. A*, 82:022107, 2010. URL: https://link.aps.org/doi/10.1103/PhysRevA.82.022107, doi:10.1103/PhysRevA.82.022107.

[81] K. Funo, N. Shiraishi, and K. Saito. Speed limit for open quantum systems. *New J. Phys.*, 21:013006, 2019. doi:10.1088/1367-2630/aaf9f5.

[82] F. Campaioli, F. A. Pollock, and K. Modi. Tight, robust, and feasible quantum speed limits for open dynamics. *Quantum*, 3:168, 2019. URL: http://dx.doi.org/10.22331/q-2019-08-05-168, doi:10.22331/q-2019-08-05-168.

[83] Tan Van Vu and Yoshihiko Hasegawa. Geometrical bounds of the irreversibility in markovian systems. *Physical Review Letters*, 126(1), jan 2021. doi:10.1103/physrevlett.126.010601.

[84] Tan Van Vu and Yoshihiko Hasegawa. Geometrical bounds of the irreversibility in markovian systems. *Physical Review Letters*, 126(1), jan 2021. doi:10.1103/physrevlett.126.010601.

[85] Tan Van Vu and Keiji Saito. Topological speed limit. *Physical Review Letters*, 130(1), jan 2023. doi:10.1103/physrevlett.130.010402.

[86] E. A. Morozova and N. N. Chentsov. Markov invariant geometry on manifolds of states. *Journal of Soviet Mathematics*, 56(5):2648–2669, 1991. doi:10.1007/BF01095975.

[87] D. Petz and H. Hasegawa. On the Riemannian Metric of α-Entropies of Density Matrices. *Letters in Mathematical Physics*, 38:221–225, 1996. doi:10.1007/BF00398324.

[88] Adolfo del Campo. Probing quantum speed limits with ultracold gases. *Physical Review Letters*, 126(18), may 2021. doi:10.1103/physrevlett.126.180603.

[89] Wei Wu and Jun-Hong An. Quantum speed limit of a noisy continuous-variable system. *Physical Review A*, 106(6), dec 2022. doi:10.1103/physreva.106.062438.

[90] Nikolai Il'in and Oleg Lychkovskiy. Quantum speed limit for thermal states. *Physical Review A*, 103(6), jun 2021. doi:10.1103/physreva.103.062204.

[91] Ryusuke Hamazaki. Speed limits for macroscopic transitions. *PRX Quantum*, 3(2), apr 2022. doi:10.1103/prxquantum.3.020319.

[92] N. Mirkin, F. Toscano, and D. A. Wisniacki. Quantum-speed-limit bounds in an open quantum evolution. *Phys. Rev. A*, 94, 2016. URL: https://doi.org/10.1103/PhysRevA.94.052125.

[93] J. Teittinen, H. Lyyra, and S. Maniscalco. There is no general connection between the quantum speed limit and non-Markovianity. *New J. Phys.*, 21:123041, 2019. doi:10.1088/1367-2630/ab59fe.

[94] Tan Van Vu and Yoshihiko Hasegawa. Lower bound on irreversibility in thermal relaxation of open quantum systems. *Physical Review Letters*, 127(19), nov 2021. doi:10.1103/physrevlett.127.190601.

[95] Tan Van Vu and Keiji Saito. Thermodynamic unification of optimal transport: Thermodynamic uncertainty relation, minimum dissipation, and thermodynamic speed limits. *Physical Review X*, 13(1), feb 2023. doi:10.1103/physrevx.13.011013.

[96] Brij Mohan and Arun K. Pati. Reverse quantum speed limit: How slowly a quantum battery can discharge. *Physical Review A*, 104(4), oct 2021. doi:10.1103/physreva.104.042209.

[97] Wenzheng Dong, Fei Zhuang, Sophia E. Economou, and Edwin Barnes. Doubly geometric quantum control. *PRX Quantum*, 2(3), aug 2021. doi:10.1103/prxquantum.2.030333.

[98] A. A. Dìaz V., V. Martikyan, S. J. Glaser, and D. Sugny. Purity speed limit of open quantum systems from magic subspaces. *Phys. Rev. A*, 102:033104, 2020. URL: https://journals.aps.org/pra/abstract/10.1103/PhysRevA.102.033104, doi:10.1103/physreva.102.033104.

[99] M. R. Frey. Quantum speed limits—primer, perspectives, and potential future directions. *Quantum Inf. Process.*, 15:3919, 2016. URL: http://dx.doi.org/10.1007/s11128-016-1405-x, doi:10.1007/s11128-016-1405-x.

[100] S. Deffner and S. Campbell. Quantum speed limits: from heisenberg's uncertainty principle to optimal quantum control. *J. Phys. A: Math. Theor.*, 50:453001, 2017. doi:10.1088/1751-8121/aa86c6.

[101] Masahito Hayashi. *Quantum information theory*. Springer, 2016. URL: https://link.springer.com/book/10.1007/978-3-662-49725-8, doi:10.1007/978-3-662-49725-8.

[102] Ronald A Fisher. On the mathematical foundations of theoretical statistics. *Philosophical transactions of the Royal Society of London. Series A, containing papers of a mathematical or physical character*, 222(594-604):309–368, 1922. doi:10.1098/rsta.1922.0009.

[103] Harold Cramer. Mathematical methods of statistics, princeton univ. *Princeton University Press*, 1946.

[104] Paolo Facchi, Ravi Kulkarni, VI Man'ko, Giuseppe Marmo, ECG Sudarshan, and Franco Ventriglia. Classical and quantum fisher information in the geometrical formulation of quantum mechanics. *Physics Letters A*, 374(48):4801–4803, 2010. URL: https://www.sciencedirect.com/science/article/pii/S0375960110013204, doi:10.1016/j.physleta.2010.10.005.

[105] Donald Bures. An extension of kakutani's theorem on infinite product measures to the tensor product of semifinite w*-algebras. *Transactions of the American Mathematical Society*, 135:199–212, 1969. URL: https://www.ams.org/journals/tran/1969-135-00/S0002-9947-1969-0236719-2/.

[106] Matthias Hübner. Explicit computation of the bures distance for density matrices. *Physics Letters A*, 163(4):239–242, 1992. URL: https://ui.adsabs.harvard.edu/abs/1992PhLA..163..239H/abstract, doi:10.1016/0375-9601(92)91004-B.

[107] Vittorio Gorini, Andrzej Kossakowski, and Ennackal Chandy George Sudarshan. Completely positive dynamical semigroups of n-level systems. *Journal of Mathematical Physics*, 17(5):821–825, 1976. doi:10.1063/1.522979.

[108] Goran Lindblad. On the generators of quantum dynamical semigroups. *Communications in Mathematical Physics*, 48:119–130, 1976. doi:10.1007/BF01608499.

[109] M. G. A. Paris. Quantum estimation for quantum technology. *Int. J. Quant. Inf.*, 7:125, 2009. URL: http://dx.doi.org/10.1142/S0219749909004839, doi:10.1142/S0219749909004839.

[110] P. Gibilisco and T. Isola. A characterisation of Wigner-Yanase skew information among statistically monotone metrics. *Infinite Dimensional Analysis, Quantum Probability and Related Topics*, 04(04):553–557, 2001. doi:10.1142/s0219025701000644.

[111] P. Gibilisco and T. Isola. Wigner-Yanase information on quantum state space: The geometric approach. *J. Math. Phys.*, 44:3752, 2003. URL: http://scitation.aip.org/content/aip/journal/jmp/44/9/10.1063/1.1598279, doi:10.1063/1.1598279.

[112] A. Uhlmann. Geometric phases and related structures. *Reports on Mathematical Physics*, 36:461–481, 1995. doi:10.1016/0034-4877(96)83640-8.

[113] E. Carolan, A. Kiely, and S. Campbell. Counterdiabatic control in the impulse regime. *Physical Review A*, 105(1):012605, 2022. doi:10.1103/PhysRevA.105.012605.

[114] J. Xuereb, P. Erker, F. Meier, M. T. Mitchison, and M. Huber. The impact of imperfect timekeeping on quantum control. *arXiv preprint arXiv:2301.10767*, 2023. doi:10.48550/arXiv.2301.10767.

[115] P. Salamon and R. S. Berry. Thermodynamic length and dissipated availability. *Phys. Rev. Lett.*, 51:1127–1130, 1983. URL: https://link.aps.org/doi/10.1103/PhysRevLett.51.1127, doi:10.1103/PhysRevLett.51.1127.

[116] G. E. Crooks. Measuring thermodynamic length. *Phys. Rev. Lett.*, 99:100602, 2007. doi:10.1103/PhysRevLett.99.100602.

[117] P. R. Zulkowski, D. A. Sivak, G. E. Crooks, and M. R. DeWeese. Geometry of thermodynamic control. *Phys. Rev. E*, 86:041148, 2012. URL: https://journals.aps.org/pre/abstract/10.1103/PhysRevE.86.041148, doi:10.1103/PhysRevE.86.041148.

[118] E. H. Feng and G. E. Crooks. Far-from-equilibrium measurements of thermodynamic length. *Phys. Rev. E*, 79:012104, 2009. URL: https://journals.aps.org/pre/abstract/10.1103/PhysRevE.79.012104, doi:10.1103/PhysRevE.79.012104.

[119] D. A. Sivak and G. E. Crooks. Thermodynamic metrics and optimal paths. *Phys. Rev. Lett.*, 108:190602, 2012. URL: https://journals.aps.org/prl/abstract/10.1103/PhysRevLett.108.190602, doi:10.1103/PhysRevLett.108.190602.

[120] M. Scandi and M. Perarnau-Llobet. Thermodynamic length in open quantum systems. *Quantum*, 3:197, 2019. doi:10.22331/q-2019-10-24-197.

[121] M. Scandi, H. J. D. Miller, J. Anders, and M. Perarnau-Llobet. Quantum work statistics close to equilibrium. *Phys. Rev. Research*, 2:23377, 2020. URL: https://journals.aps.org/prresearch/abstract/10.1103/PhysRevResearch.2.023377, doi:10.1103/physrevresearch.2.023377.

[122] S. Deffner. Optimal control of a qubit in an optical cavity. *J. .Phys. B*, 47:145502, 2014. URL: https://iopscience.iop.org/article/10.1088/0953-4075/47/14/145502https://iopscience.iop.org/article/10.1088/0953-4075/47/14/145502/meta, doi:10.1088/0953-4075/47/14/145502.

[123] V. Mukherjee, A. Carlini, A. Mari, T. Caneva, S. Montangero, T. Calarco, R. Fazio, and V. Giovannetti. Speeding up and slowing down the relaxation of a qubit by optimal control. *Phys. Rev. A*, 88:062326, 2013. URL: https://link.aps.org/doi/10.1103/PhysRevA.88.062326, doi:10.1103/PhysRevA.88.062326.

[124] P. R. Zulkowski and M. R. DeWeese. Optimal protocols for slowly driven quantum systems. *Phys. Rev. E*, 92:032113, 2015. URL: https://journals.aps.org/pre/abstract/10.1103/PhysRevE.92.032113, doi:10.1103/PhysRevE.92.032113.

[125] S. Deffner and M. V. S. Bonança. Thermodynamic control-An old paradigm with new applications. *EPL*, 131(2):20001, 2020. URL: https://iopscience.iop.org/article/10.1209/0295-5075/131/20001https://iopscience.iop.org/article/10.1209/0295-5075/131/20001/meta, doi:10.1209/0295-5075/131/20001.

[126] H. J.D. Miller, M. Scandi, J. Anders, and M. Perarnau-Llobet. Work Fluctuations in Slow Processes: Quantum Signatures and Optimal Control. *Phys. Rev. Lett.*, 123:230603, 2019. doi:10.1103/PhysRevLett.123.230603.

[127] J. Liu and H. Yuan. Quantum parameter estimation with optimal control. *Phys. Rev. A*, 96(1):012117, 2017. doi:10.1103/PhysRevA.96.012117.

[128] N. Mirkin, M. Larocca, and D. Wisniacki. Quantum metrology in a non-markovian quantum evolution. *Phys. Rev. A*, 102(2):022618, 2020. doi:10.1103/PhysRevA.102.022618.

[129] D. Basilewitsch, H. Yuan, and C. P. Koch. Optimally controlled quantum discrimination and estimation. *Phys. Rev. Research*, 2(3):033396, 2020. doi:10.1103/PhysRevResearch.2.033396.

[130] D. E Kirk. *Optimal control theory : an introduction*. Mineola, N.Y. : Dover Publications, 2004.

[131] Yusef Maleki, Bahram Ahansaz, and Alireza Maleki. Speed limit of quantum metrology. *Scientific Reports*, 13(1):12031, 2023. doi:10.1038/s41598-023-39082-w.

[132] Pablo M. Poggi, Gabriele De Chiara, Steve Campbell, and Anthony Kiely. Universally robust quantum control, 2023. arXiv:2309.14437.

[133] A. D. Cimmarusti, Z. Yan, B. D. Patterson, L. P. Corcos, L. A. Orozco, and S. Deffner. Environment-assisted speed-up of the field evolution in cavity quantum electrodynamics. *Physical Review Letters*, 114(23), jun 2015. doi:10.1103/physrevlett.114.233602.

[134] Gerhard C. Hegerfeldt. Driving at the quantum speed limit: Optimal control of a two-level system. *Physical Review Letters*, 111(26), dec 2013. doi:10.1103/physrevlett.111.260501.

[135] Xikun Li. Optimal control of quantum state preparation and entanglement creation in two-qubit quantum system with bounded amplitude. *Scientific Reports*, 13(1):14734, 2023. doi:10.1038/s41598-023-41688-z.

[136] Francesco Campaioli, Felix A. Pollock, Felix C. Binder, Lucas Cé leri, John Goold, Sai Vinjanampathy, and Kavan Modi. Enhancing the charging power of quantum batteries. *Physical Review Letters*, 118(15), apr 2017. doi:10.1103/physrevlett.118.150601.

[137] Gian Marcello Andolina, Maximilian Keck, Andrea Mari, Michele Campisi, Vittorio Giovannetti, and Marco Polini. Extractable work, the role of correlations, and asymptotic freedom in quantum batteries. *Physical Review Letters*, 122(4), feb 2019. doi:10.1103/physrevlett.122.047702.

[138] Elliott H Lieb and Derek W Robinson. The finite group velocity of quantum spin systems. *Communications in mathematical physics*, 28(3):251–257, 1972. doi:10.1007/BF01645779.

[139] Michael Murphy, Simone Montangero, Vittorio Giovannetti, and Tommaso Calarco. Communication at the quantum speed limit along a spin chain. *Physical Review A*, 82(2), aug 2010. doi:10.1103/physreva.82.022318.

[140] M. M. Feyles, L. Mancino, M. Sbroscia, I. Gianani, and M. Barbieri. Dynamical role of quantum signatures in quantum thermometry. *Phys. Rev. A*, 99(6):062114, 2019. doi:10.1103/PhysRevA.99.062114.

[141] Diego Paiva Pires, Kavan Modi, and Lucas Chibebe Cé leri. Bounding generalized relative entropies: Nonasymptotic quantum speed limits. *Physical Review E*, 103(3), mar 2021. doi:10.1103/physreve.103.032105.

[142] Paolo Abiuso, Harry JD Miller, Martí Perarnau-Llobet, and Matteo Scandi. Geometric optimisation of quantum thermodynamic processes. *Entropy*, 22(10):1076, 2020. doi:10.3390/e22101076.

[143] S. Seah, S. Nimmrichter, D. Grimmer, J. P. Santos, V. Scarani, and G. T. Landi. Collisional Quantum Thermometry. *Phys. Rev. Lett.*, 123:180602, 2019. URL: https://journals.aps.org/prl/abstract/10.1103/PhysRevLett.123.180602, doi:10.1103/PhysRevLett.123.180602.

[144] A. Shu, S. Seah, and V. Scarani. Surpassing the thermal Cramér-Rao bound with collisional thermometry. *Phys. Rev. A*, 102:042417, 2020. URL: https://journals.aps.org/pra/abstract/10.1103/PhysRevA.102.042417, doi:10.1103/PhysRevA.102.042417.

[145] F. Ciccarello, S. Lorenzo, V. Giovannetti, and G M. Palma. Quantum collision models: open system dynamics from repeated interactions. *arXiv preprint arXiv:2106.11974*, 2021. URL: https://arxiv.org/abs/2106.11974.

[146] G. O. Alves and G. T. Landi. Bayesian estimation for collisional thermometry. *arXiv preprint arXiv:2106.12072*, 2021. URL: https://arxiv.org/abs/2106.12072.

[147] V. Giovannetti, S. Lloyd, and L. Maccone. Quantum metrology. *Phys. Rev. Lett.*, 96:010401, 2006. URL: https://journals.aps.org/prl/abstract/10.1103/PhysRevLett.96.010401, doi:10.1103/PhysRevLett.96.010401.

[148] A. Acín, I. Bloch, H. Buhrman, T. Calarco, C. Eichler, J. Eisert, D. Esteve, N. Gisin, S. J. Glaser, F. Jelezko, S. Kuhr, M. Lewenstein, M. F. Riedel, P. O. Schmidt, R. Thew, A. Wallraff, I. Walmsley, and F. K. Wilhelm. The quantum technologies roadmap: A European community view. *New J. Phys.*, 20:080201, 2018. doi:10.1088/1367-2630/aad1ea.

[149] D. Braun, G. Adesso, F. Benatti, R. Floreanini, U. Marzolino, M. W. Mitchell, and S. Pirandola. Quantum-enhanced measurements without entanglement. *Rev. Mod. Phys.*, 90:035006, 2018. URL: https://journals.aps.org/rmp/abstract/10.1103/RevModPhys.90.035006, doi:10.1103/RevModPhys.90.035006.

[150] S. Razavian, C. Benedetti, M. Bina, Y. Akbari-Kourbolagh, and M. G.A. Paris. Quantum thermometry by single-qubit dephasing. *Eur. Phys. J. Plus*, 134:1–9, 2019. URL: https://link.springer.com/article/10.1140/epjp/i2019-12708-9, doi:10.1140/epjp/i2019-12708-9.

[151] L. A. Correa, M. Mehboudi, G. Adesso, and A. Sanpera. Individual quantum probes for optimal thermometry. *Phys. Rev. Lett.*, 114:220405, 2015. URL: https://journals.aps.org/prl/abstract/10.1103/PhysRevLett.114.220405, doi:10.1103/PhysRevLett.114.220405.

[152] M. T. Mitchison, T. Fogarty, G. Guarnieri, S. Campbell, Th. Busch, and J. Goold. In Situ Thermometry of a Cold Fermi Gas via Dephasing Impurities. *Phys. Rev. Lett.*, 125:080402, 2020. URL: https://journals.aps.org/prl/abstract/10.1103/PhysRevLett.125.080402, doi:10.1103/PhysRevLett.125.080402.

[153] M. Mehboudi, A. Sanpera, and L. A. Correa. Thermometry in the quantum regime: recent theoretical progress. *J. Phys. A*, 52:303001, 2019. URL: https://iopscience.iop.org/article/10.1088/1751-8121/ab2828https://iopscience.iop.org/article/10.1088/1751-8121/ab2828/meta, doi:10.1088/1751-8121/AB2828.

[154] L. Maccone. Intuitive reason for the usefulness of entanglement in quantum metrology. *Phys. Rev. A*, 88:042109, 2013. doi:10.1103/PhysRevA.88.042109.

[155] Z. Huang, C. Macchiavello, and L. Maccone. Usefulness of entanglement-assisted quantum metrology. *Phys. Rev. A*, 94:012101, 2016. doi:10.1103/PhysRevA.94.012101.

[156] K. Micadei, D. A. Rowlands, F. A. Pollock, L. C. Céleri, R. M. Serra, and K. Modi. Coherent measurements in quantum metrology. *New J. Phys.*, 17(2):023057, 2015. doi:10.1088/1367-2630/17/2/023057.

[157] D. P. Pires, I. A. Silva, E. R. Deazevedo, D. O. Soares-Pinto, and J. G. Filgueiras. Coherence orders, decoherence, and quantum metrology. *Phys. Rev. A*, 98(3):032101, 2018. doi:10.1103/PhysRevA.98.032101.

[158] A. Castellini, R. Lo Franco, L. Lami, A. Winter, G. Adesso, and G. Compagno. Indistinguishability-enabled coherence for quantum metrology. *Phys. Rev. A*, 100:012308, 2019. doi:10.1103/PhysRevA.100.012308.

[159] H. R. Jahromi. Quantum thermometry in a squeezed thermal bath. *Physica Scripta*, 95:035107, 2020. doi:10.1088/1402-4896/ab4de5.

[160] L. A. Correa, M. Perarnau-Llobet, K. V. Hovhannisyan, S. Hernández-Santana, M. Mehboudi, and A. Sanpera. Enhancement of low temperature thermometry by strong coupling. *Phys. Rev. A*, 96:062103, 2017. URL: https://journals.aps.org/pra/abstract/10.1103/PhysRevA.96.062103, doi:10.1103/PhysRevA.96.062103.

[161] K. V. Hovhannisyan and L. A. Correa. Measuring the temperature of cold many-body quantum systems. *Phys. Rev. B*, 98:045101, 2018. URL: https://journals.aps.org/prb/abstract/10.1103/PhysRevB.98.045101, doi:10.1103/PhysRevB.98.045101.

[162] P. A. Ivanov. Quantum thermometry with trapped ions. *Optics Communications*, 436:101–107, 2019. doi:10.1016/j.optcom.2018.12.013.

[163] S. Jevtic, D. Newman, T. Rudolph, and T. M. Stace. Single-qubit thermometry. *Phys. Rev. A*, 91:12331, 2015. URL: https://journals.aps.org/pra/abstract/10.1103/PhysRevA.91.012331, doi:10.1103/PhysRevA.91.012331.

[164] A. H. Kiilerich, A. De Pasquale, and V. Giovannetti. Dynamical approach to ancilla-assisted quantum thermometry. *Phys. Rev. A*, 98:042124, 2018. URL: https://journals.aps.org/pra/abstract/10.1103/PhysRevA.98.042124, doi:10.1103/PhysRevA.98.042124.

[165] L. Mancino, M. Sbroscia, I. Gianani, E. Roccia, and M. Barbieri. Quantum Simulation of Single-Qubit Thermometry Using Linear Optics. *Phys. Rev. Lett.*, 118:130502, 2017. URL: https://journals.aps.org/prl/abstract/10.1103/PhysRevLett.118.130502, doi:10.1103/PhysRevLett.118.130502.

[166] P. P. Potts, J. B. Brask, and N. Brunner. Fundamental limits on low-temperature quantum thermometry with finite resolution. *Quantum*, 3:161, 2019. URL: https://quantum-journal.org/papers/q-2019-07-09-161/, doi:10.22331/q-2019-07-09-161.

[167] C. R. Rao. *Linear statistical inference and its applications*, volume 2. Wiley New York, 1973. doi:10.1002/9780470316436.

[168] J. Liu, H. Yuan, X.-M. Lu, and X. Wang. Quantum Fisher information matrix and multiparameter estimation. *J. Phys. A*, 53:023001, 2019. URL: https://iopscience.iop.org/article/10.1088/1751-8121/ab5d4d, doi:10.1088/1751-8121/AB5D4D.

[169] Mădălin Guţă. Fisher information and asymptotic normality in system identification for quantum markov chains. *Physical Review A*, 83(6), jun 2011. doi:10.1103/physreva.83.062324.

[170] Cătălin Cătană, Merlijn van Horssen, and Mădălin Guţă. Asymptotic inference in system identification for the atom maser. *Philosophical Transactions of the Royal Society A: Mathematical, Physical and Engineering Sciences*, 370(1979):5308–5323, 2012. doi:10.1098/rsta.2011.0528.

[171] Alexander Holm Kiilerich and Klaus Mølmer. Quantum zeno effect in parameter estimation. *Physical Review A*, 92(3), sep 2015. doi:10.1103/physreva.92.032124.

[172] Daniel Burgarth, Vittorio Giovannetti, Airi N Kato, and Kazuya Yuasa. Quantum estimation via sequential measurements. *New Journal of Physics*, 17(11):113055, nov 2015. doi:10.1088/1367-2630/17/11/113055.

[173] A. De Pasquale, K. Yuasa, and V. Giovannetti. Estimating temperature via sequential measurements. *Phys. Rev. A*, 96:012316, 2017. URL: https://journals.aps.org/pra/abstract/10.1103/PhysRevA.96.012316, doi:10.1103/PhysRevA.96.012316.

[174] Pablo Zegers. Fisher information properties. *Entropy*, 17(7):4918–4939, 2015. doi:1099-4300/17/7/4918.

[175] Marco Radaelli, Gabriel T Landi, Kavan Modi, and Felix C Binder. Fisher information of correlated stochastic processes. *New Journal of Physics*, 25(5):053037, may 2023. doi:10.1088/1367-2630/acd321.

[176] Daniel Burgarth and Vittorio Giovannetti. The generalized lyapunov theorem and its application to quantum channels. *New Journal of Physics*, 9(5):150–150, may 2007. doi:10.1088/1367-2630/9/5/150.

[177] Howard M Wiseman and Gerard J Milburn. *Quantum measurement and control*. Cambridge university press, 2009. doi:10.1017/CBO9780511813948.

[178] Jing Zhang, Yu xi Liu, Re-Bing Wu, Kurt Jacobs, and Franco Nori. Quantum feedback: Theory, experiments, and applications. *Physics Reports*, 679:1–60, mar 2017. doi:10.1016/j.physrep.2017.02.003.

[179] Joseph A. Smiga, Marco Radaelli, Felix C. Binder, and Gabriel T. Landi. Stochastic metrology and the empirical distribution, 2023. arXiv:2305.16480.

[180] Karen V. Hovhannisyan, Mathias R. Jørgensen, Gabriel T. Landi, Álvaro M. Alhambra, Jonatan B. Brask, and Martí Perarnau-Llobet. Optimal quantum thermometry with coarse-grained measurements. *PRX Quantum*, 2(2), may 2021. doi:10.1103/prxquantum.2.020322.

[181] Anthony J Leggett, SDAFMGA Chakravarty, Alan T Dorsey, Matthew PA Fisher, Anupam Garg, and Wilhelm Zwerger. Dynamics of the dissipative two-state system. *Reviews of Modern Physics*, 59(1):1, 1987.

[182] Alessandro Ferraro, Stefano Olivares, and Matteo G. A. Paris. Gaussian states in continuous variable quantum information, 2005. arXiv:quant-ph/0503237.

[183] Hannes Pichler and Peter Zoller. Photonic circuits with time delays and quantum feedback. *Physical Review Letters*, 116(9), mar 2016. doi:10.1103/physrevlett.116.093601.

[184] Arne L. Grimsmo. Time-delayed quantum feedback control. *Physical Review Letters*, 115(6), aug 2015. doi:10.1103/physrevlett.115.060402.

[185] Tomá š Rybár, Sergey N Filippov, Mário Ziman, and Vladimír Bužek. Simulation of indivisible qubit channels in collision models. *Journal of Physics B: Atomic, Molecular and Optical Physics*, 45(15):154006, jul 2012. doi:10.1088/0953-4075/45/15/154006.

[186] F. Ciccarello, G. M. Palma, and V. Giovannetti. Collision-model-based approach to non-markovian quantum dynamics. *Physical Review A*, 87(4), apr 2013. doi:10.1103/physreva.87.040103.

[187] P. Strasberg, G. Schaller, T. Brandes, and M. Esposito. Quantum and information thermodynamics: A unifying framework based on repeated interactions. *Phys. Rev. X*, 7:021003, 2017. URL: https://journals.aps.org/prx/abstract/10.1103/PhysRevX.7.021003, doi:10.1103/PhysRevX.7.021003.

[188] Carlton M Caves and Gerard J Milburn. Quantum-mechanical model for continuous position measurements. *Physical Review A*, 36(12):5543, 1987. doi:10.1103/PhysRevA.36.5543.

[189] P Filipowicz, J Javanainen, and P Meystre. Theory of a microscopic maser. *Physical Review A*, 34(4):3077, 1986. doi:10.1103/PhysRevA.34.3077.

[190] Serge Haroche and J-M Raimond. *Exploring the quantum: atoms, cavities, and photons*. Oxford university press, 2006.

[191] S. Campbell, F. Ciccarello, G. M. Palma, and B. Vacchini. System-environment correlations and Markovian embedding of quantum non-Markovian dynamics. *Phys. Rev. A*, 98:012142, 2018. URL: https://journals.aps.org/pra/abstract/10.1103/PhysRevA.98.012142, doi:10.1103/PhysRevA.98.012142.

[192] A P Lund and H M Wiseman. Measuring measurement–disturbance relationships with weak values. *New Journal of Physics*, 12(9):093011, sep 2010. URL: https://doi.org/10.1088%2F1367-2630%2F12%2F9%2F093011, doi:10.1088/1367-2630/12/9/093011.

[193] Lee A. Rozema, Ardavan Darabi, Dylan H. Mahler, Alex Hayat, Yasaman Soudagar, and Aephraim M. Steinberg. Violation of heisenberg's measurement-disturbance relationship by weak measurements. *Physical Review Letters*, 109(10), sep 2012. URL: https://doi.org/10.1103%2Fphysrevlett.109.100404, doi:10.1103/physrevlett.109.100404.

[194] H. Ollivier and W. H. Zurek. Quantum discord: a measure of the quantumness of correlations. *Phys. Rev. Lett.*, 88:017901, 2001. URL: https://link.aps.org/doi/10.1103/PhysRevLett.88.017901, doi:10.1103/PhysRevLett.88.017901.

[195] L Henderson and V Vedral. Classical, quantum and total correlations. *J. Phys. A*, 34:6899, 2001. URL: http://stacks.iop.org/0305-4470/34/i=35/a=315.

[196] F. S. Luiz, A. Junior, F. F. Fanchini, and G. T Landi. Machine classification for probe based quantum thermometry. *arXiv preprint arXiv:2107.04555*, 2021. URL: https://arxiv.org/abs/2107.04555.

[197] P. Strasberg. Operational approach to quantum stochastic thermodynamics. *Phys. Rev. E*, 100:022127, 2019. URL: https://journals.aps.org/pre/abstract/10.1103/PhysRevE.100.022127, doi:10.1103/PhysRevE.100.022127.

[198] B. Vacchini. Quantum renewal processes. *Sci. Rep.*, 10:1–13, 2020. URL: https://www.nature.com/articles/s41598-020-62260-z, doi:10.1038/s41598-020-62260-z.

[199] D. A Chisholm, G. García-Pérez, M. A. C. Rossi, G. M. Palma, and S. Maniscalco. Stochastic collision model approach to transport phenomena in quantum networks. *New J. Phys.*, 23:033031, 2021. URL: https://iopscience.iop.org/article/10.1088/1367-2630/abd57d/meta, doi:10.1088/1367-2630/ABD57D.

[200] Jorge Tabanera, Iné s Luque, Samuel L Jacob, Massimiliano Esposito, Felipe Barra, and Juan M R Parrondo. Quantum collisional thermostats. *New Journal of Physics*, 24(2):023018, feb 2022. doi:10.1088/1367-2630/ac4923.

[201] J. Ehrich, M. Esposito, F. Barra, and J. M. R. Parrondo. Micro-reversibility and thermalization with collisional baths. *Physica A*, 552:122108, 2020. doi:10.1016/J.PHYSA.2019.122108.

[202] S. L. Jacob, M. Esposito, J. M. R. Parrondo, and F. Barra. Thermalization Induced by Quantum Scattering. *PRX Quantum*, 2:020312, 2021. URL: https://journals.aps.org/prxquantum/abstract/10.1103/PRXQuantum.2.020312, doi:10.1103/PRXQuantum.2.020312.

[203] H. J. D. Miller and J. Anders. Energy-temperature uncertainty relation in quantum thermodynamics. *Nat. Commun.*, 9:1–8, 2018. doi:10.1038/s41467-018-04536-7.

[204] W.-K. Mok, K. Bharti, L.-C. Kwek, and A. Bayat. Optimal probes for global quantum thermometry. *Communications Physics*, 4(1):1–8, 2021. URL: https://www.nature.com/articles/s42005-021-00572-w, doi:10.1038/s42005-021-00572-w.

[205] Mohammad Mehboudi, Mathias R. Jørgensen, Stella Seah, Jonatan B. Brask, Jan Kołodyń ski, and Martí Perarnau-Llobet. Fundamental limits in bayesian thermometry and attainability via adaptive strategies. *Physical Review Letters*, 128(13), apr 2022. doi:10.1103/physrevlett.128.130502.

[206] Mathias R. Jørgensen, Jan Kołodyń ski, Mohammad Mehboudi, Martí Perarnau-Llobet, and Jonatan B. Brask. Bayesian quantum thermometry based on thermodynamic length. *Physical Review A*, 105(4), apr 2022. doi:10.1103/physreva.105.042601.

[207] Vittorio Giovannetti, Seth Lloyd, and Lorenzo Maccone. Advances in quantum metrology. *Nature Photonics*, 5(4):222–229, mar 2011. doi:10.1038/nphoton.2011.35.

[208] Michele Campisi, Peter Hänggi, and Peter Talkner. Colloquium: Quantum fluctuation relations: Foundations and applications. *Rev. Mod. Phys.*, 83(3):771, 2011. URL: https://link.aps.org/doi/10.1103/RevModPhys.83.771.

[209] Peter Talkner, Eric Lutz, and Peter Hänggi. Fluctuation theorems: Work is not an observable. *Phys. Rev. E*, 75:050102, May 2007. URL: https://link.aps.org/doi/10.1103/PhysRevE.75.050102, doi:10.1103/PhysRevE.75.050102.

[210] Tiago B. Batalhão, Alexandre M. Souza, Laura Mazzola, Ruben Auccaise, Roberto S. Sarthour, Ivan S. Oliveira, John Goold, Gabriele De Chiara, Mauro Paternostro, and Roberto M. Serra. Experimental reconstruction of work distribution and study of fluctuation relations in a closed quantum system. *Phys. Rev. Lett.*, 113:140601, Oct 2014. URL: https://link.aps.org/doi/10.1103/PhysRevLett.113.140601, doi:10.1103/PhysRevLett.113.140601.

[211] Gabriele De Chiara, Augusto J Roncaglia, and Juan Pablo Paz. Measuring work and heat in ultracold quantum gases. *New J. Phys.*, 17(3):035004, 2015. URL: https://doi.org/10.1088/1367-2630/17/3/035004.

[212] Michele Campisi and John Goold. Thermodynamics of quantum information scrambling. *Phys. Rev. E*, 95:062127, Jun 2017. URL: https://link.aps.org/doi/10.1103/PhysRevE.95.062127, doi:10.1103/PhysRevE.95.062127.

[213] A. Chenu, I. L. Egusquiza, J. Molina-Vilaplana, and A. del Campo. Quantum work statistics, loschmidt echo and information scrambling. *Sci. Rep.*, 8(1):12634, aug 2018. doi:10.1038/s41598-018-30982-w.

[214] A. Chenu, J. Molina-Vilaplana, and A. del Campo. Work statistics, loschmidt echo and information scrambling in chaotic quantum systems. *Quantum*, 3:127, mar 2019. doi:10.22331/q-2019-03-04-127.

[215] A. del Campo. Universal statistics of topological defects formed in a quantum phase transition. *Physical Review Letters*, 121(20), nov 2018. URL: https://doi.org/10.1103/physrevlett.121.200601.

[216] Zhaoyu Fei, Nahuel Freitas, Vasco Cavina, H. T. Quan, and Massimiliano Esposito. Work statistics across a quantum phase transition. *Phys. Rev. Lett.*, 124:170603, May 2020. URL: https://link.aps.org/doi/10.1103/PhysRevLett.124.170603, doi:10.1103/PhysRevLett.124.170603.

[217] Adrián Juan-Delgado and Aurélia Chenu. First law of quantum thermodynamics in a driven open two-level system. *Phys. Rev. A*, 104:022219, Aug 2021. URL: https://link.aps.org/doi/10.1103/PhysRevA.104.022219, doi:10.1103/PhysRevA.104.022219.

[218] María García Díaz, Giacomo Guarnieri, and Mauro Paternostro. Quantum work statistics with initial coherence. *Entropy*, 22(11), 2020. URL: https://www.mdpi.com/1099-4300/22/11/1223.

[219] Kamil Korzekwa, Matteo Lostaglio, Jonathan Oppenheim, and David Jennings. The extraction of work from quantum coherence. *New J. Phys.*, 18(2):023045, feb 2016. doi:10.1088/1367-2630/18/2/023045.

[220] John Goold, Francesco Plastina, Andrea Gambassi, and Alessandro Silva. The role of quantum work statistics in many-body physics. *Thermodynamics in the Quantum Regime*, pages 317–336, 2018. URL: https://link.springer.com/chapter/10.1007/978-3-319-99046-0_13.

[221] James Klatzow, Jonas N. Becker, Patrick M. Ledingham, Christian Weinzetl, Krzysztof T. Kaczmarek, Dylan J. Saunders, Joshua Nunn, Ian A. Walmsley, Raam Uzdin, and Eilon Poem. Experimental demonstration of quantum effects in the operation of microscopic heat engines. *Phys. Rev. Lett.*, 122:110601, Mar 2019. URL: https://link.aps.org/doi/10.1103/PhysRevLett.122.110601, doi:10.1103/PhysRevLett.122.110601.

[222] Marcus Huber, Martí Perarnau-Llobet, Karen V Hovhannisyan, Paul Skrzypczyk, Claude Klöckl, Nicolas Brunner, and Antonio Acín. Thermodynamic cost of creating correlations. *New J. Phys.*, 17(6):065008, 2015. URL: https://doi.org/10.1088/1367-2630/17/6/065008.

[223] Avijit Misra, Uttam Singh, Samyadeb Bhattacharya, and Arun Kumar Pati. Energy cost of creating quantum coherence. *Phys. Rev. A*, 93(5):052335, 2016. URL: https://link.aps.org/doi/10.1103/PhysRevA.93.052335.

[224] Harry J. D. Miller, Giacomo Guarnieri, Mark T. Mitchison, and John Goold. Quantum fluctuations hinder finite-time information erasure near the landauer limit. *Phys. Rev. Lett.*, 125:160602, Oct 2020. URL: https://link.aps.org/doi/10.1103/PhysRevLett.125.160602.

[225] Krissia Zawadzki, Anthony Kiely, Gabriel T Landi, and Steve Campbell. Non-gaussian work statistics at finite-time driving. *Phys. Rev. A*, 107(1):012209, 2023. URL: https://link.aps.org/doi/10.1103/PhysRevA.107.012209, doi:10.1103/PhysRevA.107.012209.

[226] Krissia Zawadzki, Roberto M. Serra, and Irene D'Amico. Work-distribution quantumness and irreversibility when crossing a quantum phase transition in finite time. *Phys. Rev. Research*, 2:033167, Jul 2020. URL: https://link.aps.org/doi/10.1103/PhysRevResearch.2.033167, doi:10.1103/PhysRevResearch.2.033167.

[227] Alexander Streltsov, Gerardo Adesso, and Martin B. Plenio. Colloquium: Quantum coherence as a resource. *Reviews of Modern Physics*, 89(4), oct 2017. doi:10.1103/revmodphys.89.041003.

[228] T. Baumgratz, M. Cramer, and M. B. Plenio. Quantifying coherence. *Phys. Rev. Lett.*, 113:140401, Sep 2014. URL: https://link.aps.org/doi/10.1103/PhysRevLett.113.140401, doi:10.1103/PhysRevLett.113.140401.

[229] Andreas Winter and Dong Yang. Operational resource theory of coherence. *Physical Review Letters*, 116(12), mar 2016. doi:10.1103/physrevlett.116.120404.

[230] C. Jarzynski. Nonequilibrium equality for free energy differences. *Physical Review Letters*, 78(14):2690–2693, apr 1997. doi:10.1103/physrevlett.78.2690.

[231] Peter Talkner and Peter Hänggi. The tasaki–crooks quantum fluctuation theorem. *Journal of Physics A: Mathematical and Theoretical*, 40(26):F569, 2007. doi:10.1088/1751-8113/40/26/F08.

[232] Gavin E Crooks. Nonequilibrium measurements of free energy differences for microscopically reversible markovian systems. *Journal of Statistical Physics*, 90:1481–1487, 1998.

[233] John Goold, Marcus Huber, Arnau Riera, Lídia Del Rio, and Paul Skrzypczyk. The role of quantum information in thermodynamics—a topical review. *J. Phys. A*, 49(14):143001, 2016. URL: https://doi.org/10.1088/1751-8113/49/14/143001.

[234] L. Fusco, S. Pigeon, T. J. G. Apollaro, A. Xuereb, L. Mazzola, M. Campisi, A. Ferraro, M. Paternostro, and G. De Chiara. Assessing the nonequilibrium thermodynamics in a quenched quantum many-body system via single projective measurements. *Phys. Rev. X*, 4:031029, Aug 2014. URL: https://link.aps.org/doi/10.1103/PhysRevX.4.031029, doi:10.1103/PhysRevX.4.031029.

[235] Markus Greiner, Olaf Mandel, Tilman Esslinger, Theodor W Hänsch, and Immanuel Bloch. Quantum phase transition from a superfluid to a mott insulator in a gas of ultracold atoms. *nature*, 415(6867):39–44, 2002.

[236] Markus Greiner, Olaf Mandel, Theodor W. Hänsch, and Immanuel Bloch. Collapse and revival of the matter wave field of a bose–einstein condensate. *Nature*, 419(6902):51–54, sep 2002. doi:10.1038/nature00968.

[237] Ehud Altman and Assa Auerbach. Oscillating superfluidity of bosons in optical lattices. *Physical Review Letters*, 89(25), dec 2002. doi:10.1103/physrevlett.89.250404.

[238] Pasquale Calabrese and John Cardy. Time dependence of correlation functions following a quantum quench. *Physical Review Letters*, 96(13), apr 2006. doi:10.1103/physrevlett.96.136801.

[239] F. Pietracaprina, C. Gogolin, and J. Goold. Total correlations of the diagonal ensemble as a generic indicator for ergodicity breaking in quantum systems. *Phys. Rev. B*, 95:125118, Mar 2017. URL: https://link.aps.org/doi/10.1103/PhysRevB.95.125118, doi:10.1103/PhysRevB.95.125118.

[240] Aslı Çakan, J Ignacio Cirac, and Mari Carmen Bañuls. Approximating the long time average of the density operator: Diagonal ensemble. *Phys. Rev. B*, 103:115113, Mar

2021. URL: https://link.aps.org/doi/10.1103/PhysRevB.103.115113, doi:10.1103/PhysRevB.103.115113.

[241] J. Goold, C. Gogolin, S. R. Clark, J. Eisert, A. Scardicchio, and A. Silva. Total correlations of the diagonal ensemble herald the many-body localization transition. *Phys. Rev. B*, 92:180202, Nov 2015. URL: https://link.aps.org/doi/10.1103/PhysRevB.92.180202, doi:10.1103/PhysRevB.92.180202.

[242] Zakaria Mzaouali, Ricardo Puebla, John Goold, Morad El Baz, and Steve Campbell. Work statistics and symmetry breaking in an excited-state quantum phase transition. *Phys. Rev. E*, 103:032145, Mar 2021. URL: https://link.aps.org/doi/10.1103/PhysRevE.103.032145, doi:10.1103/PhysRevE.103.032145.

[243] Qian Wang and Francisco Pérez-Bernal. Characterizing the lipkin-meshkov-glick model excited-state quantum phase transition using dynamical and statistical properties of the diagonal entropy. *Phys. Rev. E*, 103:032109, Mar 2021. URL: https://link.aps.org/doi/10.1103/PhysRevE.103.032109, doi:10.1103/PhysRevE.103.032109.

[244] J. Q. You and Franco Nori. Superconducting circuits and quantum information. *Physics Today*, 58(11):42–47, nov 2005. doi:10.1063/1.2155757.

[245] Floris A. Zwanenburg, Andrew S. Dzurak, Andrea Morello, Michelle Y. Simmons, Lloyd C. L. Hollenberg, Gerhard Klimeck, Sven Rogge, Susan N. Coppersmith, and Mark A. Eriksson. Silicon quantum electronics. *Reviews of Modern Physics*, 85(3):961–1019, jul 2013. doi:10.1103/revmodphys.85.961.

[246] E Dupont-Ferrier, B Roche, B Voisin, X Jehl, R Wacquez, M Vinet, M Sanquer, and S De Franceschi. Coherent coupling of two dopants in a silicon nanowire probed by landau-zener-stückelberg interferometry. *Physical review letters*, 110(13):136802, 2013.

[247] Takuya Higuchi, Christian Heide, Konrad Ullmann, Heiko B. Weber, and Peter Hommelhoff. Light-field-driven currents in graphene. *Nature*, 550(7675):224–228, sep 2017. doi:10.1038/nature23900.

[248] Thomas Faust, Johannes Rieger, Maximilian J. Seitner, Peter Krenn, Jörg P. Kotthaus, and Eva M. Weig. Nonadiabatic dynamics of two strongly coupled nanomechanical resonator modes. *Physical Review Letters*, 109(3), jul 2012. doi:10.1103/physrevlett.109.037205.

[249] Oleh V. Ivakhnenko, Sergey N. Shevchenko, and Franco Nori. Nonadiabatic landau–zener–stückelberg–majorana transitions, dynamics, and interference. *Physics Reports*, 995:1–89, jan 2023. doi:10.1016/j.physrep.2022.10.002.

[250] Alexandre M Zagoskin. *Quantum engineering: theory and design of quantum coherent structures*. Cambridge University Press, 2011.

[251] Subir Sachdev. Quantum phase transitions. *Physics world*, 12(4):33, 1999.

[252] Dung-Hai Lee, Guang-Ming Zhang, and Tao Xiang. Edge solitons of topological insulators and fractionalized quasiparticles in two dimensions. *Physical Review Letters*, 99(19), nov 2007. doi:10.1103/physrevlett.99.196805.

[253] K. Sengupta, Diptiman Sen, and Shreyoshi Mondal. Exact results for quench dynamics and defect production in a two-dimensional model. *Physical Review Letters*, 100(7), feb 2008. doi:10.1103/physrevlett.100.077204.

[254] Adolfo del Campo, Marek M. Rams, and Wojciech H. Zurek. Assisted finite-rate adiabatic passage across a quantum critical point: Exact solution for the quantum ising model. *Physical Review Letters*, 109(11), sep 2012. doi:10.1103/physrevlett.109.115703.

[255] Philip W Anderson. Absence of diffusion in certain random lattices. *Physical review*, 109(5):1492, 1958.

[256] G A Domínguez-Castro and R Paredes. The aubry–andré model as a hobbyhorse for understanding the localization phenomenon. *Eur. J. Phys.*, 40(4):045403, jun 2019. doi:10.1088/1361-6404/ab1670.

[257] Elihu Abrahams, PW Anderson, DC Licciardello, and TV Ramakrishnan. Scaling theory of localization: Absence of quantum diffusion in two dimensions. *Physical Review Letters*, 42(10):673, 1979. doi:10.1103/PhysRevLett.125.196604.

[258] Serge Aubry and Gilles André. Analyticity breaking and Anderson localization in incommensurate lattices. *Proceedings, VIII International Colloquium on Group-Theoretical Methods in Physics*, 3, 1980.

[259] P. G. Harper. Single band motion of conduction electrons in a uniform magnetic field. *Proceedings of the Physical Society. Section A*, 68(10):874–878, 1955. doi:10.1088/0370-1298/68/10/304.

[260] J. E. Lye, L. Fallani, C. Fort, V. Guarrera, M. Modugno, D. S. Wiersma, and M. Inguscio. Effect of interactions on the localization of a bose-einstein condensate in a quasiperiodic lattice. *Phys. Rev. A*, 75:061603, Jun 2007. URL: https://link.aps.org/doi/10.1103/PhysRevA.75.061603, doi:10.1103/PhysRevA.75.061603.

[261] Luca Tanzi, Eleonora Lucioni, Saptarishi Chaudhuri, Lorenzo Gori, Avinash Kumar, Chiara D'Errico, Massimo Inguscio, and Giovanni Modugno. Transport of a bose gas in 1d disordered lattices at the fluid-insulator transition. *Phys. Rev. Lett.*, 111:115301, Sep 2013. URL: https://link.aps.org/doi/10.1103/PhysRevLett.111.115301, doi:10.1103/PhysRevLett.111.115301.

[262] Chiara D'Errico, M Moratti, E Lucioni, L Tanzi, B Deissler, M Inguscio, G Modugno, Martin B Plenio, and F Caruso. Quantum diffusion with disorder, noise and interaction. *New J. Phys.*, 15(4):045007, 2013. URL: https://doi.org/10.1088/1367-2630/15/4/045007.

[263] Georgios Styliaris, Namit Anand, Lorenzo Campos Venuti, and Paolo Zanardi. Quantum coherence and the localization transition. *Phys. Rev. B*, 100:224204, Dec 2019. URL: https://link.aps.org/doi/10.1103/PhysRevB.100.224204, doi:10.1103/PhysRevB.100.224204.

[264] Shane Dooley and Graham Kells. Enhancing the effect of quantum many-body scars on dynamics by minimizing the effective dimension. *Phys. Rev. B*, 102:195114, Nov 2020. URL: https://link.aps.org/doi/10.1103/PhysRevB.102.195114, doi:10.1103/PhysRevB.102.195114.

[265] S Das Sarma, Song He, and XC Xie. Mobility edge in a model one-dimensional potential. *Physical review letters*, 61(18):2144, 1988. doi:10.1103/PhysRevLett.61.2144.

[266] Sriram Ganeshan, J. H. Pixley, and S. Das Sarma. Nearest neighbor tight binding models with an exact mobility edge in one dimension. *Physical Review Letters*, 114(14), apr 2015. doi:10.1103/physrevlett.114.146601.

[267] Yucheng Wang, Xu Xia, Long Zhang, Hepeng Yao, Shu Chen, Jiangong You, Qi Zhou, and Xiong-Jun Liu. One-dimensional quasiperiodic mosaic lattice with exact mobility edges. *Physical Review Letters*, 125(19), nov 2020. doi:10.1103/physrevlett.125.196604.

[268] Alexander Duthie, Sthitadhi Roy, and David E. Logan. Self-consistent theory of mobility edges in quasiperiodic chains. *Physical Review B*, 103(6), feb 2021. doi:10.1103/physrevb.103.l060201.

[269] Fangzhao Alex An, Karmela Padavić , Eric J. Meier, Suraj Hegde, Sriram Ganeshan, J. H. Pixley, Smitha Vishveshwara, and Bryce Gadway. Interactions and mobility edges: Observing the generalized aubry-andré model. *Physical Review Letters*, 126(4), jan 2021. doi:10.1103/physrevlett.126.040603.

[270] Yunfei Wang, Jia-Hui Zhang, Yuqing Li, Jizhou Wu, Wenliang Liu, Feng Mei, Ying Hu, Liantuan Xiao, Jie Ma, Cheng Chin, and Suotang Jia. Observation of interaction-induced mobility edge in an atomic aubry-andré wire. *Physical Review Letters*, 129(10), sep 2022. doi:10.1103/physrevlett.129.103401.

[271] G. Semeghini, M. Landini, P. Castilho, S. Roy, G. Spagnolli, A. Trenkwalder, M. Fattori, M. Inguscio, and G. Modugno. Measurement of the mobility edge for 3d anderson localization. *Nature Physics*, 11(7):554–559, jun 2015. doi:10.1038/nphys3339.

[272] G. Francica, J. Goold, and F. Plastina. Role of coherence in the nonequilibrium thermodynamics of quantum systems. *Physical Review E*, 99(4), apr 2019. URL: https://doi.org/10.1103/physreve.99.042105.

[273] Adalberto D Varizi, Mariana A Cipolla, Martí Perarnau-Llobet, Raphael C Drumond, and Gabriel T Landi. Contributions from populations and coherences in non-equilibrium entropy production. *New J. Phys.*, 23(6):063027, jun 2021. doi:10.1088/1367-2630/abfe20.

[274] PG De Gennes. Collective motions of hydrogen bonds. *Solid State Communications*, 1(6):132–137, 1963. doi:10.1016/0038-1098(63)90212-6.

[275] Harry J Lipkin, N Meshkov, and AJ Glick. Validity of many-body approximation methods for a solvable model:(i). exact solutions and perturbation theory. *Nuclear Physics*, 62(2):188–198, 1965. doi:10.1016/0029-5582(65)90862-X.